Material Science and Technology Division

Propulsion Materials Program
Quarterly Progress Report for
January through March 2011

David P. Stinton
Technical Project Manager

Prepared for
U.S. Department of Energy
Assistant Secretary for Energy Efficiency and Renewable Energy
Office of Vehicle Technologies Program
VT 05 04 000

Prepared by the
OAK RIDGE NATIONAL LABORATORY
Oak Ridge, Tennessee 37831-6066
Managed by
UT-Battelle, LLC
for the Department of Energy
Under contract DE-AC05-00OR22725

CONTENTS

Project 18516 – Materials for Hybrid and Electric Drive Systems

Agreement 23279 - Improved Organics for Power Electronics and Electric Motors *(ORNL)*

Agreement 23278 - Low-Cost Direct Bonded Aluminum (DBA) Substrates *(ORNL)*

Agreement 19201 – MBD Non-Rare Earth Magnetic Materials *(ORNL)*

Project 18518 – Materials for High Efficiency Engines

Agreement 11752 – Materials for HCCI Engines *(ORNL)*

Agreement 13329 – Design Optimization of Piezoceramic Multilayer Actuators for Heavy Duty Diesel Engine Fuel Injectors *(ORNL)*

Agreement 15050 – Evaluation of Materials via ACERT Engine *(ORNL)*

Agreement 16303 – Materials for High Pressure Fuel Injection Systems *(ORNL)*

Agreement 16304 – Materials for Advanced Engine Valve Train *(ORNL)*

Agreement 17257 – Materials for Advanced Turbocharger Design *(ORNL)*

Agreement 17894 – NDE for ACERT Engine Components *(ANL)*

Agreement 18570 – Engine Materials Compatibility with Alternate Fuels *(ORNL)*

Agreement 18571 – Materials Issues Associated with EGR Systems *(ORNL)*

Agreement 19202 – Titanium Friction and Wear *(ORNL)*

Agreement 23284 – Friction Reduction Through Surface Modification *(ORNL)*

Agreement 23285 - Efficiency Implications of Advanced Materials in Advanced Combustion Internal Engines *(ORNL)*

Project 18519 – Materials for Exhaust and Energy Recovery

Agreement 9130 – Catalyst Characterization *(ORNL)*

Agreement 10461 – Durability of Diesel Engine Particulate Filters *(ORNL)*

Agreement 10635 – Catalysts via First Principles *(ORNL)*

Agreement 19214 - Biofuels Impact on Diesel Particulate Filters *(ORNL)*

Agreement 20091 – Electrically Regenerated DPF Material *(ORNL)*

<u>Project 18865 – Materials by Design</u>

Agreement 9105 – Characterization of Catalyst Microstructures *(ORNL)*

Agreement 14957 – Thermoelectric Mechanical Reliability *(ORNL)*

Agreement 16308 – MBD - Thermoelectrics Theory and Structure *(ORNL)*

Agreement 23279: Improved Organics for Power Electronics and Electric Motors

A. A. Wereszczak, C. W. Ayers, R. H. Wiles, and H. Wang
Oak Ridge National Laboratory

Objective/Scope

Identify lower-cost and better-performing organic compounds for dielectric and thermal management applications in power electronics and electric motors. Candidate and new organic compounds (e.g., epoxy molded compounds or EMCs) will be characterized and developed to promote low-cost fabrication, volume reduction, mechanical resilience, and improved and alternative thermal management exploitation. They include compounds presently used in dielectrics in power electronic devices, potting compounds used with capacitors, and pottings used in motors. For dielectrics, improved performance represents a higher-temperature capability and the sustainment of dielectric and gel-like mechanical damping properties under thermal cycling and vibratory conditions. For potting compounds used with capacitors or motors, interest exists to identify alternatives that have higher thermal conductivity (or that enhance the thermal conductivity of existing compounds) or that benefit structural or damping performance without compromising thermal performance.

Technical Highlights

Thermal property measurement of existing EMCs

The thermal conductivities of a first set of approximately 20 different EMC samples and electronic components with EMCs were measured with a hot-disk thermal constants analyzer.

The electronic components included EMCs used with film capacitors (Fig. 1), IGBT power electronic modules, and motors (Fig. 1) used with hybrid vehicles. These components are unused and their measured thermal conductivity will serve as a reference. Used components will also be analogously sectioned up, and the thermal conductivities of the used epoxy molding compounds will also be measured and compared. This will help us understand how thermal conductivity (and consequential thermal management and reliability) changes as a function of service time and conditions. And then as we make high-thermal conductivity EPMs (which these components do not employ), we will be able to guide and predict improvements in their thermal management.

Testing was completed and the results are being reduced and will be reported in Q3 reporting.

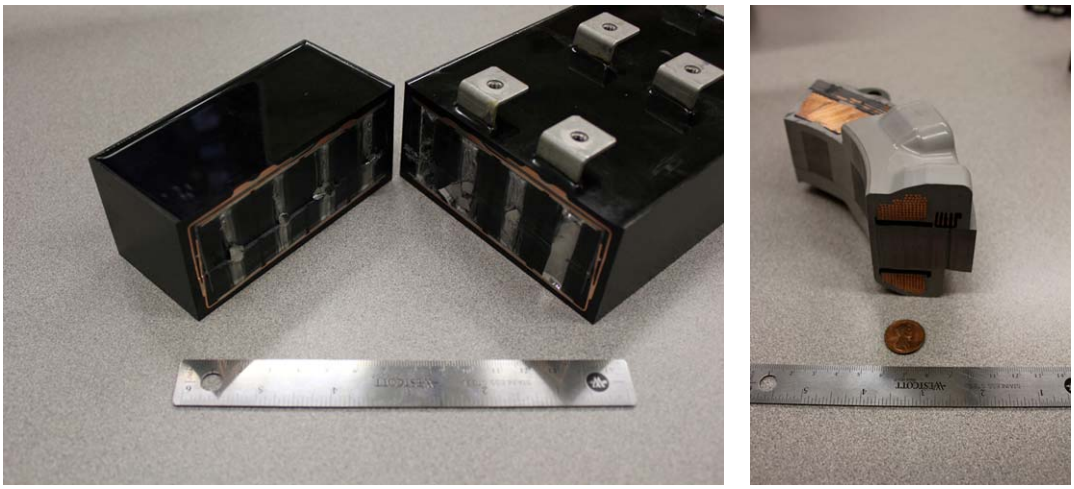

Figure 1. The thermal conductivities of the EMCs enveloping a sectioned film capacitor (left) and a sectioned motor component (right) used hybrid vehicles are being measured.

Processing of ceramic-filler EMCs

The introduction of non-metallic mineral particles is known to increase the thermal conductivity of an electrically insulative EMC and that practice has been utilized for many years now. An example of filler-EMC structure is shown in Fig. 2. Metallic particles are not candidate fillers for these applications because they ultimately cause those EMCs to exhibit electrically conductive character. Traditionally, starting about 40 years ago, typical non-metallic mineral fillers included milled silica, quartz, and glass (all silicon-dioxide- or silica- or SiO_2-based derivatives). During the past 25 years the use of fused silica, and its fumed filler form, have became dominant as they could be combined in controlled particle size distribution that favored low viscosity flow at temperature, good spiral flow, and high solids loading (as high as 80% or more). Additionally, the use of silica in an EMC causes the EMC to have a low coefficient of thermal expansion (CTE); consequently, that promotes near-matching of EMC's CTE and the CTEs of the material constituents the EMC encapsulations, and minimizes the introduction of high thermomechanical stresses. This CTE matching promotes long-lifetime of protection at higher use temperatures and during thermal cycling. If a filler material in an EMC has too large a CTE, then it would cause the EMC to have relatively high expansion or swelling response at high temperature that can damage the constituents it is meant to protect. But the primary drawback of all these silica-based options for EMCs is silica has a low thermal conductivity thus its use limits thermal management options with these EMCs.

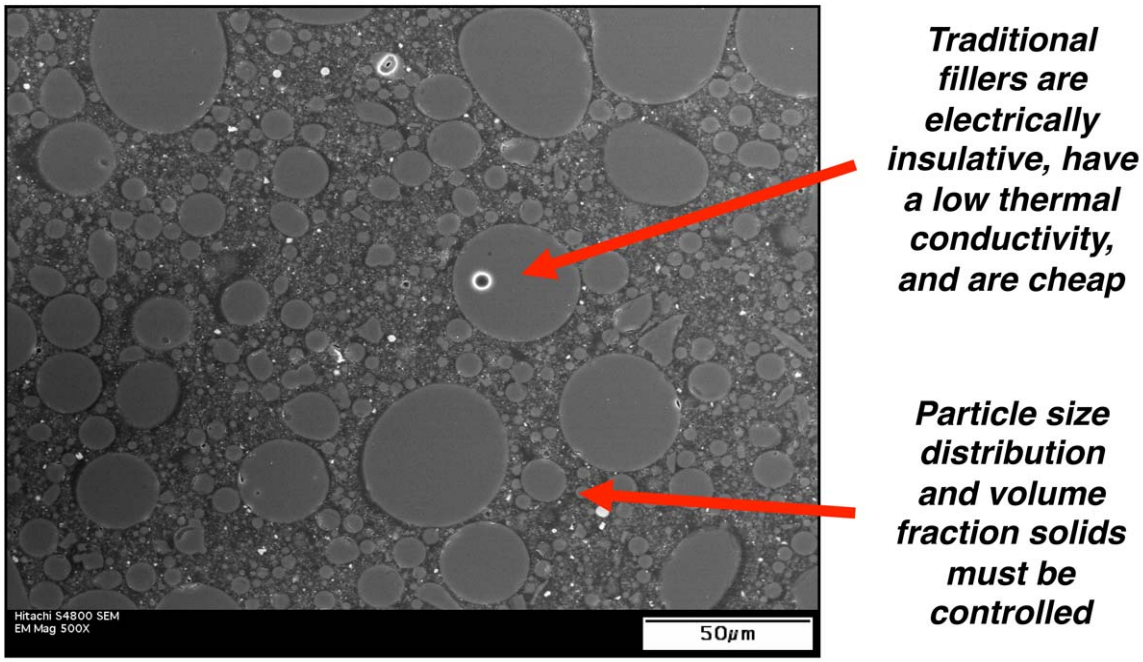

Photo used with permission of Z. Liang (NTRC/ORNL)

Figure 2. Example of epoxy molding compound with ceramic filler used in a power electronic module from a hybrid vehicle's inverter.

There are other non-metallic, non-electrically-conducting minerals that conceivably could be used for EMC fillers. They are listed in Table 1. Silica (SiO_2), while having a low density and being inexpensive, has a very low thermal conductivity (consequences of the latter already described) compared to Si. Aluminum oxide (Al_2O_3), magnesium oxide (MgO), and boron nitride (BN) have moderate thermal conductivities and are inexpensive; however, they are denser than Si and have higher CTEs than Si. Silicon carbide (SiC) is several times more expensive than Si. Lastly, highly desirable high thermal conductivities of aluminum nitride (AlN) and beryllium oxide (BeO) are offset by high costs for both materials (more than one order of magnitude costlier than Si) and also toxicity issues associated with the latter (Si is not toxic). Among those listed candidate filers, Si perhaps has the best combination of high thermal conductivity, low density, low CTE, and low cost.

Table 1. Properties for candidate fillers and epoxy.

Material	Electrical Resistivity at 25°C (Ω•cm)	Thermal Conductivity at 25°C - □ - (W/m•K)	Heat Capacity - Cp - (J/kg•K)	Density - □ - (kg/m^3)	Coefficient of Thermal Expansion - CTE - (x 10^{-6}/°C)
Silica silicon dioxide (SiO_2)	> 10^{14}	2	700	2600	0.5
Alumina aluminum oxide (Al_2O_3)	> 10^{14}	30	900	3900	8
Boron nitride (BN) * has anisotropy	> 10^{14}	30/33*	1600	1900	12/3*
Magnesia magnesium oxide (MgO)	> 10^{14}	40	900	3600	10
Silicon carbide (SiC)	> 10^{14}	120	800	3100	4
Aluminum nitride (AlN)	> 10^{14}	250	700	3200	5
Beryllia berylium oxide (BeO)	> 10^{14}	280	600	2900	9
Silicon (Si)	10^2	150	700	2300	3
Epoxy	> 10^{12}	0.05 - 0.4	1500	1200	30-60

During Q2 we initiated the processing of several ceramic-filler EMCs. These fillers so far include Al_2O_3, MgO, AlN, and Si. We are controlling the volume fraction and particle size distribution, and measuring the produced thermal conductivity using a hot disk thermal constants analyzer. Lastly, we are modeling the thermal conductivity of these filler-EMCs taking into account volume fraction and particle size distribution, and examining percolation threshold limits based on those.

Status of FY 2010 Milestones

1. Establish baselines by measuring thermal properties of unused and serviced organics of each of three classes of organics. [Jun11] *May be difficult to satisfy by Jun11 because initial funding commenced during Q2.*
2. Develop test methods that representatively thermal cycle each of the three classes of organic materials. [Sep11] *On schedule.*

Communications/Visits/Travel

- Several technical discussions have occurred with Mossey Creek's J. Carberry about epoxy molding compounds.
- Numerous discussions held with NTRC staff members (Ayers, Wiles, and Miller).
- A visit to Henkel (Olean, NY) in Q3 or Q4 is being organized. Henkel's Olean Division manufactures EMCs for the electronics industry.
- Poster on this project to be presented at DOE Merit Review on 11 May 2011.

Problems Encountered

Funding for project did not begin until Q2.

Publications/Presentations/Awards

An invention disclosure was filed. A. A. Wereszczak and J. Carberry, "Thermally-Conductive, Electrically-Insulating, Silicon-Containing Epoxy Molding Compounds (Si-EMCs)," DOE S-Number S-124,118, Invention Disclosure Number 201102561, February 28, 2011.

References

None.

Agreement 23278: Low-Cost Direct Bonded Aluminum (DBA) Substrates

H. -T. Lin and A. A. Wereszczak
Oak Ridge National Laboratory

Objective/Scope

This project seeks to develop low-cost, high quality, and thermomechanically robust direct-bonded aluminum (DBA) substrates. Low-cost DBA substrates will lessen the cost of the inverter insulated gate bipolar transistor (IGBT) power modules while concomitantly sustaining or improving thermal management and improving thermomechanical reliability. Compared to copper and DBC substrates, aluminum has a lower elastic modulus so it imparts a lower stress on the ceramic substrate it sandwiches, and this contributes to improved mechanical reliability of the entire substrate. Wire and ribbon for bonding in power electronic modules tends to be aluminum, so the apparent coefficient of thermal expansion of DBAs is compatible with them unlike DBCs. The use of a DBA substrate will also lessen the weight up to 50% compared to presently used DBC substrates, and this would contribute to the weight reduction goals of the inverter and converter in the APEEM program as well.

Technical Highlights

A literature search was conducted during this reporting period on the conventional and alternative processing methods to directly bond aluminum (Al) to alumina (Al_2O_3) or alumina nitride (AlN). In general, Al could be bonded to Al_2O_3 (and AlN) substrates by placing and then melting a piece of brazing film (e.g., Al-Si alloys) between the two materials [1-4]. The diffusion of brazing element (like Si) into Al would result in a good bonding. The other approach involved in the direct melting or casting of Al on Al_2O_3 (and AlN) substrate without the use of brazing film [5]. On the other hand, the transient-liquid-phase (TLP) approach has been widely applied to manufacture direct bonded aluminum (DBA) substrates [6-9]. Aluminum is known to form transient eutectic liquid phase products with elements of Si (577°C), Ge (420°C), Ag (567°C), and Cu (548°C). These elements could be deposited on the Al surface via the vapor deposition or slurry screen-printing process prior to the final bonding step carried out above the eutectic liquid temperatures. Results showed that the use of Si and Cu exhibited relatively better reliability and lifetime performance after thermal cycle testing [7].

The purchase of commercially available DBA and direct bonded copper (DBC) substrates was in progress during this reporting period. A cross-sectional view of one of those DBAs is shown in Fig. 1.

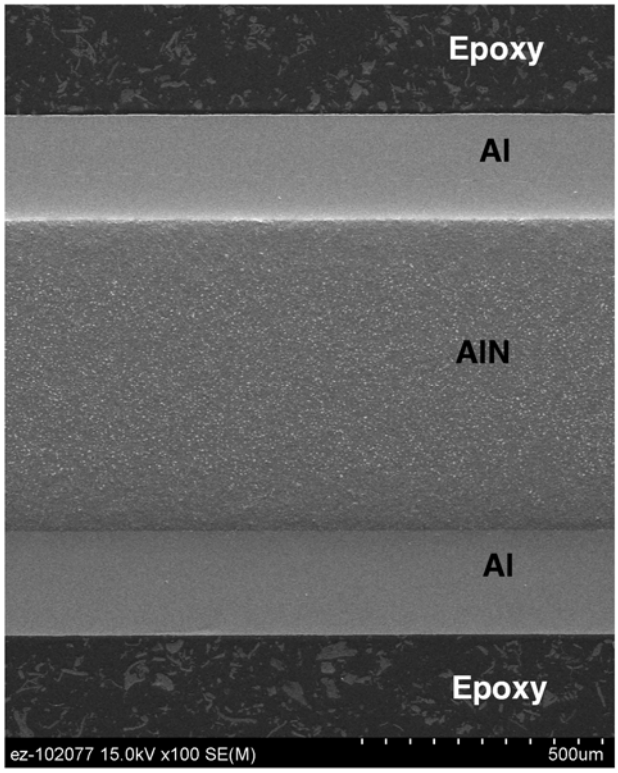

Figure 1. Cross-section example of a commercially available DBA substrate. Aluminum is cladded on both sides of an aluminum nitride ceramic substrate.

These commercial DBA and DBA substrates will be characterized and tested under thermal cycle condition to provide a database for reference. The purchase of commercial Al_2O_3 and AlN substrate was also completed. The physical properties (e.g., Young's modulus, Poisson ratio, and coefficient of thermal expansion) of both substrates will be characterized and be reported in next quarterly report. These physical properties would be used for modeling the temperature profile and thermomechanical stress under simulated application condition and thus probabilistic reliability prediction.

Status of FY 2011 Milestones

1. Survey conventional and alternative processing methods to directly bond Al to Al_2O_3 (and AlN). [April11] – On schedule.
2. Down-select processing method most likely to produce high strength bonding. [Sep11] – On schedule.

Communications/Visits/Travel

- Several discussions have occurred with ORNL/NTRC, USCAR EETT, General Motors, and NREL staff members about the plans for this project.
- Poster on this project to be presented at DOE Merit Review on 11 May 2011.

Problems Encountered
Funding for project did not begin until Q2.

Publications/Presentations/Awards
None.

References

1. H. Yoshida, Y. Kuromitsu, M. Toriumi, M. Yuzawa, Ceramic substrate used for fabricating electric or electronic circuit, US Patent No. 5130498, 1992.
2. Y. Nagatomo, R. Muranaka, H. Hayashi, Y. Kuromitsu, N. Kuwano, Fracture Process of Aluminum/Aluminum Nitride Interfaces during Thermal Cycling, *Materials Science Forum*, 638-642, 3895, 2010.
3. S. Gerhard, Method for manufacturing a power semiconductor device and direct bonded substrate thereof, US Patent No. 6670216, 2003.
4. J.Y. Kim, J.S. Hardy, and K.S. Weil, Aluminum Air Brazing for Joining Ceramics, in Advances in Ceramic Coatings and Ceramic-Metal Systems: *Ceramic Engineering and Science Proceedings*, 26, 3, 2008.
5. X.S. Ning, C. Nagata, M. Sakuraba, T. Tanaka: Process for preparing a ceramic electronic circuit board and process for preparing aluminum or aluminum alloy bonded ceramic material, US patent No. 5965193, 1999.
6. M. Nobuyuki, K. Hajime, S. Yasuyuki, Method for directly bonding ceramic and metal members and laminated body of the same, US Patent No. 4849292, 1989.
7. Y. Kuromitsu, Y. Nagatomo, H. Tonomura, K. Akiyama, C.M. Montesa, N. Shibata, T. Tohei, and Y. Ikuhara, Direct Bonded Aluminum (DBA) on Aluminum Nitride (AlN) substrates through Transient Liquid Phase and its Application, *6th International Conference on Integrated Power Electronic Systems (CIPS) Proceedings*, 2010.
8. H. Knoll, W. Weidenauer, P. Ingram, S. Bennemann, S. Brand, M. Petzold, , Ceramic substrates with aluminum metallization for power application, *Electronic System-Integration Technology Conference (ESTC), 2010 3rd* ,1-5, 13-16, 2010.
9. A. Lindemann, Properties of Direct Aluminum Bonded Substrates for Power Semiconductor Components, *IEEE Transactions on Power Electronics*, 22 (2), 2007.

Agreement 19201: Non-Rare Earth Magnetic Materials

Michael A. McGuire
Oak Ridge National Laboratory

Objective/Scope

We will examine rare-earth-free chemical systems which hold promise for the discovery of new high-temperature ferromagnets with the large magnetic moments and strong anisotropies required for technologically useful permanent magnet materials. This research will focus on the development of new rare-earth free permanent magnet materials. Understudied chemical systems which are likely to contain materials with properties required for useful ferromagnets (large moments, high Curie temperatures, strong magnetic anisotropy) will be synthesized and characterized. First principle calculations will be performed to aid in the identification of promising target materials and to guide chemical tuning of magnetic properties through element substitutions and alloying. The focus will be on materials based on elements, such as Mn, Fe and Cr, suitable for application in vehicles.

The primary challenge in this work is to obtain high magnetic anisotropy without rare-earth elements, while maintaining high saturation magnetization. The two main sources of anisotropy are magneto-crystalline anisotropy and shape anisotropy. Magneto-crystalline anisotropy is an intrinsic property determined by energy required to rotate a magnetic moment relative to the crystal lattice. Shape anisotropy is an extrinsic property related to the domain structure of individual crystallites. We are targeting intermetallic compounds with large magneto-crystalline anisotropy, which could then be further enhanced by materials processing to optimize magnetic domain configurations. To obtain anisotropic magnetic properties, heavy transition metal elements will be incorporated instead of rare earths.

Technical Highlights

Work has continued on the promising Hf-Co materials. In an effort to learn more about the crystal structure of these complex and interesting materials, metal flux single crystal growth reactions were attempted. The main concern with these types of syntheses is the solubility of reactants in the chosen flux. A low melting metal flux was chosen, and dissolution of Hf, Zr, and Co was achieved under the selected reaction conditions. The single crystals that resulted were ternary phases containing (Hf/Zr), Co and an element from the metal flux. The target materials (Hf_2Co_{11} and Zr_2Co_{11}) were not obtained, but these initial results show the methodology to be appropriate for the crystallization with these elements. Tuning the flux composition and reaction condition may produce the desired result.

First principles calculations were performed to assess the potential for large coercivity in the ferromagnetic Laves phase $HfFe_2$. The results show little magnetic anisotropy, and suggest that the realization of hard magnetic behavior in this compound would require further chemical manipulation. Some related experiments are ongoing.

Materials selection for this work is shifting from binary to ternary compounds. The role of a third, non-magnetic, light element (like boron in NdFeB magnets) can play an important role in magnetic anisotropy. Nitrogen is of interest, but presents synthetic challenges and stability issues. Some commercial iron nitride powder containing mostly Fe_4N was acquired and preliminary experiments have been conducted to determine its usefulness as a starting material for ternary intermetallic nitrides. Decomposition to Fe and N_2 proceeded under even relatively mild conditions, suggesting limited usefulness as a nitrogen source for solids. Reaction under flowing ammonia gas is the most reasonable route to metal nitrides. The infrastructure for such experiments will be available to us in the last quarter of FY2011. Other light elements, in particular Si and P, are being examined as well. In this quarter, work on this effort has focused on known ternary compounds with both Si and P, as well as the search for new transition metal phosphides in selected chemical systems.

Status of FY 2011 Milestones

Analysis of (Hf/Zr)-(Co/Fe) systems: on schedule. Crystal growths initiated in Hf-Co and Zr-Co systems. Dissolution and reaction of elements demonstrated, although target compositions not yet stabilized.

Interstitial nitrogen in iron compounds: on schedule. Commercial iron nitride powder was investigated as a nitrogen source for intermetallic sub-nitride synthesis. Other light atoms are being investigated in parallel.

Communications/Visits/Travel

None to report for this Quarter

Problems Encountered

Technical difficulties with the melt-spinner has hindered progress on Hf-Co and related materials. Diagnostics and repairs have been initiated.

Publications/Presentations/Awards

None to report for this Quarter.

References

None

Agreement 11752: Materials for High Efficiency Engines

Govindarajan Muralidharan, Rick Battiste, and Bruce G. Bunting
Oak Ridge National Laboratory

Objective/Scope

To identify and catalog the materials operating conditions in the HCCI engines and utilize computational design concepts to develop advanced materials for such applications. The primary emphasis of this project is the identification and development of advanced

Technical Highlights

In this quarter, work was continued on Ni-based alloys for valve applications. As reported earlier, using thermodynamic modeling, microstructure evaluation, and mechanical property evaluation, high temperature fatigue was identified as a property of critical interest in Ni-based alloy valve materials for the next generation automotive engines. In order to develop relationships between the microstructures of the alloys and their mechanical properties, high-temperature fatigue property data were obtained on all down-selected alloys as a part of the project. Using the approximate correlation between the fatigue lives obtained using the rotating beam and fully reversed fatigue testing techniques several alloys with required microstructures have been identified as candidates for high temperature valve applications.

Using the microstructures of these alloys as a guide, computational thermodynamics was used to identify additional alloys with microstructure similar to the commercial alloys with desirable properties. In contrast to the commercially available alloys with Ni-contents in the range of 50 wt. % to 60 wt. %, the Ni-content in these alloys ranges from about 30 wt. % to 45 wt. % with the potential to achieve comparable properties. This implies that the alloys will be of lower cost but comparable mechanical properties.

In the previous quarter two alloys (HCCI-9, HCCI-16) (see figure 1) have been down-selected and prepared in the form of large plates. In this quarter, rotating beam tests have been carried out on HCCI-9, HCCI-16, and HCCI-35. Results from the fatigue tests show that at a stress level of 35 Ksi, the baseline alloy performs better than the newly developed alloys. However, at a stress level of 25 Ksi, HCCI-9 and HCCI-16 performed significantly better than the baseline alloy. Work will continue this quarter on further development of new alloys.

Status of FY 2011 Milestones

Work is on target to meet the following milestones:

- Present progress detailing results on the high temperature tensile testing and fatigue testing of new ORNL-developed alloys at the Annual Merit Review
- Identify a path for the further development of exhaust valve alloys (7/2011)

Communications/Visits/Travel

Problems Encountered

Difficulties were encountered in testing alloys that were of diameter less than 0.5”. Testing smaller diameter alloys was abandoned due to lack of rigidity of specimens.

Publications/Presentations/Awards

None at this time

References

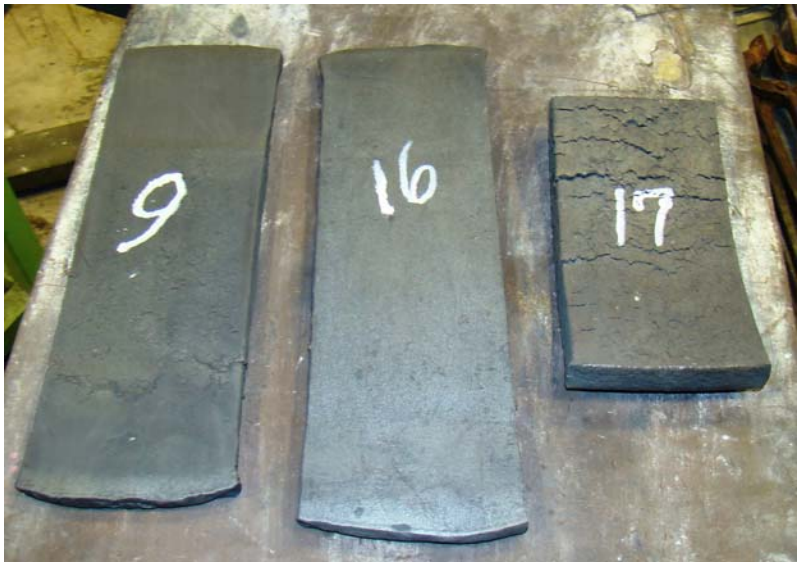

Figure 1. Two Large Heats of Alloys Were Cast (HCCI-9, HCCI-16) and Successfully Fabricated into Plates For Specimen Machining

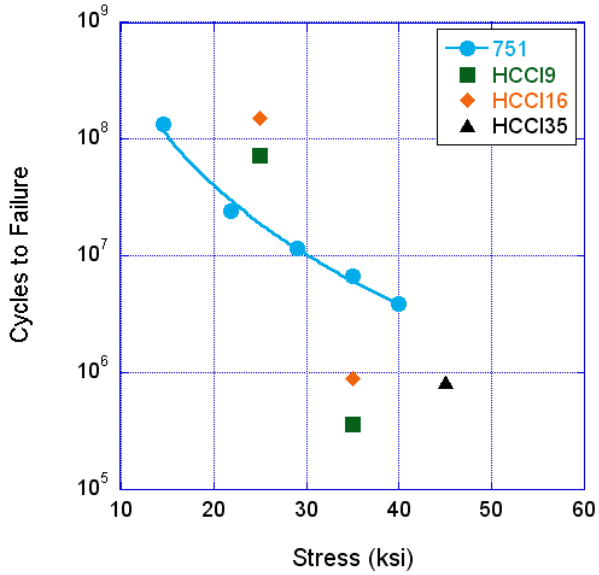

Figure 2. Rotating beam fatigue results from baseline alloy 751 and several newly developed alloys HCCI-9, HCCI-16, and HCCI-35.

Agreement 13329: Design Optimization of Piezoceramic Multilayer Actuators for Heavy Duty Diesel Engine Fuel Injectors

H.-T. Lin, H. Wang, K. Zhang, A. A. Wereszczak
Oak Ridge National Laboratory
and
R. Stafford and D. Memering
Cummins Inc.

Objective/Scope

This project seeks to enable confident utilization of piezo stack actuator in fuel injectors for heavy vehicle diesel engines. The use of such actuators in diesel fuel injectors has the potential to reduce injector response time, provide greater precision and control of the fuel injection event, and lessen energy consumption. Though piezoelectric function is the obvious primary function of lead zirconate titanate (PZT) ceramic stacks for fuel injectors, their mechanical reliability can be a performance and life limiter because PZT is brittle, lacks high strength, and is susceptible to fatigue. However, that brittleness, relatively low strength, and fatigue susceptibility can be overcome with the use of appropriate probabilistic design methods.

Technical Highlights

1. Mechanical Testing and Characterization of PZT Ceramics

1.1 Single-layer PZT testing

Ball-on-ring setup was used to test single-layer PZT materials. The ball-on-ring testing is a part of proposed research tasks to generate the input data for reliability design of PZT stack in targeted electric field, temperature, and humidity environments.

As reported in the last quarterly report, an oil bath/container has been designed and fabricated to include electronic fluid (i.e., FC-40) as a working environment of ball-on-ring setup. The inclusion of FC-40 allows the application of high electric field to the PZT specimens when mechanical test is being conducted due to the enabled control of the partial charge. Results on the mechanical strength of KCI at the electric field as high as 2 times the coercive field revealed no significant difference from those obtained without electric field. The effects of both FC-40 and the electric field on PZT materials were then confirmed.

At the same time, the focus of Cummins EPCOS piezo stack demands more data on tape-cast PZT. The supply of single-layer PZT specimens by the manufacturer has not been shown to be feasible. As a result, alternative approaches are being pursued in

this project for PZT mechanical strength characterization. These approaches include the use of commercial PSI PZT as alternative material. Note that PZT 5A4E and 5H4E are all soft PZT, especially the PZT 5A4E has the properties equivalent to those used in the target stack, and were tested and characterized in the beginning stage of this project. Tape-cast PZT sheets are commercially available and the technique of specimen preparation from the sheets has been well developed. The other approach is to use 10-layer short PZT stacks or PZT plates. The mentioned PZT plates are not readily available from the supplier. Chemical dissolving of the supplied PZT stack was proven to be effective for the previous PZT stacks (7mm x 7mm x 30mm) offering a sound base for the current PZT stacks. Thus, PSI PZT specimens from earlier purchases were proposed to be used in this task; in addition, new purchase has been made and specimens have been prepared using the same procedure.

Ball-on-ring tests under OC (open circuit) were conducted on PSI 5H4E specimens that had a nominal size of 10mm x 10mm x 0.267mm, and the part of results are presented in Fig. 1. It was stated in the previous report that the biaxial flexure strength of PZT from sheet 1 was relative higher than that from sheet 3 and that this was attributed to the difference in fracture mode.[1] Based on fractographic analysis, the failure in sheet 1 was dominated by transgranular fractures, while in sheet 3 it was by intergranular fractures. The transgranular fractures involved more energy dissipation and thus delivered a higher fracture toughness. It is interested to note that the aged 5H4E specimens based on sheet 4 seemingly did not demonstrate any degradation in mechanical strength as compared to the fresh specimens from sheet 3. This comparison is reasonable because both sheet 3 and sheet 4 came from the same purchase order. The fracture mode of sheet 3 and 4 is now under investigation by using SEM-based fractography. The insensitivity of mechanical strength of PSI 5H4E on aging is distinctly different from the results on PSI 5A4E.[2]

1.2 10-layer PZT testing

As mentioned above, mechanical testing on 10-layer PZT plates has been proposed as an alternative approach to characterizing EPCOS PZT in this project. The work to remove the PZT plates from the newly supplied PZT stacks has been initiated by using Dynasol 750. However, the chemical solution has not been very effective in dissolving the bonding agent of the new stacks supplied by Cummins. This is probably in part because of the improved high temperature epoxy bonding and/or the larger dimensions used in the new stack's cross-section. Nevertheless, an effective chemical solution is needed in order to pursue along this avenue. Searching for the mentioned chemical solution has been addressed and discussed with Cummins. In addition, ORNL is also exploring other method, especially via the means of mechanical splitting.

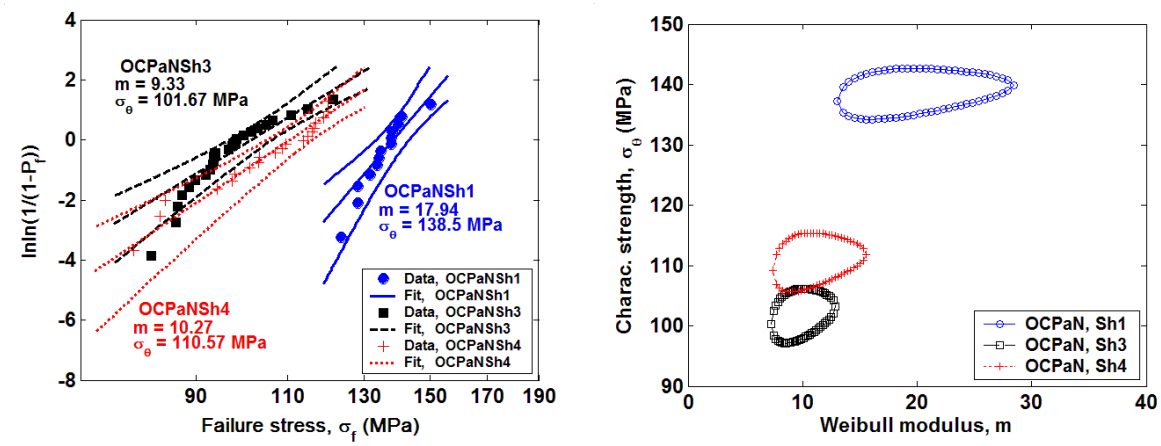

(a) (b)

Fig. 1 (a) Weibull plots of mechanical strength data and (b) 95% confidence ratio rings for PSI 5H4E specimens under open circle (OC). Data points were obtained using ball-on-ring setup with steel loading ball diameter 2 mm (sheet 1 and 3) and 6.35 mm (sheet 4). A steel support ring of 7.44 mm was used in all the tests. Displacement rate of the cross head was 0.001 mm/s. Sheet 3 and 4 were purchased at the same time but different from sheet 1. The specimens from sheet 1 and 3 were tested in fresh state, whilst those from sheet 4 were aged more than 54 months.

1.3 PZT humidity mechanical testing

PZT stack in a fuel injection system is subjected to high humidity, in addition to high temperature and high electric field during operation. Under extreme case, the water is attracted by the electric field and ionized by electrolysis.[3] Ag^+ ions move as Ag(OH) from the anode through cracks, voids, and defects to the cathode where they are recovered into metallic silver. This could cause the silver dendrite to form and grow from the anode to the cathode resulting in the reduced resistance and ultimately dielectric breakdown. Therefore, the mechanical reliability of PZT layers in humidity environment needs to be carefully addressed because the oxides such as alumina, zirconia, and PZT indeed showed a sharp drop of K_{IC} in a certain level of RH (relative humidity).[4] Moisture plays an important role in the degradation of PZT materials. The approach proposed in this task includes: (1) pre-treat the PZT specimens in a controlled humidity chamber for a specific period of time; (2) transfer the treated specimen into a chamber that hosts the ball-on-ring setup, and perform the mechanical test.

A specimen chamber has been purchased recently and potassium bromide was ordered for the chemical solution preparation. This setup is able to provide an 80% R.H. environment at room temperature so that the PZT specimen can be treated under the desired condition in a specified period of time.

2. Piezoelectric Testing and Characterization of PZT Stacks

When the PZT stacks are set and working at an optimized condition, the fatigue prevails and usually sustains during the lifetime of service. In the extreme case, the fatigue directly results in failure in various modes. ORNL has performed extensive fatigue tests during the course of this project, and the work covered various scenarios,[5,6] including PZT-5H, PZT-5A, unipolar and bipolar electrical driving, PZT single layer and multilayer stacks.

The research plan for testing piezo stacks has been exchanged and discussed in details with Cummins during the recent conference call. Expected works in association with Cummins would include, (1) test short stacks or single-layer PZT in piezodilatometer using electric cycling; (2) test PZT stacks using fatigue test facility with mechanical preload. These proposed tests will help the design and control to identify the fatigue trend of PZT materials and PZT stacks beyond 10,000 cycles. The current ORNL test facility would also need to be modified or reconfigured to accommodate the various requirements from Cummins.

Status of FY 2010 Milestones

Measure and compare reliability of competing commercially available piezoactuators under consideration for use in diesel fuel injectors, *on schedule*.

Communications/Visits/Travel

1. Communications with Cummins, Inc. were made on CRADA update.
2. An oral presentation on this project will be presented at DOE Merit Review, May 11, 2011.

Publications/Presentations/Awards

1. Wang, H., Matsunaga, T., Lin, H.-T., and Mottern, A. M., Piezoelectric and dielectric performance of poled lead zirconate titanate in electric cyclic fatigue, in review.
2. Wang, H., Matsunaga, T., and Lin, H.-T., Effects of temperature and electric field on mechanical strength of single-layer PZT plate, in preparation.

References

1. Wang, H. and Wereszczak, A. A., Effects of electric field on the biaxial strength of poled PZT, Ceram. Eng. Sci. Proc., 28 (8), 2007, 57-67.
2. Wang, H., Lin, H.-T., and Wereszczak, A. A., Strength properties of poled PZT subjected to biaxial flexural loading in high electric field, J. Am. Ceram. Soc., 93 (9), 2010, 2843-2849.

3. P. Pertsch, S. Richter, D. Kopsch, N. Kramer, J. Pogodzik, and E. Hennig, Reliability of piezoelectric multilayer actuators, ACTUATOR 2006 Conference, Bremen, Germany, Jun14-16, 2006
4. N. J. van der Laag, L. J. M. G. Dortmans, and G. de With, Influence of relative humidity on mechanical properties of alumina, PZT and Zirconia, Key Engineering Materials, 206-213, 751-754 (2001).
5. Wang, H., Wereszczak, A. A., and Lin, H.-T., Fatigue response of a PZT multilayer actuator under high-field electric cycling with mechanical preload, J. Appl. Phys., 105 (1), 2009, 014112.
6. Wang, H., Cooper, T. A., Lin, H.-T., and Wereszczak, A. A., Fatigue responses of PZT stacks under semi-bipolar electric cycling with mechanical preload, J. Appl. Phys., 108 (8), 2010, 084107.

Agreement 15050: Evaluation of Materials via ACERT Engine

Michael Kass, Brian Kaul, Norberto Domingo, Robert M. Wagner,
K. Dean Edwards, H. T. Lin and D. Ray Johnson
Oak Ridge National Laboratory

Objective/Scope

This project is focused on improving the performance, emissions and efficiency of heavy-duty diesel engines through the application of materials enabled technologies. The range of material systems is comprehensive and includes 1) improved structural materials to accommodate higher cylinder pressures and temperatures, 2) improved durability and corrosion resistance, 3) low inertial components to improve transient response, 4) improved emissions control performance, and 5) waste heat recovery systems.

To date a dynamometer engine research cell was constructed for use with heavy-duty engines. A 2004 C15 ACERT Caterpillar engine was provided by the Caterpillar materials research staff for materials-based efficiency evaluations. The engine was instrumented for combustion and thermal assessment. During FY09, the engine performance was assessed according to thermal availability and opportunities for efficiency improvements were identified. ORNL also completed a WFO with Caterpillar to evaluate a novel turbo concept. The novel turbo design was found to deliver efficiency and thermal improvements over the baseline turbo design. At the conclusion of these efforts, several materials-related efficiency improvement concepts were discussed and debated. The decision was to consider advanced alloy utilization in key components and emission control technologies.

Progress This Quarter

Several projects were proposed for FY 2011; they include valve material durability and high temperature exhaust manifold performance. Caterpillar has provided ORNL with a set of valves that composed of a novel high temperature nickel-based alloy for improved durability. The valves durability study was started on January 27 of 2011. For this study, the engine is to be run for 200 hours according to the transient cycle shown in Fig. 1. The transient cycle consists of several high load settings and idle engine operation. In addition the valve lash was measured for the untested condition and after 25 and 50 hours of engine operation. The lash results are shown in Fig. 2 and indicate that the valve recession for those composed of the nickel-based alloy are identical to the lash measurements obtained for the standard valves. Upon completion of the 200 hour run, the valves will be removed and the valve performance will be evaluated by a team of materials researchers from ORNL and Caterpillar.

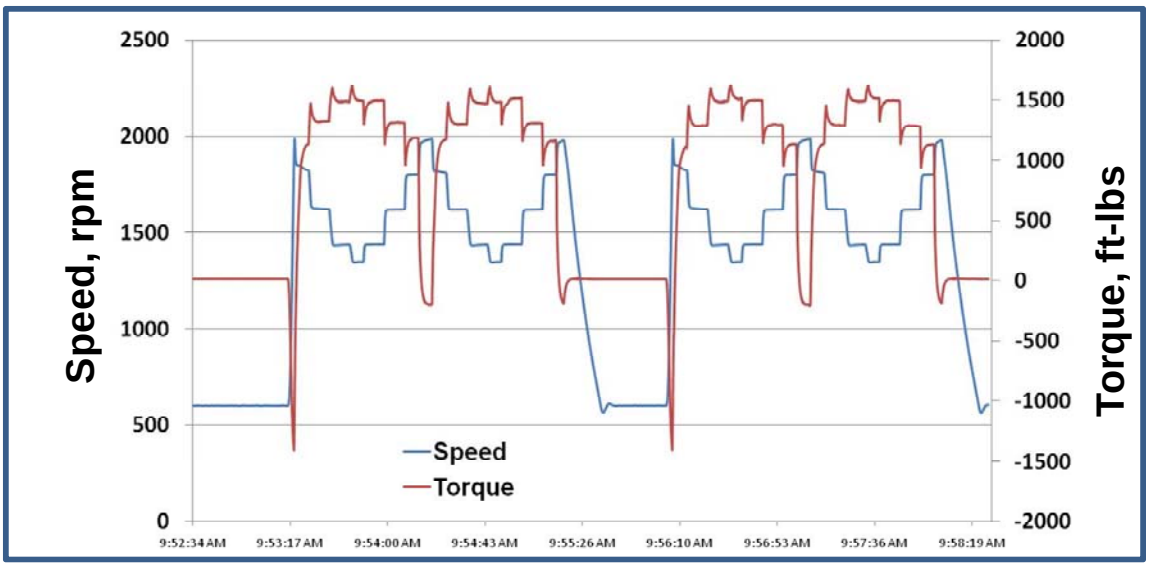

Fig. 1. Schematic of transient test cycles used to evaluate valve performance.

Table 1. Valve lash measurements for each valve as a function of operating time.

Cylinder Number	Valve Material	Valve Number	Time of Exposure		
			0 hours	30 hours	50 hours
1	Ni alloy	1	0.030	0.028	0.028
		3	0.030	0.028	0.028
2	Standard	5	0.030	0.028	0.028
		7	0.030	0.028	0.028
3	Ni alloy	9	0.030	0.028	0.028
		11	0.030	0.028	0.028
4	Standard	13	0.030	0.028	0.027
		15	0.030	0.028	0.027
5	Ni alloy	17	0.030	0.029	0.028
		19	0.030	0.028	0.028
6	Standard	21	0.030	0.028	0.027
		23	0.030	0.028	0.027

Publications/Presentations/Awards

None reported during this quarterly period.

Plans for Next Reporting Period

- Complete engine evaluation for novel valve materials.

Agreement 16303: Materials for High Pressure Fuel Injection Systems

Peter J. Blau and Amit Shyam
Oak Ridge National Laboratory
and
Nan Yang
Caterpillar Corporation

Objective/Scope

The objective of this Cooperative Research and Development Agreement (CRADA) between UT-Battelle, LLC and Caterpillar Corporation is to investigate and understand the performance limitations of current alloy steels for high-pressure diesel engine fuel injector nozzles.

During recent decades, fuel efficient, low-emissions diesel engine designs for heavy trucks have relied upon increasing fuel injection pressures to optimize combustion characteristics. Precise fuel metering is required. This key functional requirement has raised concerns over the ability of spray holes to be machined to sufficiently close tolerances to provide desired spray patterns and for the materials of construction to withstand hundreds of millions of high-pressure pulses without succumbing to fatigue damage. The data and analyses obtained in the course of this three-year effort are expected to provide vital information for designers and material selectors for high-performance fuel systems for energy-efficient diesel engines.

A three-pronged approach has been developed. It involves: (1) characterization of current fuel injector hole geometry and alloy metallurgy, (2) measuring the residual stress in nozzle tips near spray holes, and (3) development and use of specialized fatigue test methods to address the special requirements of the next generation of high-pressure fuel injectors.

Technical Highlights

*Fatigue testing on fuel injector materials***.** A dual-pronged approach for characterizing the effects of small holes on the fatigue life and crack growth mechanisms of fuel injector alloys is being implemented. The first approach is to conduct axial-fatigue tests on smooth specimens without holes. A summary of the smooth specimen stress life behavior of a tool steel having a composition used in high-pressure fuel injectors, and with two different heat treatments, is summarized in Figure 1. These data demonstrate that heat treatment can have a significant effect on the fatigue life of fuel injector tip materials. Initial results show as much as a 20% reduction in life for one heat treatment compared with another. The same approach has been implemented to discern the crack initiation mechanisms that operate over a range of applied loads. Some failures were seen to initiate from surface flaws and others subsurface flaws.

The second approach is to conduct a fracture mechanics characterization of cracks initiating and propagating from artificial defects machined on both axial and bending specimens. The artificial defects were fabricated by electro-discharge machining (EDM) to approximate dimensions of a spray hole in a fuel injector tip.

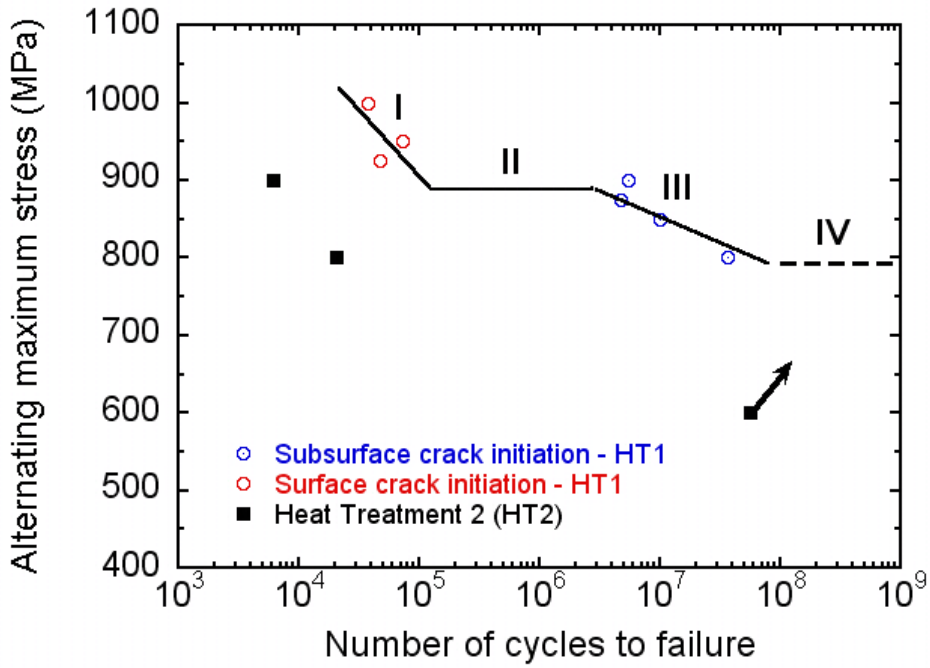

Figure 1. The effect of heat treatment on SN-behavior of a tool steel alloy. A heat treatment alone can modify the endurance limit of the alloy by more than 200 MPa.

An artificial defect with fatigue cracks propagating from it is shown in Figure 2. Tests like this have been run for more than ten million cycles. To better understand the range in material properties at low and high applied loads, fatigue crack propagation curves were determined for specimens such as this under various experimental conditions.

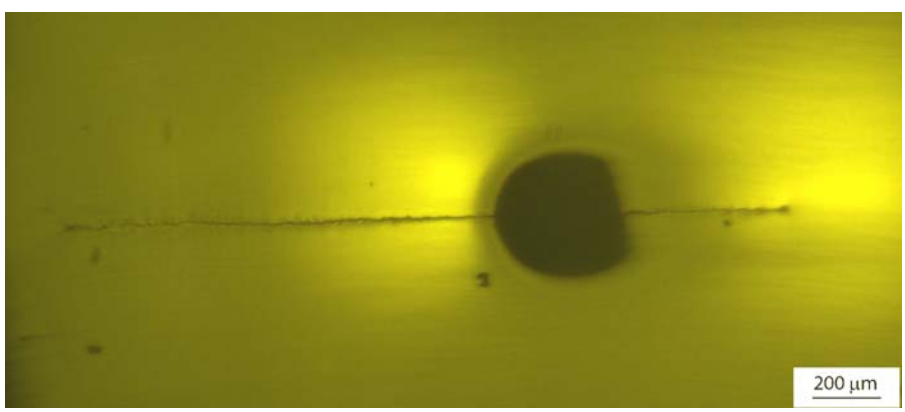

Figure 2: Image of a fatigue crack that is emanating from an EDM notch at a maximum stress of 800 MPa and R = -1. The testing conditions including the geometry of the EDM hole simulate the loading conditions observed in a diesel fuel injector during service.

In addition to the work presented in Figure 2, fatigue crack propagation thresholds were determined for the small cracks by modifying the procedure available for long fatigue

cracks in the standard ASTM E647-05. The generated experimental information can be applied to implement a damage tolerant design for fuel injector materials.

Plans for the Next Quarter

1) Continue to investigate the axial fatigue life and fatigue crack propagation behavior for fuel injector steels containing controlled flaws.
2) Begin final experiments to investigate the effects of diesel fuel environment on smooth specimen axial fatigue failures.

Status of FY 2011 Milestones

1) Complete baseline fatigue tests on smooth specimens without artificial flaws. **(3/31/2011) Status:** *Complete*.
2) Complete fatigue tests on steel specimens containing EDM holes in the presence of diesel fuel and prepare a final report. **(9/30/2011) Status**: *Not yet started*.

Communications/Visits/Travel

Dr. Nan Yang, the new Caterpillar principal investigator, visited ORNL on March 21, 2011, to make plans for the remainder of this project and to discuss possible follow-on efforts. The visit also included a tour of laboratory where the fatigue tests are being done.

Problems Encountered

Delays in the availability and characterization of specimens have compressed the schedule to the point where fatigue tests cannot be completed by the end of June as was planned. A no-cost-time extension to move the end date of the CRADA from mid-July to September has been requested.

Publications/Presentations/Awards

P. J. Blau, J. Y. Howe, D. Coffey, R. M. Trejo, E. Kenik, B. C. Jolly, and N. Wang, "Microstructure, Morphology, and Nanomechanical Properties Near Fine Holes Produced by Electro-Discharge Machining," in preparation for the journal *Materials Engineering and Performance* (2011).

A. Shyam, P. Blau, T. Jordon and N. Yang, "The fatigue behavior of high performance steels," in preparation for ASM Materials Science and Technology Conference and Expo, Columbus, OH (October 16-20, 2011).

References

None

Agreement 16304: Materials for Advanced Engine Valve Train

P.J. Maziasz and N.D. Evans
Oak Ridge National Laboratory
and
M.D. Veliz
Caterpillar, Inc.

Objective/Scope

This is an ORNL CRADA project with Caterpillar, NFE-07-00995 and DOE OVT Agreement 16304, which was extended for 24 months last year, and is now scheduled to end in Dec., 2012. This CRADA project focused on addressing the wear and failure modes of current on-highway heavy-duty diesel exhaust valves and seats, and then evaluated changes in valve-seat design or advanced alloy selection. Advanced alloy selection will enable higher temperature capability, as well as better performance and durability. Requests for more detailed information on this project should be directed to Caterpillar, Inc.

Highlights

Caterpillar, Inc.

Caterpillar completed very high temperature wear-rig tests of new prototype exhaust valves made from upgrade Ni-based superalloys with higher temperature capability than standard 31V superalloy valves. Additional testing included variations in seat-alloys in combination with the new upgraded Ni-based superalloys.

ORNL

ORNL has completed some of the initial creep-rupture testing at 816 - 871°C of specimens from the same upgrade Ni-based superalloys used to make new prototype exhaust valves for testing at Caterpillar. Both Ni-based alloys 1 and 2 show higher temperature capability and performance compared to the standard 31V superalloy.

Technical Progress, 2nd Quarter, FY2011

Background

This OVT Agreement 16304 is an ongoing ORNL CRADA project with Caterpillar, NFE-07-00995, which will last for about 5.5 years, after last year's new 24 month extension. This CRADA project has addressed the wear and failure modes found for current on-highway heavy-duty diesel exhaust valves and seats. It then identified changes in valve-seat advanced alloys that will enable higher temperature capability, as well as better performance and durability. The need for such upgraded valve-seat alloys is driven by the demand to meet new emissions and fuel economy goals, which continue to push diesel exhaust component temperature higher. The CRADA was extended for 24 more months due to outstanding technical progress and success at mitigating wear between exhaust valves and seat-inserts at above 800°C. Requests for more detailed information on this project should be directed to Caterpillar, Inc.

Approach

Caterpillar provides the baseline wear and mechanical behavior characteristics of engine-exposed standard valves and seats, and provides exposure of similar components from simulation-rig testing at Caterpillar. ORNL provides more in-depth characterization and microcharacterization of those valves and seats, and provides knowledge and understanding of the full range of commercially available heat-resistant alloys, to select those most suitable for upgraded valve performance. ORNL and Caterpillar have developed an understanding of the underlying degradation mechanisms, which is the technical basis for selecting and testing alternate valve and seat alloys with upgraded performance and temperature capability. Caterpillar and ORNL are working with Caterpillar's various component and materials suppliers, to enable prototype production of upgraded exhaust valves and seats for evaluation in Caterpillar's wear-test rig, and parallel testing and characterization of the same advanced alloys at ORNL.

Technical Progress – Caterpillar, Inc.

Caterpillar previously obtained new prototype exhaust valves from a major valve supplier, forged from two heats of advanced, alternate Ni-based superalloys with upgraded high-temperature properties. These new upgrade Ni-based superalloys have improved performance and higher temperature capability compared to the standard 31V alloy. Last quarter, Caterpillar completed some of the initial testing and evaluation of Ni-based 1 and 2 alloys in the wear-test rigs with the standard Co-based seat alloys, and this quarter included testing with alternate seat alloys as well. A summary of all the testing done to date at 850°C is shown in Figure 1. Ni-based alloy 1 had 2.7 times better seat-valve wear life at 850°C than the standard production 31V valve alloy, and is better than Ni-based alloy 2. Similar data on testing of the various valve and seat alloys at 740°C will be summarized next quarter. Additional wear-rig testing of Ni-based alloys 1 and 2 is planned, and Caterpillar is also obtaining more new prototype valves of these Ni-based 1 and 2 alloys engine-testing. Caterpillar has sent some of the new alloy valves to ORNL for characterization.

Technical Progress – ORNL

ORNL previously obtained new forged valves and various mechanical properties test specimens from one of Caterpillar's exhaust valve suppliers of two alternate alloys, Ni-based 1 and 2. Both Ni-based alloys have more temperature capability and performance than the standard 31V alloy. Previously it was shown that both alternate Ni-based alloys have higher tensile yield strength (YS) of 90-100 ksi when tested at 816°C (1500°F) in the age-hardened condition with no service, compared to the YS of about 70 ksi for the standard 31V alloy. The initial creep-rupture tests run at 816°C and 30 ksi (207 MPa) were completed last quarter, and data shown previously indicated that Ni-based alloy 1 had much better creep-resistance than the standard 31V alloy. Ni-based 1 alloy was also several times better than Ni-based 2 alloy. This quarter, the initial creep-rupture testing done at 871°C and 15 ksi (104 MPa) was completed, and is

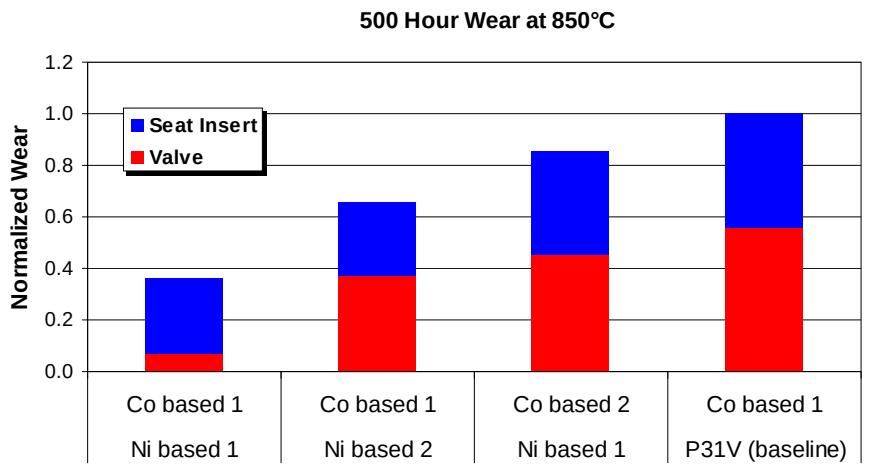

Figure 1 – Summary of Caterpillar wear-rig testing data, showing the separate wear of seat and valve components, and the cumulative wear (valve and seat-insert), for standard 31V alloy exhaust valves and new Ni-based 1 and 2 superalloy prototype valves at 850°C in air. The Ni-based 1 alloy shows showed a 2.7x improvement in total wear life with the standard Co-based seat alloy (1) relative to the standard 31V valve alloy.

shown in Figure 2. Again, both Ni-based alloys 1 and 2 have much better creep-resistance than standard 31V, and Ni-based alloy 1 has significantly better creep-resistance than Ni-based alloy 2. The differences in creep-rupture life among the various alloys is much larger than their differences in YS. Creep-testing of these various alloys at 816°C at a lower stress continued this quarter.

Tensile/creep specimens of these alloys were also being aged at 800 and 850°C for 5000h, and that was completed this quarter. Tensile and creep-rupture testing of these aged specimens will begin next quarter. Microcharacterization of the rig-tested valves from Caterpillar continued this quarter.

Communications/Visits/Travel

Detailed team communications between ORNL and Caterpillar occur regularly in multi-party conference calls. Caterpillar has extended team discussions to include their commercial seat-insert supplier as well as one of their exhaust valve suppliers.

Status of Milestones (ORNL for DOE)

Milestone for Caterpillar rig-testing of prototype valves and seats of new advanced alloys (Nov., 2010) was completed last quarter. Milestone for completing the initial creep-rupture testing of new Ni-based superalloys with upgraded performance at ORNL (Feb., 2011) was mainly satisfied this quarter.

Publications/Presentations/Awards

None

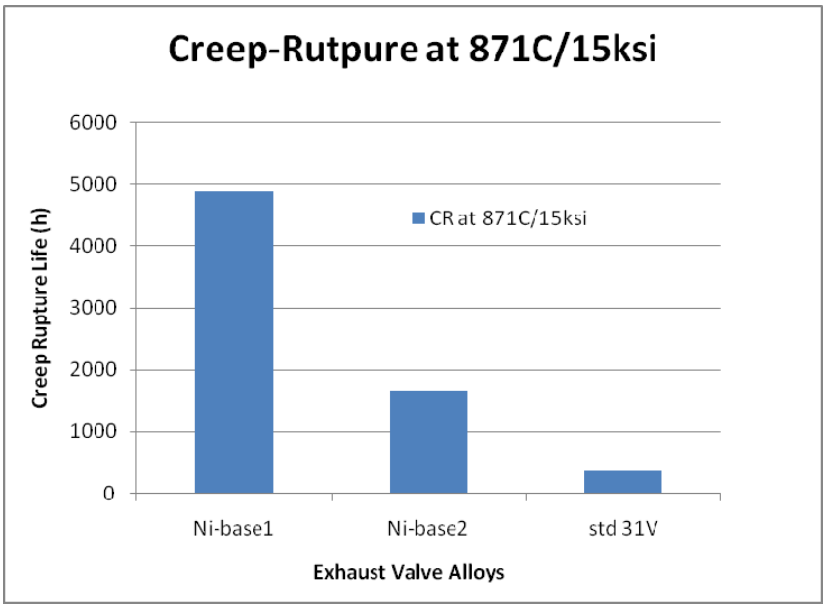

Figure 2 – Creep-rupture life of the standard 31V exhaust valve alloy and two alternate upgrade Ni-based superalloys, for creep tests run in air at 871°C (1600°F) and 15 ksi (104 MPa).

Agreement 17257: Materials for Advanced Turbocharger Designs

P.J. Maziasz and A. Shyam
Oak Ridge National Laboratory
and
K. Pattabiraman
Honeywell Turbo Technologies

Objective/Scope

This ORNL CRADA project with Honeywell, NFE-08-01671 (DOE/EERE/OVT Agreement 17257) began last year, and is scheduled to last for about 3 years. This CRADA project addresses the limitations of lifetime or use-temperature for the various components (casing, wheel, shaft, bearings) of both the turbine and compressor parts of the turbocharger system. As exhaust temperatures increase, to provide higher engine efficiency and lower emissions, turbocharger component temperatures also increase, so the need for more heat-resistant materials must be addressed. Requests for more detailed information on this CRADA project should be directed to Honeywell, Inc.

Highlights

Neutron-scattering experiments at ORNL to measure residual-stresses in critical locations of wheel/shaft assemblies and turbine housings began this quarter. Long-term creep-testing of cast CF8C-Plus austenitic stainless steel at 600°C continued this quarter. Assessments of the oxidation-resistance of CF8C-Plus steel relative to other exhaust component cast-irons and steels continued this quarter.

Technical Progress, 2nd Quarter, FY2011

Background

This CRADA project began last year, and will extend for 3 years, and covers several different tasks. The first task was to assess and prioritize the various components that need or would most benefit from materials upgrades to increase temperature capability and performance, as well as durability and reliability. The next tasks examine current performance and degradation modes of wheel/shaft assemblies for turbines and compressors, housings for turbines and compressors, and bearings. These tasks may then obtain and test new materials with upgraded performance, and provide the results to Honeywell for designing advanced turbocharger systems, or for manufacturing of new prototype components for testing and evaluation.

Approach

This CRADA project began early last year. This project is comprised of six tasks, which will span the next 36 month period. Activity began with ORNL and Honeywell discussing the priority of the various turbocharger components for materials upgrades. A turbocharger system includes the hot (turbine) end, driven by exhaust gas from the engine, a cold (compressor) end to increase air pressure into the combustion changer, and a transition region that connects these two ends. The turbine and compressor wheels are connected to a common shaft, supported by bearings. For the first task, the turbine wheel-shaft assembly was chosen as the first component for consideration, with analysis focused on residual stresses near the weld-joint of the Ni-based superalloy wheel to the steel shaft, which can upset balance during service. Another task of this new CRADA project continues previous work between ORNL and Honeywell on testing of the new CF8C-Plus cast stainless steel as a significant performance upgrade for the turbine housings relative to standard SiMo or Ni-resist cast irons. This CRADA project for turbine housings covers a broad range of other high temperature properties, including creep and fatigue strength, and includes turbine housing applications for passenger vehicle gasoline engines.

Technical Progress

For Task 1, Honeywell identified neutron-scattering experiments to measure residual stresses in welded wheel/shaft assemblies as one of their highest priority items. For Task 2, these experiments were defined, and the proposal needed to obtain neutron scattering time at the HFIR Residual Stress User- Facility, was approved last quarter. Figure 1 shows a typical Honeywell wheel/shaft assembly. Preliminary neutron-scattering experiments for diffraction analysis of the steel shaft began last quarter, and additional experiments on wheel/shaft assemblies with variations in processing parameters began and continued this quarter. The Neutron Residual Stress Facility 2 (NRSF2) at HFIR is shown in Figure 2.

For Task 3, ORNL continued long-term creep-rupture tests at 600°C of the cast CF8C-Plus stainless steel this quarter, with one test at a higher stress rupturing after 7,300 h, and another test at a lower stress continuing beyond about 8500 h. ORNL completed aging of as-cast CF8C-Plus tensile/creep specimens at 700 and 800°C to 2500 h this quarter, and mechanical properties testing of the aged specimens will begin next quarter. ORNL also identified additional longer-term creep-rupture testing at 700-800°C that will add to previous creep-rupture data on CF8C-Plus and HK30-Nb steels, which will begin next quarter. Honeywell is addressing the next steps necessary to commercially produce some prototype turbocharger housing using CF8C-Plus steel for certain turbocharger models. This is the next step required so that new housings can be evaluated and tested on engines.

Figure 1 – Honeywell turbocharger wheel/shaft assembly used for neutron-scattering experiments, consisting of a Ni-based superalloy turbine wheel welded to a steel shaft.

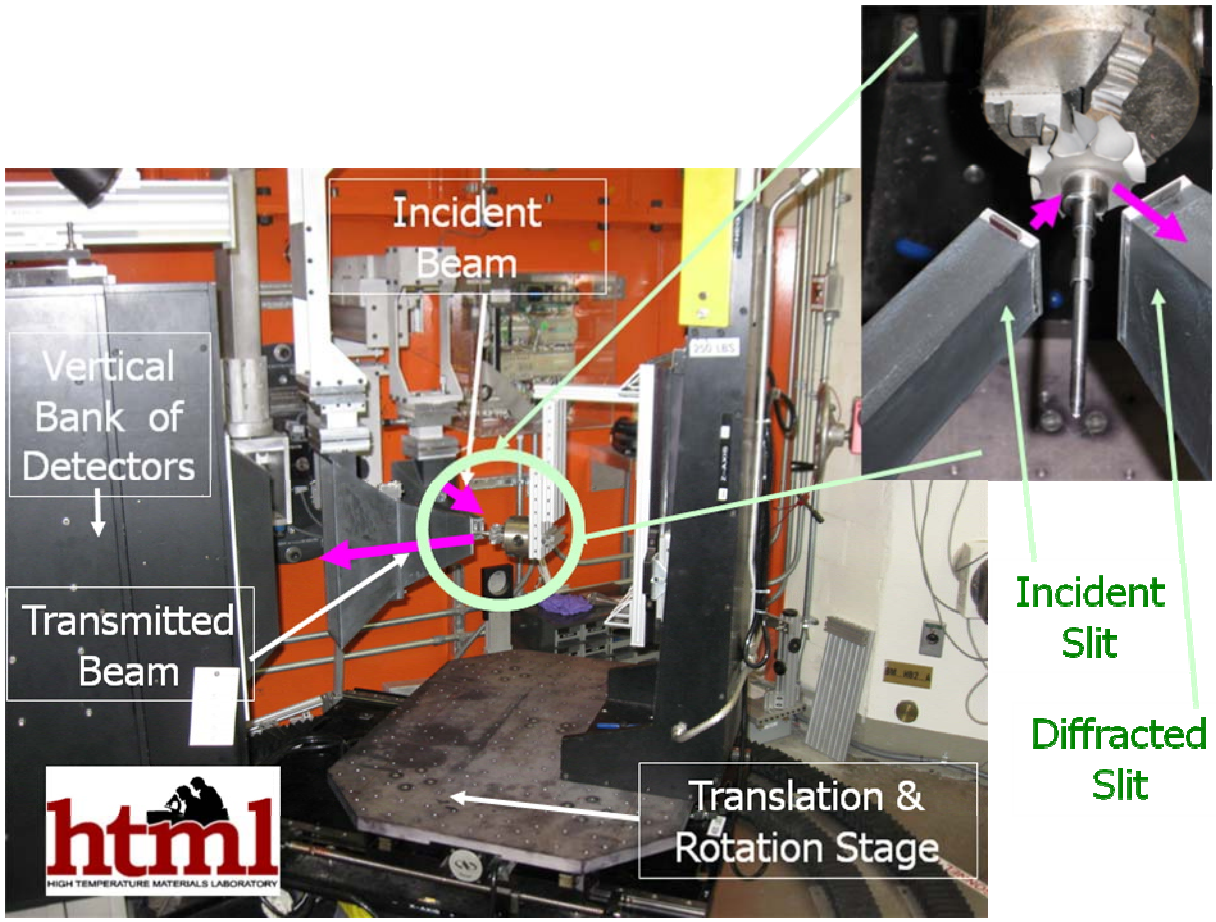

Figure 2 – The Neutron Residual-Stress Facility 2 (NRSF2) at the HFIR beam port, with the specific neutron scattering geometry used for the Honeywell turbocharger wheel/shaft assembly shown in the magnified inset. The NRSF2 is part of the High Temperature Materials Laboratory (HTML) at ORNL, and these experiments were run by Tom Watkins and Cam Hubbard of the Residual Stress User Center.

Oxidation experiments to assess the oxidation-resistance of cast CF8C-Plus relative to several cast-irons used for conventional turbochargers and exhaust system components began last quarter, and continued this quarter.

Communications/Visits/Travel

Periodic conference calls are held between ORNL and Honeywell Turbo Technologies, and email communications help to coordinate the work.

Status of Milestones (ORNL for DOE)

The FY2011 milestone to begin initial neutron-scattering residual-stress measurements on wheel/shaft assemblies for turbochargers (12/2011) was achieved, and the other milestones for FY2011 are on-track.

Publications/Presentations/Awards

None

Agreement 17894: NDE for ACERT™ Engine Components

J. G. Sun and Mark Veliz*
Argonne National Laboratory
***Caterpillar Inc.**
Technical Center

Objective/Scope

Applications of advanced materials in diesel engines may enhance combustion and reduce parasitic and thermal losses, thereby improving engine efficiency. Engine components developed from advanced materials, however, require rigorous assessment to assure their reliability and durability in more stringent operating conditions. The objective of this work is to develop and assess various nondestructive evaluation (NDE) methods for characterization of advanced engine components in a CAT heavy-duty ACERT™ experimental engine at ORNL. NDE technologies established at ANL, including optical scanning, infrared thermal imaging, ultrasonics, and x-ray computed tomography (CT), will be further developed for detection of volumetric, planar, and other types of flaws that may limit the performance of these components. NDE development will be focused on achieving higher spatial resolution and detection sensitivity. Current efforts are directed in applications of optical methods for valvetrain components, x-ray and ultrasonic for joinings, and thermal imaging for thermal barrier coatings (TBC).

Technical Highlights

Work during this period (January-March 2011) focused on synchrotron x-ray CT characterization of friction-welded joints between TiAl turbine wheel and Ti-6Al-4V shaft, a TiAl turbine wheel cast, and a power module for compact hybrid vehicles.

1. Synchrotron X-Ray CT Characterization of Friction-Welded Joints

During this period we continued x-ray CT investigation of friction-welded joint between a TiAl wheel and a Ti-6Al-4V shaft in diesel-engine turbochargers received from Dr. Nan Yang of Caterpillar. Although the joining process is becoming mature [Yang et al, 2005], NDE inspection is required for all joints to ensure component reliability. Joint inspection in industry is mostly based on ultrasonic techniques. Synchrotron x-ray CT, on the other hand, has superior inspection capability and accuracy so is pursued to assist the development of industrial inspection techniques. Figure 1 shows a photograph of the high-energy synchrotron x-ray CT facility at the advanced photon source (APS) at ANL. The synchrotron x-ray source has high peak energy to penetrate thick metals. The cross section of the x-ray beam is rectangular, >2” wide and ~0.7mm high. The intensity of transmitted x-ray is detected by a scintillation plate, which is imaged by a CCD camera. By using the scintillator/camera configuration, a high spatial resolution (40 to <10 µm) can be obtained.

Figure 2a shows a friction-welded joint. The flash material pressed out during the welding process was not removed from this joint. The ultrasonic NDE inspection at Caterpillar detected some flaws. However, it could not identify the flaw types as well as the exact location and size of the flaws within the sample. The synchrotron x-ray inspection scanned a region of 24.5mm axial length around the joint, at a pixel size of

43.7µm. Figure 2b shows a cross-section CT slice, which is located within the TiAl cast at ~1.5 mm below the joint plane. The CT slice image shows clearly the geometry and the length of axial cracks inside the TiAl cast. All cross-section slices acquired from this sample, total of 560 slices, were then composed together into a 3D volume data and sliced in the axial direction. Figure 3 is an axial CT slice at the location marked in Fig. 2b. In this image, the geometry and length of cracks along the welding interface and inside the TiAl casting are clearly visualized.

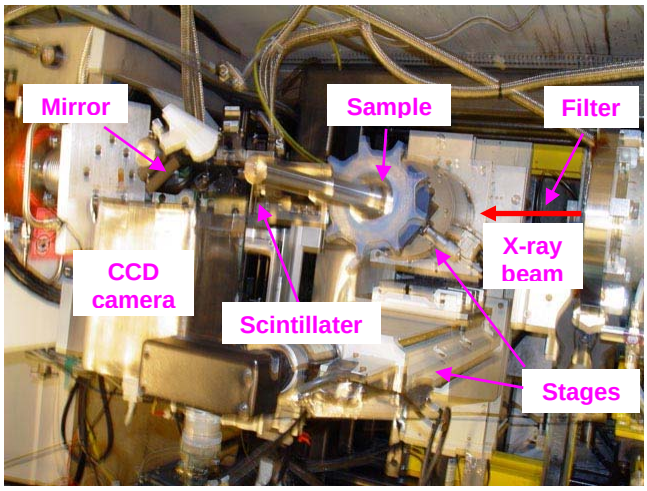

Fig. 1. Top view of synchrotron x-ray CT facility at ANL's Advanced Phone Source (APS).

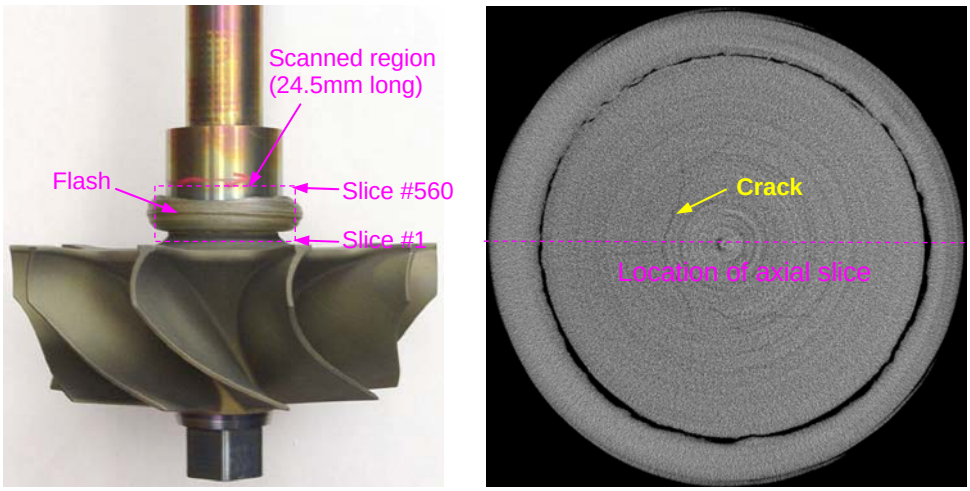

(a) (b)

Fig. 2. (a) Friction-welded turbocharger component and (b) a typical cross-section CT slice.

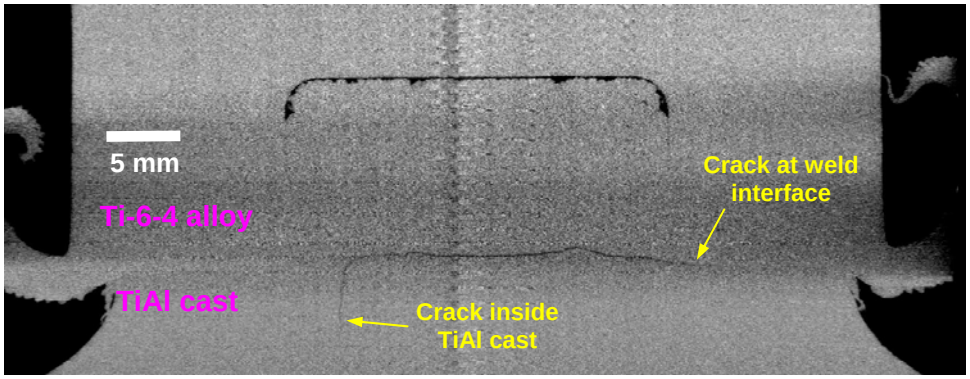

Fig. 3. Reconstructed axial CT slice image for the sample in Fig. 2a.

2. Synchrotron X-Ray CT Characterization of TiAl Turbine-Wheel Casts

Titanium aluminide (TiAl) has been identified as a promising material for rotating and oscillating components in gasoline and diesel engines. Its application can lead to decreased fuel consumption, reduced noise and pollution, and enhanced lifetime and reliability. Two components that benefit most from the use of TiAl were identified to be the turbocharger wheel and exhaust valve [Baur et al., 2003]. Development of TiAl turbine wheel has been very challenging because of its complex shape and high-strength requirement. These wheels are made from casting followed by hot-isostatic pressing (HIPing) to close the internal porosity. Cast TiAl wheels may contain various types of defects. One type of defects is micro and macro porosities in the cast core region (see Fig. 4). Although these porosities may be closed by the HIPing process, they may lead to strength reduction of geometry distortion. Destructive methods are normally used to examine the core porosities. Another type of defects is subsurface voids that open to the surface. These voids cannot be closed by the HIPing process, and may limit the wheel strength if they are located near the blade base. Although fluorescence penetration inspection (FPI) may detect such open voids, it cannot determine void size and geometry that are important to predict the wheel performance. These two types of casting defects are investigated using the synchrotron x-ray CT method.

Figure 4 shows a TiAl turbine-wheel cast used in this synchrotron x-ray CT study. The original intention was to scan the cast core (~2” diameter) along the entire axial length of the blades. However, this was found impossible because the large dimension of the blades significantly limited the x-ray transmission (x-ray beam passes wheel horizontally during scan) so a much longer imaging time was required. As a result, only a 14.5-mm-long axial region marked in Fig. 4 was scanned, for a total of 380 cross-sectional slices (each at 38.1µm thick). Figure 5 shows two cross-sectional slices: Slice #1 is at the elevation with thicker core and Slice #380 with thinner core. It is seen that some line artifacts are presents within the images. These lines are induced because most of the blades are outside the width of the CCD camera’s field of view. The artifacts are more intense in Slice #1 where imaged material is thicker (so low signal to noise ratio). However, they in general should not affect the identification of voids within the casting. Nevertheless, the large volume of CT data is still a challenge for identification of small voids near the level of pixel (voxel) size. It is desirable to find or develop 3D image analysis tools to enhance and automatically detect such small defects.

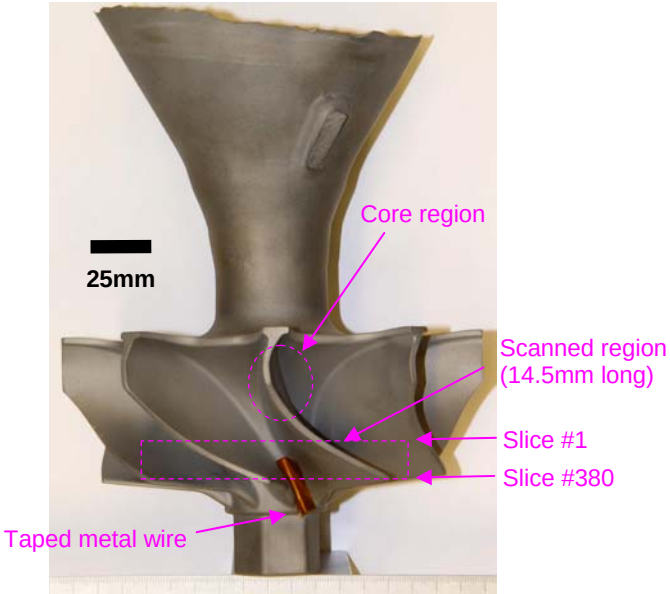

Fig. 4. A TiAl turbine-wheel cast used in synchrotron x-ray CT inspection.

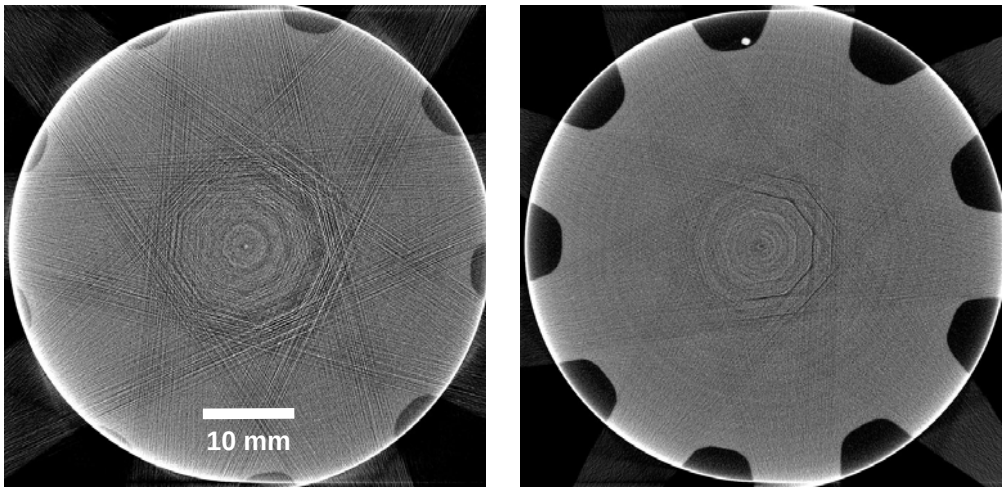

Slice #1 Slice #380

Fig. 5. Typical x-ray CT slices at locations of the TiAl cast shown in Fig. 4.

It should be noted that experimental procedure and setup may also affect data quality. This is especially critical to synchrotron tests because only limited test time is usually available. Figure 6 shows a cross-section CT slice of a shaft section. Because the shaft has uniform material, a uniform shaft density is expected in the CT image. However, both ring artifact and gross density variation are introduced due to improper test procedure. Such problems have now been resolved and a more robust and accurate test procedure has been established.

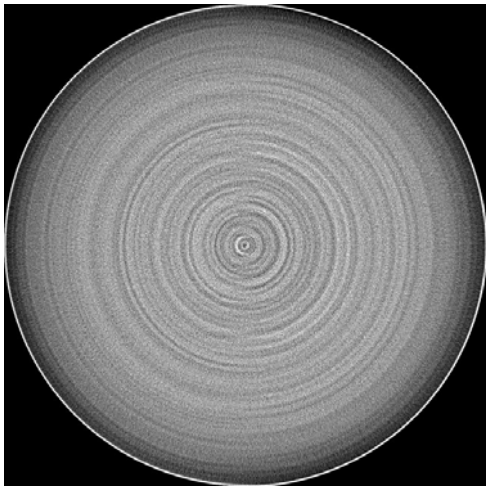

Fig. 6. A poorly reconstructed cross-sectional CT slice from a shaft section.

3. Synchrotron X-Ray CT Characterization of Power Module

A new generation of power control unit (PCU) was developed for compact-size hybrid vehicles [Nozawa, et al., 2009]. The PCU features size reduction, light weight, and high efficiency. Among the improvements includes a direct cooling structure for the power module that greatly improves the cooling efficiency. The structure consists of a punched-hole plate between the insulating substrate and the cold plate to reduce the thermal stress (see Fig. 7a). Therefore, the bonding of the punched plate is important to the power module performance. In this period, a power module (Fig. 7b) received from Dr. A. Wereszczak of ORNL was examined by synchrotron x-ray CT. Typical plane and cross-sectional CT slices for the punched plate are shown in Fig. 7c. It is apparent that the CT data can be used to determine detailed hole geometry as well as any change from its use.

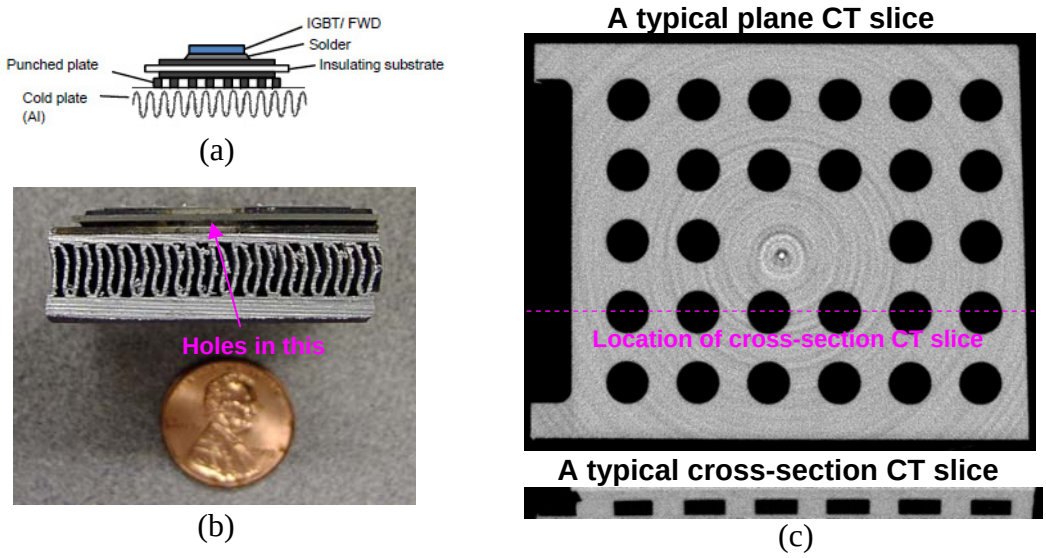

Fig. 7. Power module (a) schematic [Nozawa, et al., 2009], (b) sample, and (c) typical plane and cross-section CT slices of punched layer.

4. High-Resolution Imaging of Thermal Barrier Coatings by Thermal Tomography
No activity for this task during this period.

Status of FY 2010 Milestones
Current ANL milestones are on schedule.

Communications/Visits/Travel
J. G. Sun attended the 35th International Conference and Exposition on Advanced Ceramics and Composites, Daytona Beach, FL, January 23-28, 2011.

J.G. Sun plans to present an invited talk "NDE of composite materials" at the Composite Workshop organized by United Technologies Research Center, East Hartford, CT, May 8, 2011.

J.G. Sun plans to attend the DOE Vehicle Technologies Program Annual Merit Review Meeting at Washington, DC, May 9-13, 2011.

Problems Encountered
None this period.

Publications/Presentations/Awards
J. G. Sun presented a paper entitled "Thermal Imaging Measurement Accuracy for Thermal Properties of Thermal Barrier Coatings" and an oral talk on "Nondestructive Evaluation of Ceramic Materials by Thermal Tomography" at the 35th International Conference and Exposition on Advanced Ceramics and Composites, Daytona Beach, FL, January 23-28, 2011.

References
H. Baur, et al., "Titanium Aluminides for Automotive Applications," in Gamma Titanium Aluminides 2003, pp. 23-31, The Minerals, Metals & Materials Society, 2003.

N. Nozawa, et al., "Development of Power Control Unit for Compact-Class Vehicle" SAE International Journal of Passenger Cars - Electronic and Electrical Systems, v 2, n 1, p 376-382, 2009.

Nan Yang, et al., "Development of Titanium Alloys for Heavy-Duty Diesel Engines," Quarterly Progress Report for April through June 2005, Heavy Vehicle Propulsion Materials Program.

Agreement 18570: Engine Materials Compatibility with Alternate Fuels

S. J. Pawel
Oak Ridge National Laboratory

Objective/Scope

The purpose of this Cooperative Research and Development Agreement (CRADA) between Oak Ridge National Laboratory and USCAR is to systematically evaluate compatibility between engine materials and ethanol fuel blends over a range of temperatures consistent with engine operation. Four primary tasks are included in the overall program:

1) surface analysis of materials exposed in field and lab exposures
2) in-situ extraction of gas and/or fluid from the valve seat crevice
3) development of electrochemical testing protocols
4) laboratory corrosion exposures of coupon materials

Technical Highlights

Emphasis in the second quarter of FY11 was placed on initiation of surface analysis of engine components in/around the valve seat crevice to examine corrosion products and patterns of attack in the affected substrate. Where possible, comparisons have been made between components revealing corrosion and otherwise identical components that have not been exposed during engine operation/testing. Representative figures appear below.

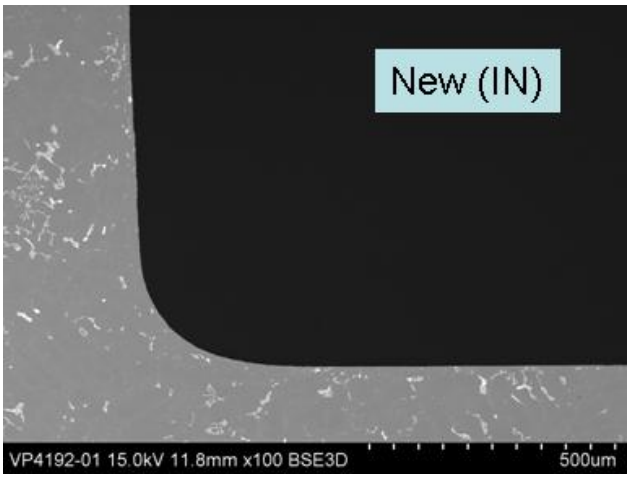

Figure 1. Representative valve seat crevice area of a new (unexposed) aluminum engine head.

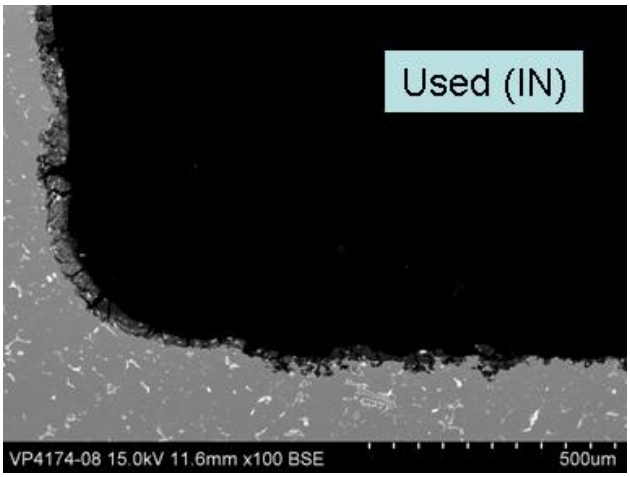

Figure 2. Representative valve seat crevice area of an aluminum engine head operated under test conditions. Surface has been substantially roughened and corrosion product has accumulated.

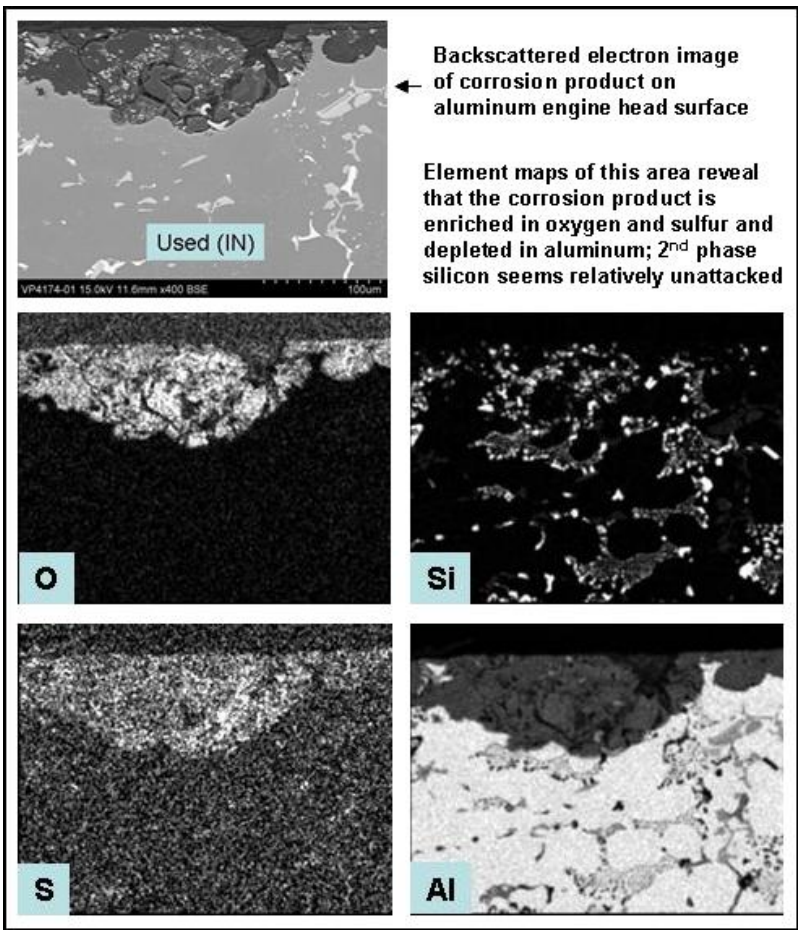

Figure 3. Element maps of representative corrosion product from the valve seat crevice. In this case, aluminum is consumed while the silicon component of the casting remains largely unattacked. Corrosion product is rich in oxygen and sulfur (products of combustion).

Other activities this quarter included finalizing the capillary sampling port design for analysis of engine fluids/gases; the first head was successfully machined and tested and five others are now being similarly processed. Testing is expected to begin in Summer 2011.

In addition, the laboratory corrosion testing has been redesigned to incorporate much smaller autoclaves (~ 50 ml rather than 1000 ml) to provide more nimble temperature/pressure assessments and more rapid evaluations. Materials and equipment are on order and data gathering is expected to recommence as soon as these orders are delivered.

Status of FY2011 Milestones

Ongoing.

Communications/Visits/Travel

Routine electronic mail and regular telephone contact (bimonthly conference calls) is being maintained between the USCAR Partners and the ORNL team. No travel occurred this quarter.

Problems Encountered

None.

Publications/Presentations/Awards

none

References

none

Agreement 18571: Materials Issues Associated with Exhaust Gas Recirculation Systems

M. J. Lance, C. S. Sluder and J. M. E. Storey
Oak Ridge National Laboratory

Objective/Scope

Provide information to industry specialists about fouling deposit properties so as to enable improved models and potential design improvements to reduce fouling and its impact on the performance of EGR (exhaust gas recirculation) coolers.

Technical Highlights

Two baseline operating conditions are being used to generate deposits that will be used for subsequent aging studies using our bench-top tube reactor. The first simulates a light-duty condition with the engine running at 2.6 Bar BMEP and a high hydrocarbon content (144 ppm) and a low inlet temperature (225°C). The second baseline condition is more relevant to heavy-duty use; 7-8 Bar BMEP, 28 ppm HC and 325°C inlet temperature. Both deposits were formed using a 1.9 L GM engine with an EGR loop, 1500 rpm, EGR flow rate of ~30 SLPM, coolant temperature of 90°C for 4 hours. Figs. 1 and 2 show cross-sections of the light-duty and the heavy-duty deposits, respectively. The density of the light-duty deposit was 0.0230 g/cm^3 and the heavy duty was 0.0133 g/cm^3. This difference may explain why the effectiveness loss for the heavy duty condition was higher since the thermal conductivity of the deposit would be lower which would prevent the gas from being cooled as effectively. In addition, the heavy-duty deposit also appeared thicker. This project will proceed by addressing both the light-duty and heavy-duty diesel communities using these two baseline conditions to better understand changes in deposit properties and microstructure while aging in gas that simulates the engine exhaust.

In addition to successfully forming deposits using our engine and tube sampling system, the bench-top reactor is now nearly assembled. The heat exchanger shown in Fig. 3 was redesigned to have a Marmon cap on its end to accept the feedgas from our mass flow controllers. The system has been initially tested and appears to work with the exception of the thermocouples which still need to be connected to our computer. Labview was purchased so as to control the system.

Finally, a second round of coolers has been requested from all nine members of our industry consortium of EGR technicians for late-stage deposit characterization. This round will focus on coolers that will represent specific applications.

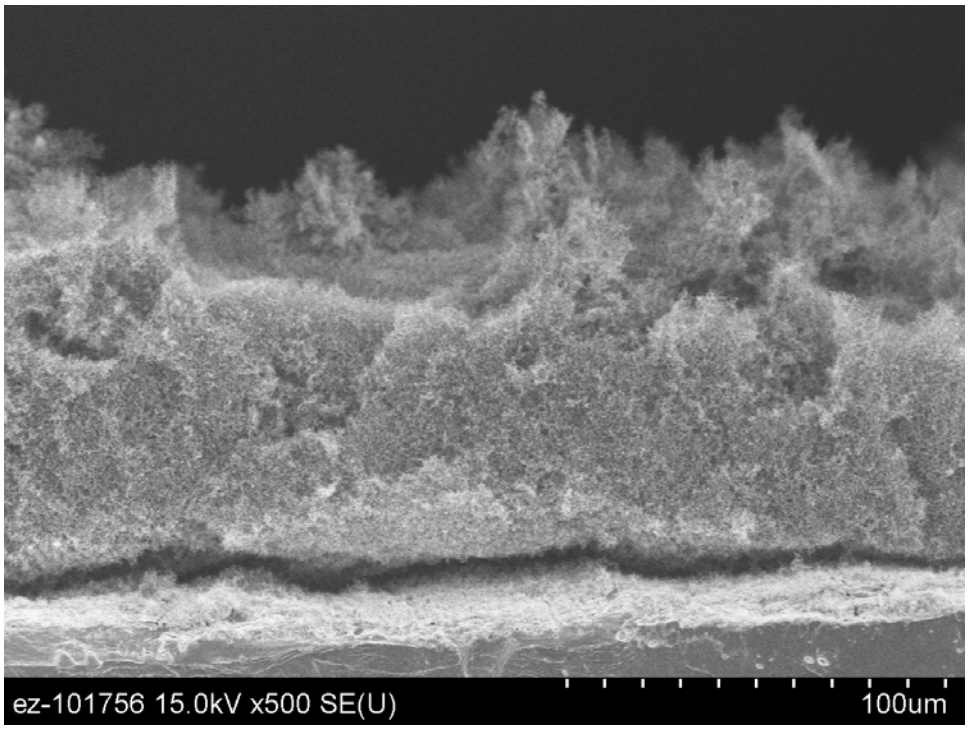

Figure 1. Deposit formed using light-duty conditions: 2.6 Bar BMEP, ~225°C inlet, 144 ppm HC, 95 ppm NO_x, 1.36 FSN.

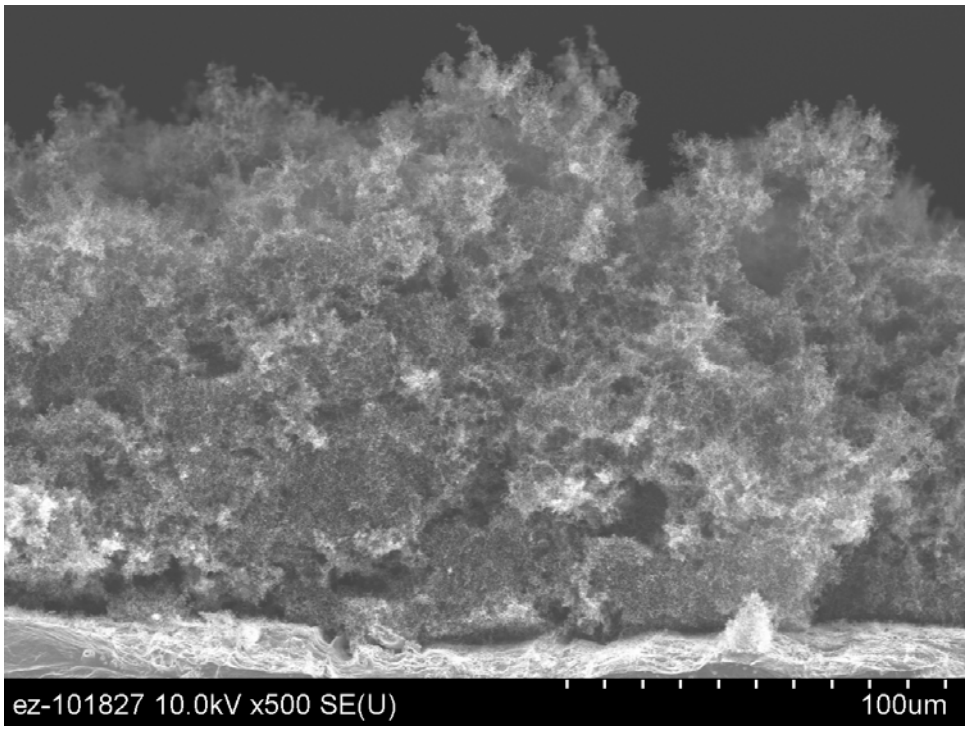

Figure 2. Deposit formed using light-duty conditions: 7-8 Bar BMEP, ~325°C inlet, 28 ppm HC 310 ppm NO_x, 0.97 FSN.

Figure 3. Heat exchanger that will be used to age deposit-loaded tubes in a controlled manner.

Status of FY2011 Milestones

1. Assemble and test sampling system for controlled deposit formation. (10/10) *On Schedule.*
2. Generate fouling deposits using an engine and sampler tube system and age them in controlled environments to investigate changes in deposit properties. (09/11) *On Schedule.*

Communications/Visits/Travel

All 10 engine companies were contacted to discuss the possibility of receiving a 2nd round of coolers for forensic analysis of the deposit.

Problems Encountered

None.

Publications/Presentations/Awards

Presentations:

- Michael J. Lance, Hassina Bilheux, C. Scott Sluder, Sophie Voisin, and John M.E. Storey "Materials Issues Associated with EGR Systems," Advanced Engine Cross-cut Team Meeting, January 13, 2011.
- Michael J. Lance, C. Scott Sluder and John M.E. Storey, "Materials Issues Associated with EGR Systems," Advanced Engine Cross-cut Team Meeting, March 17, 2011.

References

None.

Agreement 19202: Titanium Friction and Wear (Surface Engineering of Bearing Components)

Peter Blau and Dinesh Bansal
Oak Ridge National Laboratory

Objective/Scope

The energy efficiency and durability of internal combustion engines (ICEs), whether fueled by conventional or alternative fuels, benefit from the use of lightweight materials. Examples include polymer composites and alloys of aluminum, magnesium, and titanium. While such materials offer attractive efficiency gains, their use also presents technical and economic challenges. One class of ICE applications involves tribological aspects: that is, those which concern friction, wear, and lubrication. Studies in the United States, Japan, and the United Kingdom have shown that mechanical losses comprise about fifteen percent of the energy dissipation from fuel in a typical ICE, and that of those, energy losses by friction comprise about eighty percent. The two major subsystems, in terms of engine frictional losses, are the piston ring/cylinder interface and the crankshaft bearings, including those on the connecting rods. Past research at ORNL has focused on the piston ring/cylinder interface. The current project which began in FY 2010 not only addresses the connecting rod bearings, but it also demonstrates how surface engineering and coating technologies that could benefit other friction- and wear-critical applications as well.

The objective of this project is to *enable the use of strong, lightweight titanium (Ti) alloys for wear and friction-sensitive engine components like connecting rods (CRs) and crankshafts.* The goal is to identify the most promising surface engineering methods, whether commercialized or experimental, to reduce friction and wear of Ti alloys under engine-like conditions. This work compliments recent developments in Ti processing technology that is aimed at reducing raw materials cost. It utilizes the experience of ORNL tribology staff to effect changes in surface-critical properties via a variety of potential treatments and combinations of treatments. The phases of this planned three-year effort are: 1) *Friction and wear baseline screening* of multiple surface treatments and coatings for titanium using ASTM test methods to down-select leading performers for more rigorous year 2 evaluation, 2) *Design and construction of a computer-controlled, variable load bearing tester* (VLBT) to simulate the contact pressure and lubricant regime excursions experienced by connecting rod bearings, and 3) *Development of a prototype diesel engine Ti-based connecting rod concept* using surface-engineered Ti bearing surfaces.

Technical Highlights

Down-selection of candidate surface treatments is completed. As reported in FY 2010, nineteen candidate materials, including combinations of experimental and commercial coatings and surface treatments, were screened using an ASTM standard test method for reciprocating friction and wear behavior under lubricated conditions. Of those candidates, eight passed the dual criteria of (1) having friction coefficients less than 0.15 (placing them in the boundary or mixed lubrication regime). and (2) lasting for the full 400 m of sliding distance without excessive noise or vibration. These results of those screening tests were accepted for publication in *Wear* journal, and will be

reported in the next quarter at the International Conference on Wear of Materials in Philadelphia (see **Publications and Presentations**, below).

Construction of the Variable Load Bearing Test System (VLBT). Engine bearings, such as the large end bearing on diesel engine connecting rods, are attractive candidates for titanium-enabled lightweighting. Such rotating parts operate under varying pressures and lubrication regimes, which means that simple constant load and constant speed tests do not offer a realistic simulation of service. Therefore, a variable load, bearing tester (VLBT) was designed and is nearing completion at ORNL. It will enable leading candidate Ti alloy surface treatments to be evaluated under transient conditions more simulative of engines. The drivetrain build is shown in Figure 1. The programmable 3-phase drive motor is visible at the lower left. Its output shaft is coupled to a torque cell, then to specimen chucks for the rotating specimen, and finally a support bearing assembly at the upper right. A programmable load actuator forces a lever to raise the test specimen underneath the rotating rod. This first prototype VLBT is expected to be ready to begin baseline tests during the next quarter.

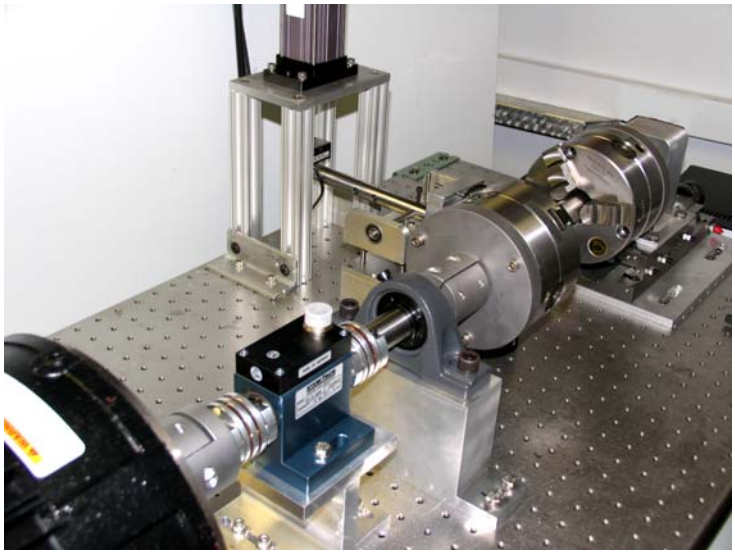

Figure 1. Drivetrain and loading system assembly for the VLBT.

Future Plans. Plans for the upcoming quarter include: (1) complete aligning and calibrating the VLBT, (2) establishing test parameters for bearing tests, (3) conducting bench-mark tests on non-treated titanium and bearing bronze in preparation for evaluating the friction and wear performance of the down-selected candidate surface treatments and coatings.

Status of Milestones

Design friction and wear testing apparatus to simulate connecting rod motions, loads, and speeds, and complete a series of baseline experiments on small test coupons of candidate titanium alloys, with and without surface treatments. **(09/10)** *Status: design completed***.**

Complete construction of a variable-load bearing test system and conduct baseline experiments to establish its operating characteristics. **(03/11)** *Status: completion delayed due to a combination of budget uncertainties and unforeseen alignment issues with the new machine.*

Complete tests of candidate coatings and multiple surface treatments using the variable-load bearing test system**. (09/11)** *Status: to begin in Quarter 3.*

Communications/Visits/Travel

None this quarter.

Problems Encountered

A delay occurred in completing the variable-load bearing test system due to problems in achieving the precise alignment needed for all the drivetrain components. Progress is now on track for a late-Spring completion of the apparatus and the beginning of baseline tests to verify the VLBT performance characteristics.

References

None

Publications and Presentations

1) D. Bansal and P. Blau, "Surface engineering to improve the durability and lubricity of Ti-6Al-4V alloy," accepted for presentation at the 2011 International Conference on Wear of Materials (April 3-7, 2011, Philadelphia), and for publication in the journal *Wear*.

Agreement 23284: Friction Reduction Through Surface Modification

Peter Blau
Oak Ridge National Laboratory

Objective/Scope

The primary objective of this new two-year effort is to improve the fuel efficiency of diesel-powered vehicles by reducing the friction of contacting surfaces by employing specific patterns of micro-scale features. These features function in two ways: (1) by increasing the lubricant film thickness to separate bearing surfaces, and (2) by trapping harmful wear debris in depressions below the contact surface. One bearing surface of particular interest is that between the piston ring and cylinder liner, although other frictional surfaces like those of bucket lifters and cam lobes are of interest as well.

The scope of this effort includes the preparation and testing of textured bearings by various surface engineering methods. During FY 2011, ORNL will select appropriate laboratory-scale friction test methods, prepare textured surfaces on bearing materials, and investigate the effects of specific patterns and feature depths on frictional characteristics as a function of sliding time. Changes in the morphology of the surfaces during the running-in stages will be correlated with the friction coefficient versus time sliding history. Understanding the running-in period is key to separating the contributions of as-finished surface roughness, wear-in, and lubricant conditioning as the bearing system approaches its longer-term, steady-state condition. A university subcontract will complement in-house efforts by developing a new masking technology to enable the surface patterning of curved surfaces like those on piston rings and cylinder bores.

Technical Highlights

Approach and initial progress. A dual approach leverages national laboratory investigations with university efforts in texture development. A subcontract, dated 3/28/2011, and titled: “Fuel Economy Improvement through Surface Technology and Weight Reduction,” was awarded to George Washington University with Prof. Stephen M. Hsu as principal investigator. This work will involve the demonstration of a novel method of texturing surfaces that enables patterns to be placed on curved surfaces like many types of engine components. That capability can help to move the surface texturing approach from a laboratory-scale effort of flat coupons to a commercially-viable technology on real parts. The weight reduction component of the subcontract work, comprises a smaller portion of the effort. It involves fundamental studies to characterize the bonding of nanofibers to polymer matrices using atomic force microscopy, and supports an existing International Energy Agency (IEA) effort to provide better research tools for developing polymer nanocomposites. Initial progress on both texturing and nanocomposites will be reported in the next quarterly report.

ORNL in-house studies of texturing effects on friction and wear are based on the recognition that friction control and durability require a systems-level approach involving: material selection, surface morphology control, lubrication regime control (film thickness to roughness ratio), lubricant entrainment, and the dynamic attributes of the contact environment (load, sliding speed, relative motion: unidirectional vs reciprocating,

temperature, debris particle effects, and more). Work during this quarter has focused on identifying and down-selecting options for surface texturing from among various possibilities such: micro-machining, etching, and dimpling. Prior studies of modulated surfaces at the Massachusetts Institute of Technology, DOE funded work on laser dimpling at the Technion (Israel), and research on dimpling of ceramics at ORNL will help in designing the initial series of in-house experiments. Metallic substrate materials (bearing steels and non-ferrous alloys) will be selected and prepared for initial study. An ASTM test method will be used to characterize patterning effects on the wear-in of bearing surfaces.

Status of FY 2011 Milestones

(a) Put in place a university subcontract to produce textured surfaces for further study. (3/31/2011). *Completed*.

(b) Complete baseline lubricated friction tests on flat laboratory test coupons and correlate their frictional running-in behavior with the features of surface textures. (9/30/2011). *In progress.*

Communications/Visits/Travel

None.

Problems Encountered

None this quarter.

Publications/Presentations/Awards

None.

References

None.

Agreement 23285: Efficiency Implications of Advanced Materials in Advanced Combustion Internal Engines

C.E.A. Finney
Oak Ridge National Laboratory

Objective/Scope

Internal combustion engines can realize efficiency gains if operated at higher cylinder pressures. One limitation on thermal efficiency gains is engine materials allowing higher cylinder operating pressures and with favorable heat-transfer characteristics. Recent developments of affordable and favorable materials, such as CF8C-Plus, offer promise in increasing overall thermal efficiency of engines. To date, their potential has not been quantified in engines or engine models.

This study will examine the efficiency effects of materials changes enabling higher operating cylinder pressures and having altered heat-transfer characteristics. An existing late-model, six-cylinder, heavy-duty diesel engine model, constructed in GT-Power, will be used to examine the effects of increased operating pressures, with both real (cylinder geometry) and effective (elevated boost pressures) higher compression ratios. Additionally, heat-transfer characteristics of the cylinder, piston and valves will be changed to mimic materials differences. Of primary interest will be changing the combustion rates to simulate various high-efficiency combustion modes currently under active industrial R&D.

Technical Highlights

Work began in March, on collecting input data and adapting an existing HD engine model for simulations of alternative combustion regimes and using advanced materials to enable these regimes. This preparatory work will continue into early Q3 and evolve into simulations and analysis to meet the project objectives.

Status of FY 2011 Milestones

This project is on track to meet its target objectives.

Communications/Visits/Travel

None.

Problems Encountered

Some input data are not readily available but are being synthesized or estimated to within reasonable ranges.

Publications/Presentations/Awards

None.

References

None.

Agreement 9130: Catalyst Characterization

Thomas Watkins, Larry Allard, Michael Lance and Harry Meyer
Oak Ridge National Laboratory

Krishna Kamasamudram and Alex Yezerets
Cummins Inc.

Objective

The objective of this effort is to produce a quantitative understanding of the process/product interdependence leading to catalyst systems with improved final product quality, resulting in diesel emission levels that meet the prevailing emission requirements.

Goals, Barriers, Relevance & Integration:

In the study area of OVT's Materials Technology subprogram, the Propulsion Materials Technology activity provides materials R&D expertise to enable advanced materials and supports the goals of several OVT subprograms.[1] Within the Advanced Combustion Engine subprogram-Combustion and Emission Control R&D activity, one primary R&D direction is to: Develop aftertreatment technologies integrated with combustion strategies for emissions compliance and minimization of an efficiency penalty. [1] Correspondingly, one *goal* is to: by 2015, improve the fuel economy of light-duty gasoline vehicles by 25 percent and of light-duty diesel vehicles by 40 percent, compared to the baseline 2009 gasoline vehicle. In support of these, this project addresses four *barriers* [1] related to the Emission Control: Lack of fundamental knowledge of advanced engine combustion regimes, improving durability and improving market perception. This project is *relevant* to this goal as the understanding of materials changes underlying the Ammonia Oxidation (AMOX) catalyst performance degradation with age increases, efficient and durable AMOX with higher NO_x conversion efficiencies can be attained. This minimizes constraints on engine-out NO_x emissions and allowing engines to be tuned for optimal fuel efficiency, cost and durability. This project also addresses three *barriers* [1] related to the Propulsion Materials Technology activity itself: Changing internal combustion engine combustion regimes, long lead times for materials commercialization and costly precious metal content. This project supports clean diesel, which increases acceptance by the public. Larger acceptance, in turn, results in larger percentages of conversion to diesel, with the resulting reduction in petroleum usage/dependency upon foreign oil. This project is *integrated* within Vehicle Technologies program as it utilizes characterization tools acquired and maintained by the High Temperature Materials Laboratory (HTML) Program.

Technical Highlights

The main focus in FY2011 is to continue to characterize the ammonia oxidation (AMOX) catalyst characterization of a practically-relevant zeolite catalyst subjected to hydrothermal aging for lifetime prediction model input. The technical approach will be as before: experimentally characterize materials, supplied by Cummins, from all stages of the catalyst's lifecycle: fresh, de-greened, aged, regenerated, on-engine and off-engine,

etc. Determinations include: crystal structure, morphology, phase distribution, particle size and surface species of catalytically active materials; seek the atomic mechanisms and chemistry of adsorption and regeneration processes. Ultimately, an understanding of the thermal and hydrothermal aging processes and other degradation mechanisms is sought throughout the lifecycle of the catalytic material. {Acronyms are used liberally through out this report and are defined in Table I.}

New samples were hydrothermally aged at 650°C in air with 7% H_2O for 0, 2, 3, 5, 10, 25, 50, 100 hours. The x-ray diffraction patterns of a zeolite-based AMOX catalyst on a cordierite honeycomb support is shows a slight narrowing of the zeolite peaks (see Figure 1), suggesting the structure is becoming more crystalline with aging time. The intensity differences seem to support this as well (except for the 50 hour sample, which could be due to loss of catalyst powder/washcoat). In addition to the zeolite phases shown, the cordierite from the honeycomb substrate is also observed. In Figure 2, the Fourier Transform-Infrared Spectrum (FT-IR) is shown for the samples aged at 0, 10 and 100 hours. FTIR spectroscopy is sensitive to the skeletal modes of the zeolite framework that occur below 1400 cm^{-1}.[2] The hydrothermal aging in 7% H_2O at 650ºC causes the zeolite structure to become more ordered as indicated by the narrower FT-IR band widths. This structural change occurs within the first 2 hours at temperature, and subsequent aging for up to 100 hours does not significantly alter the zeolite structure. X-ray Photoelectron Spectroscopy (XPS) shows similar chemistry and valence in the samples as a function of hydrothermal aging time (see inset Table). The O, Si, Al, and Fe core level spectra show that the chemical bonding (gray highlighted areas) is similar in each. XPS also indicates the Si/Fe and Si/Al atomic ratios at the surface are slightly depleted in Fe as the hydrothermal aging time increases. {Note the Si/Al change is an order of magnitude smaller than that of Si/Fe.}

The STEM results presented in Figures 5-8 were obtained using the HTML's JEOL 2200FS aberration-corrected STEM-TEM instrument that provides simultaneous bright field (BF) and high angle-annular dark-field (HA-ADF) images in scanning transmission mode. Energy-dispersive x-ray spectra and spectrum images were acquired using a Bruker-AXS silicon-drift detector (SDD) system on the microscope. At zero hours, the samples show a SiO_x particle size of 0.3 µm (see Figure 5). The elemental maps show the locations of the Al and Fe to be coincident and some segregation of Al and Fe to boundaries and surfaces of primarily SiO_x particles. The Mg remains uniformly distributed, and the Pt map shows only background levels. Figure 6A indicates that the Pt particles are 1-4 nm in size. The SiO_x particle size appears to have has grown slightly in Figure 7 after 10 hours at 650°C in air with 7% H_2O. Again the elemental maps show segregation of Al with Fe with a primary grain composition of SiOx; note that the Pt is still at background level. Figure 6B indicates that the Pt particles are an order of magnitude larger than those at 0 hours at 650°C in air with 7% H_2O. In Figure 8, the elemental maps show qualitatively that the Al and Fe segregation may have increased with time under hydrothermal treatment (100 hours at 650°C in air with 7% H_2O). Figure 6C shows the Pt particle size is unchanged after 100 hours relative to that after 10 hours at 650°C in air with 7% H_2O. Microscopy studies concerning the growth of SiO_x/zeolite grains will be pursued in the future as well as the elemental maps of the

other hydrothermally aged samples at 650°C in air with 7% H_2O (i.e., at 2, 3, 5, 25, 50 hours).

Status of FY 2011 Milestones

In the reporting period, the ORNL team continued characterizing an ammonia oxidation (AMOX) catalyst characterization of a practically-relevant zeolite catalyst subjected to hydrothermal aging for lifetime prediction model input. The milestone is on target.

Communication/Visits/Travel

Email and telephone conversations as needed.

Publications/Presentations/Awards

None.

References

1. Vehicle Technologies Program, Multi-Year Program Plan 2011-2015, Dec 2010, pp. 2.3-1, 2 ; 2.5-8.
2. Paze´ et al., J. Phys. Chem. B 1997, 101, 4740-4751.

Table I – Acronyms

AMOX	ammonia oxidation
BF	bright-field
EDS	Energy dispersive spectroscopy
HA-ADF	high-angle annular dark-field
HTML	High Temperature Materials Laboratory
NOx	Nitrogen and Oxygen containing compounds
ORNL	Oak Ridge National Laboratory
STEM	Scanning Transmission Electron Microscopy
XPS	X-ray photoelectron spectroscopy
XRD	X-Ray Diffraction

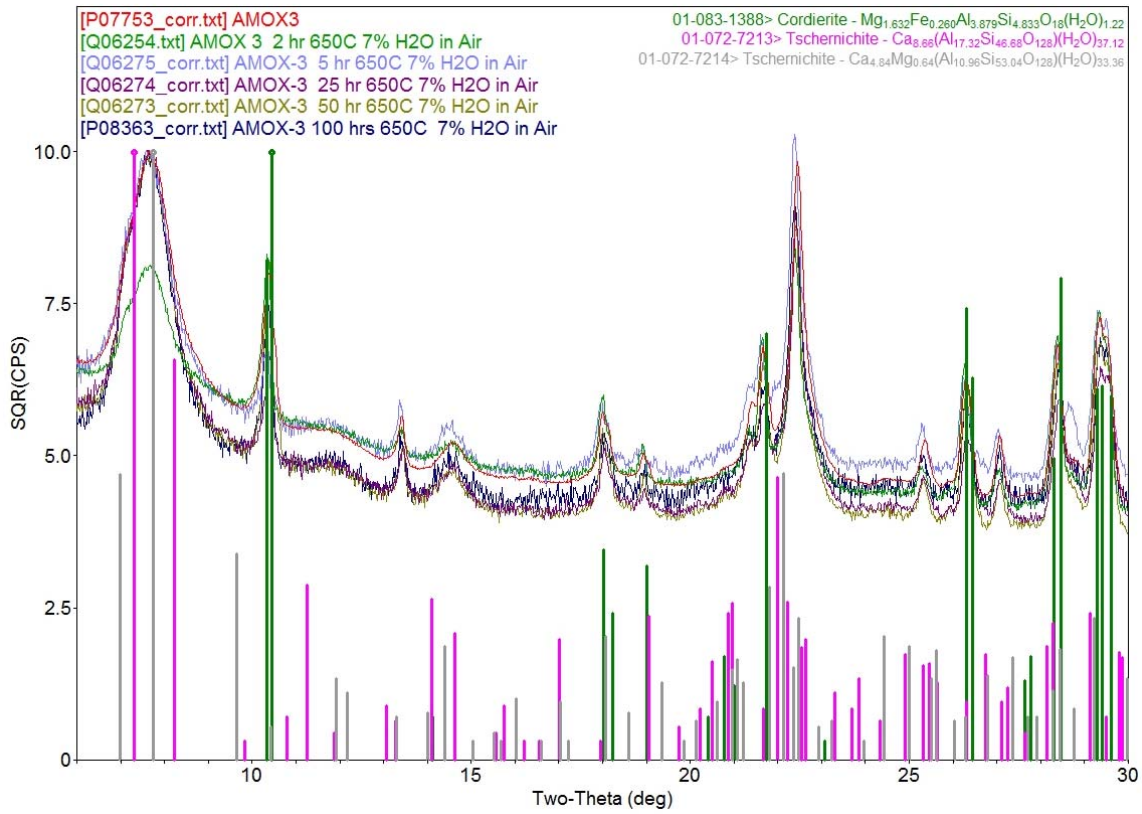

Figure 1 - The x-ray diffraction patterns of an AMOX catalyst as a function of time at 650°C in air with 7% H_2O.

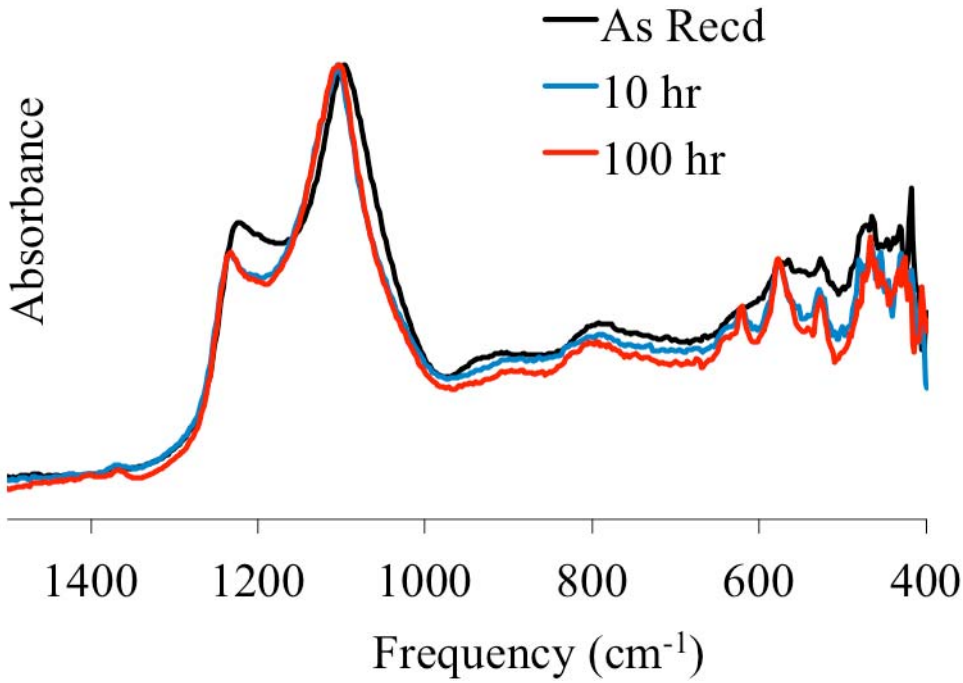

Figure 2 – The FTIR spectrum showing the absorbance as a function of frequency as a function of time at 650°C in air with 7% H_2O.

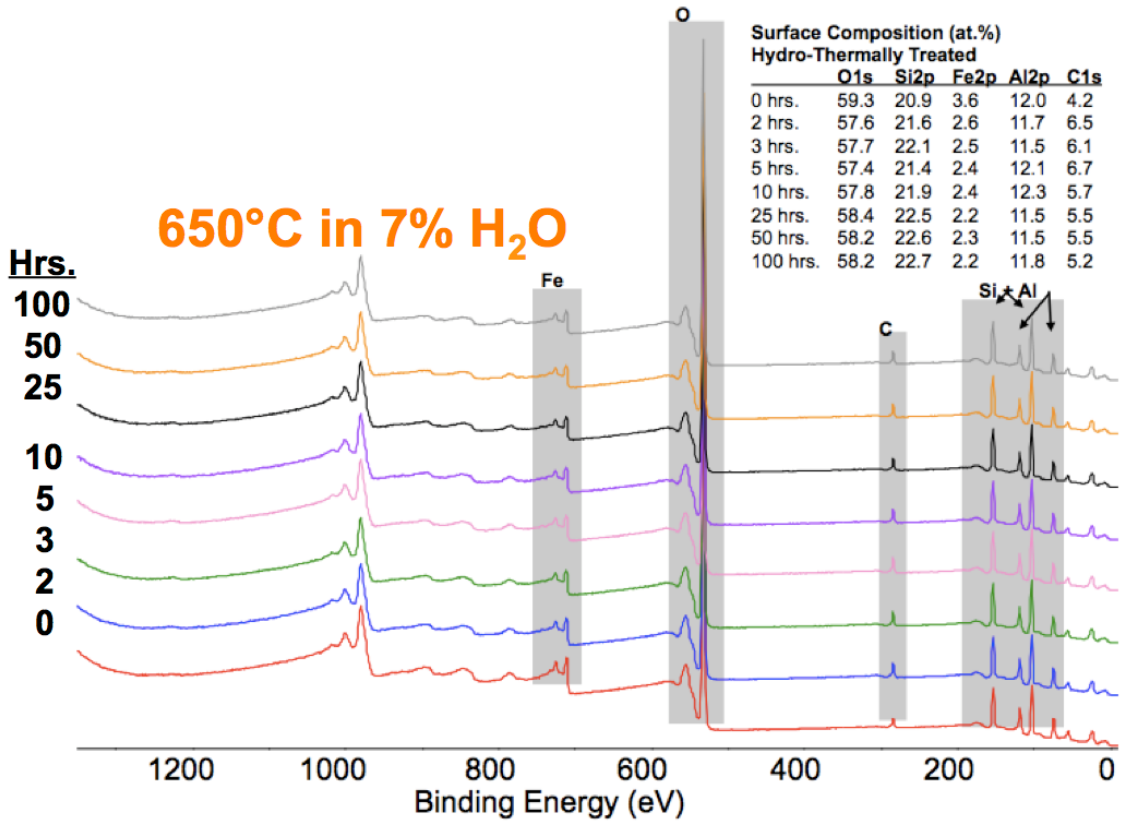

Surface Composition (at.%)
Hydro-Thermally Treated

	O1s	Si2p	Fe2p	Al2p	C1s
0 hrs.	59.3	20.9	3.6	12.0	4.2
2 hrs.	57.6	21.6	2.6	11.7	6.5
3 hrs.	57.7	22.1	2.5	11.5	6.1
5 hrs.	57.4	21.4	2.4	12.1	6.7
10 hrs.	57.8	21.9	2.4	12.3	5.7
25 hrs.	58.4	22.5	2.2	11.5	5.5
50 hrs.	58.2	22.6	2.3	11.5	5.5
100 hrs.	58.2	22.7	2.2	11.8	5.2

Figure 3 - The intensity (arb. units) as a function of binding energy as a function of time at 650°C in air with 7% H_2O.

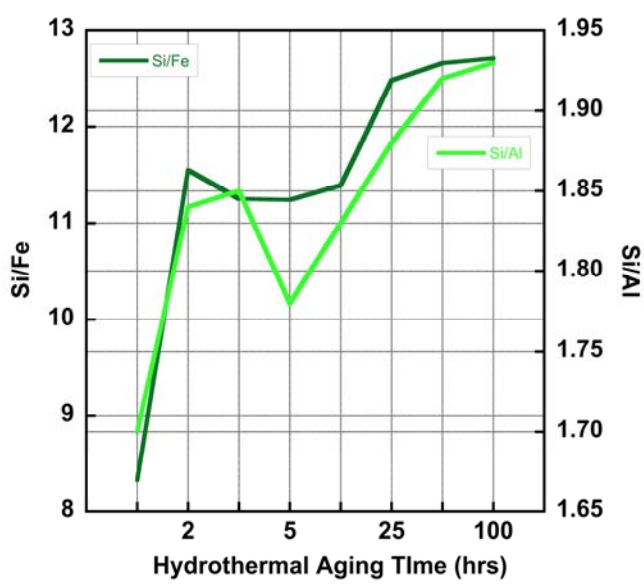

Figure 4 The atomic ratios of Si/Fe and Si/Al as a function of time at 650°C in air with 7% H_2O.

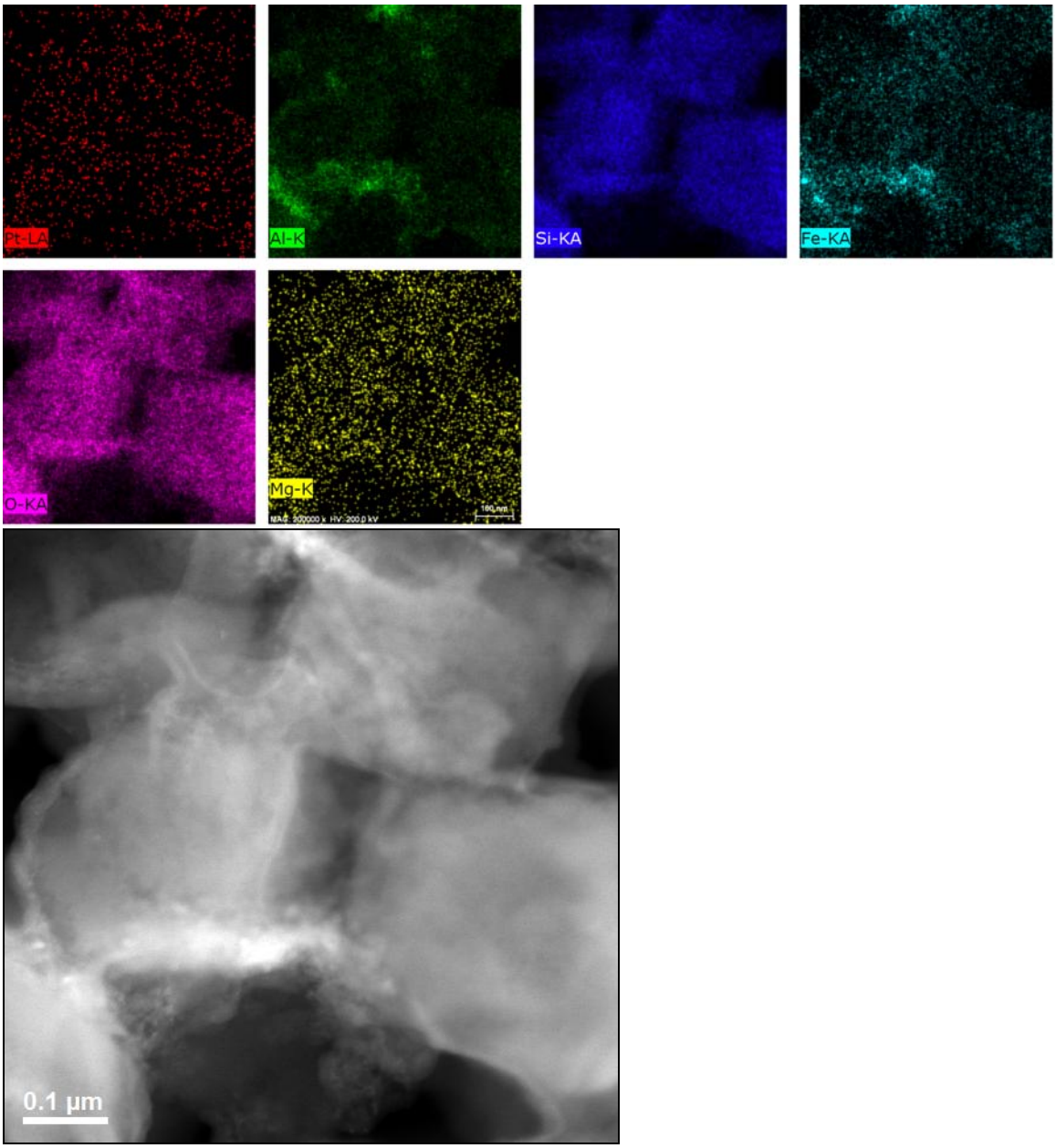

Figure 5 – The elemental maps (top) of the region shown in the dark field image (bottom) after 0 hours at 650°C in air with 7% H_2O.

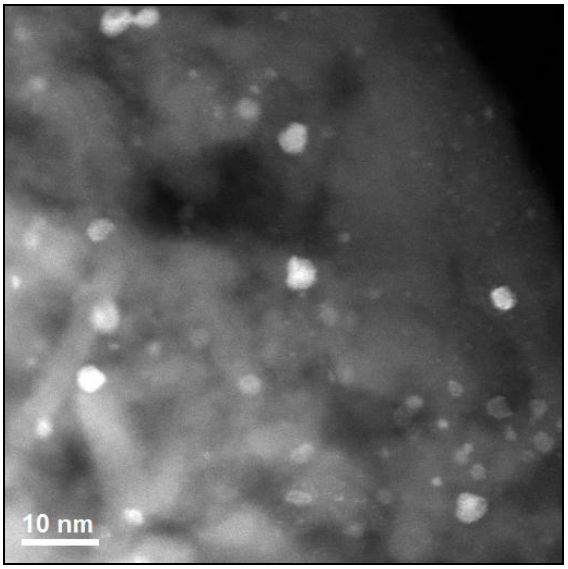

A.

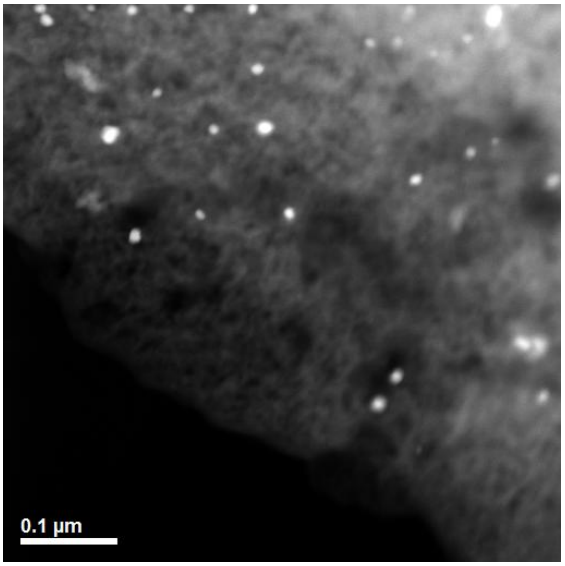

B.

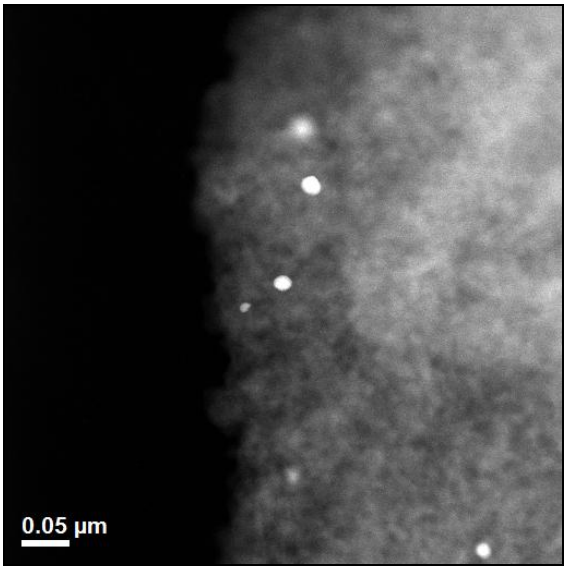

C.

Figure 6 – A.) The HA-ADF image showing nominal Pt particles 1-4 nm after 0 hours at 650°C in air with 7% H_2O. B.) The HA-ADF image showing nominal Pt particles 10-30 nm after 10 hours at 650°C in air with 7% H_2O. C.) The HA-ADF image showing nominal Pt particles 10-30 nm after 100 hours at 650°C in air with 7% H_2O.

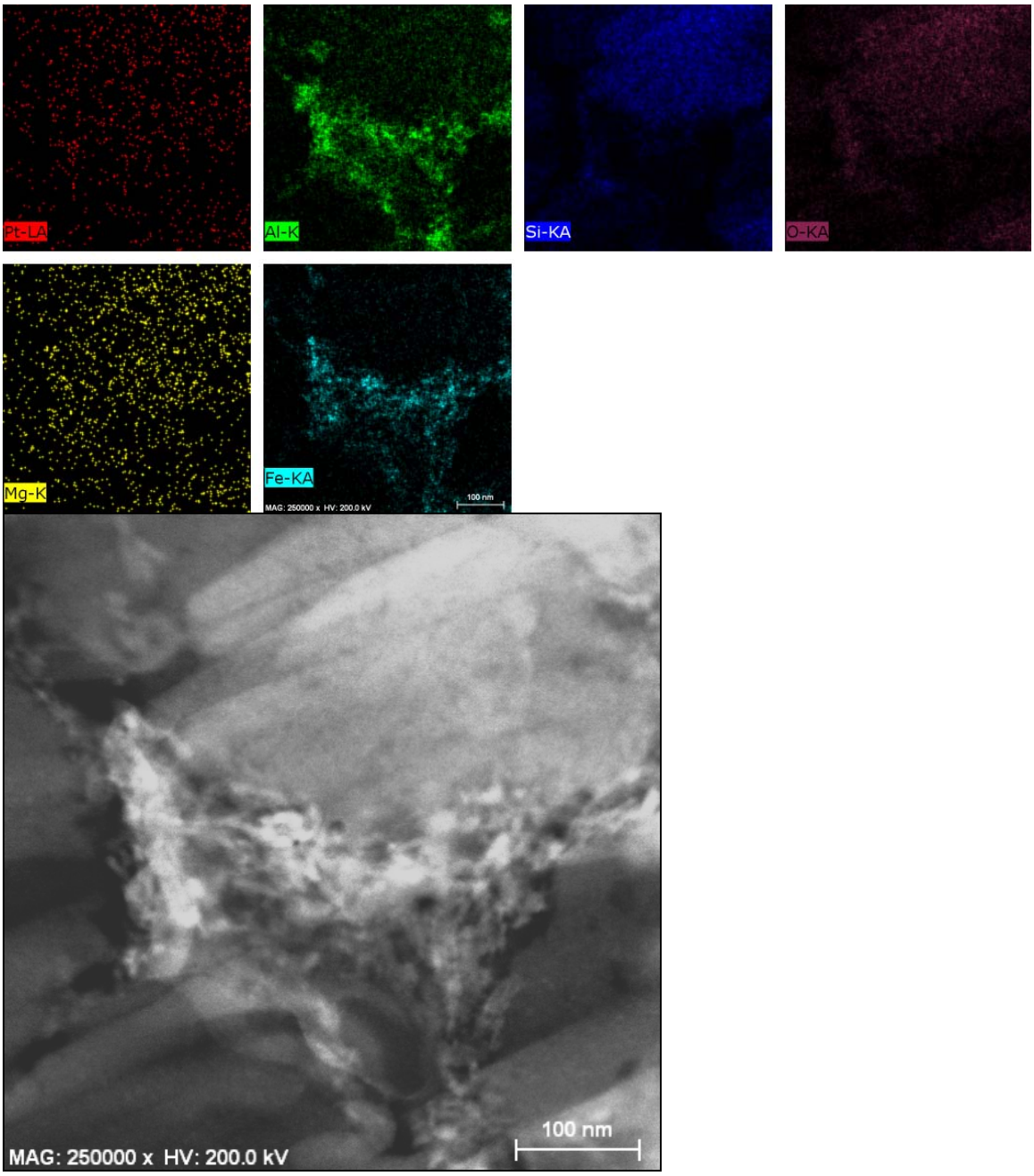

Figure 7 – The elemental maps (top) of the region shown in the dark field image (bottom) after 10 hours at 650°C in air with 7% H_2O.

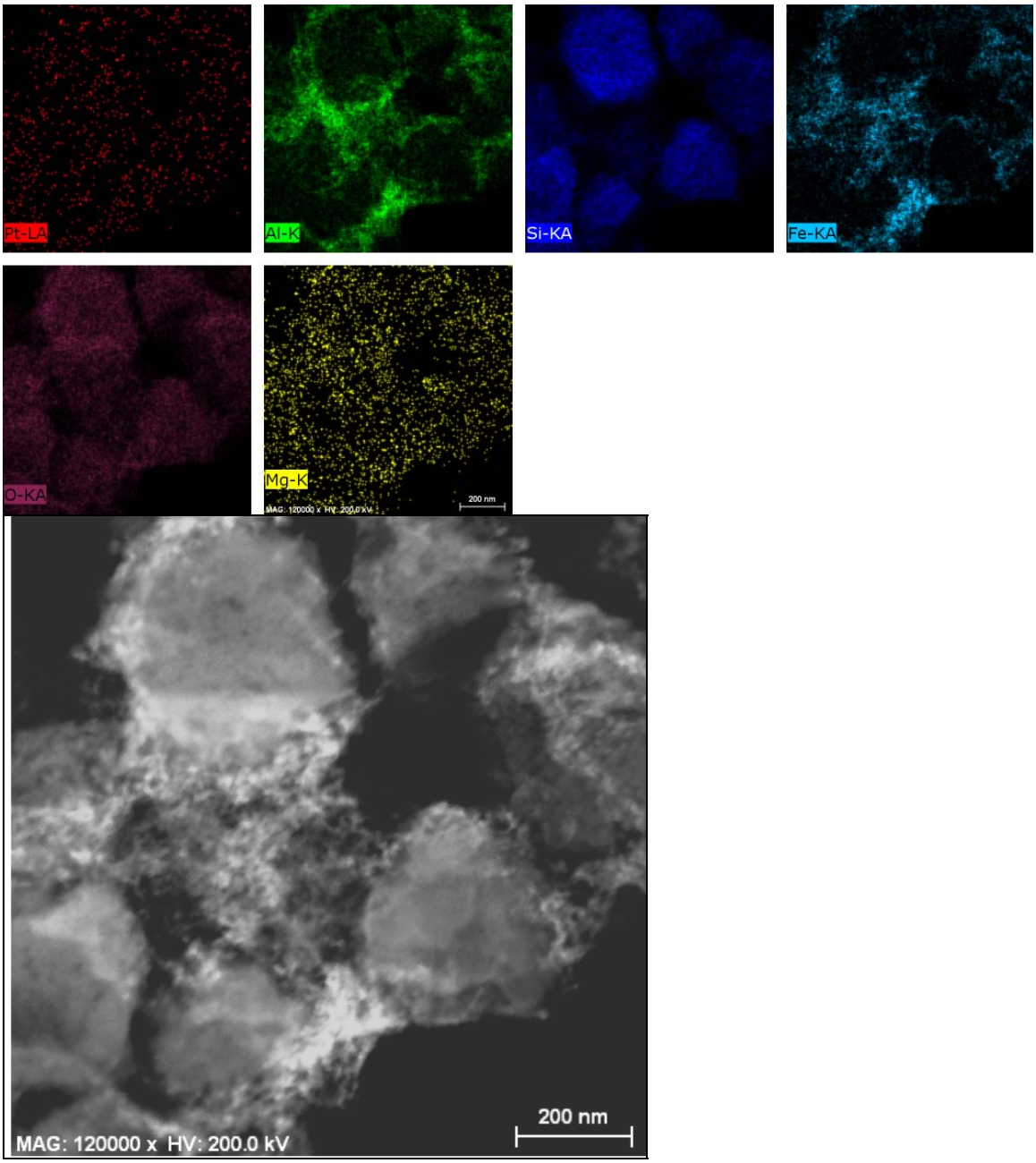

Figure 8 – The elemental maps (top) of the region shown in the dark field image (bottom) after 100 hours at 650°C in air with 7% H_2O.

Agreement 10461: Durability of Diesel Engine Particulate Filters

Thomas R. Watkins, Amit Shyam, Hua-Tay Lin, Edgar Lara-Curzio
Oak Ridge National Laboratory

Randall J. Stafford
Cummins, Inc.

Objective

The objective of this effort is to identify and implement test techniques to characterize the physical and mechanical properties of ceramic diesel particulate filters (DPFs), to identify the mechanisms responsible for the degradation and failure of DPFs and to develop analysis tools for predicting their reliability and durability.

Goals, Barriers, Relevance & Integration

In the study area of OVT's Materials Technology subprogram, the Propulsion Materials Technology activity provides materials R&D expertise to enable advanced materials and supports the goals of several OVT subprograms.[1] Within the Advanced Combustion Engine subprogram-Combustion and Emission Control R&D activity, one *goal* is to: by 2015, develop materials, materials processing, and filter regeneration techniques that reduce the fuel economy penalty of particle filter regeneration by at least 25 percent relative to the 2008 baseline. This project addresses four *barriers* [1] related to the Emission Control: Lack of cost-effective emission control, lack of modeling capability for emission control, improving durability and costly precious metal content. This project is *relevant* to this goal as the understanding of the relationships of the material properties for the filter (and catalyst) substrates enables optimization of porosity, strength, elastic modulus, thermal conductivity, thermal expansion, etc. leading to improved materials processing and models and optimized regeneration strategies that improve fuel economy and increase DPF life. This project also addresses two *barriers* [1] related to the Propulsion Materials Technology activity itself: Changing internal combustion engine combustion regimes and costly precious metal content. This project supports clean diesel, which increases acceptance by the public. Larger acceptance, in turn, results in larger percentages of conversion to diesel, with the resulting reduction in petroleum usage/dependency upon foreign oil. This project is *integrated* within Vehicle Technologies program as it utilizes characterization tools acquired and maintained by the High Temperature Materials Laboratory (HTML) Program.

Technical Highlights

In the reporting period, the ORNL team continued characterizing a new SiC-based DPF material. The DPF honeycomb monoliths were sectioned, and samples were machined as before.[2] The x-ray diffraction pattern of powder from a crushed piece of the SiC-based material shows three phases present: 6H-SiC, free Si, a triclinic form of SiO_2 and an unidentified phase (see Figure 1). Prior x-ray work showed that the cordierite ($2MgO \bullet 2Al_2O_3 \bullet 5SiO_2$) was orthorhombic while the aluminum titanate (AT) –based material contained three phases: Al_2TiO_5, ($SrO \bullet Al_2O_3 \bullet 2SiO_2$, a feldspar, monoclinic) and an unidentified phase which is not mullite. The amount of free Si is yet to be

determined. The SiC-based material is compared to previously characterized materials and references in Tables I and II. The skeletal densities are all within 13% of the dense literature reference values, indicating that there is at most 13 % closed porosity. The SiC based material is relatively more porous than either the cordierite or the aluminum titanate. The skeletal density of the SiC based material will obviously vary with free Si content and is compared to values for reaction-bonded silicon carbide (RBSC). In Table II, the Young's moduli are quite low relative to the values for dense materials, which is directly related to the high porosity as well microcracking for the cordierite, AT-based materials.[3,4] There is some variability (factors 2-4X) of Young's moduli values amongst the available measurement techniques: load deflection, resonant ultrasound spectroscopy (RUS), pulse echo and dynamic mechanical analysis (DMA, reported here). Understanding this variability is the subject of an on-going HTML user proposal.

Double torsion fracture toughness testing was performed at RT and 500 °C as described elsewhere.[2] Figure 2 shows the experimental set-up of the double torsion testing. A successfully fractured test specimen is displayed and defined as one where the crack propagates to the opposite/far end of the sample. The double torsion plate samples were 40 x 20 mm (L x W). The thicknesses of same were governed by the starting wall thickness of the honeycomb monoliths; after machining, typical double torsion sample thicknesses were 0.38, 0.30 and 0.28 mm for the cordierite, AT-based and SiC-based materials, respectively. The fracture surfaces of successfully tested double torsion samples were examined using the SEM (see Figures 3-6). In examining these micrographs, it is often difficult to discern pre-fracture/pre-existing surfaces from post-failure fracture related surface features. During sample machining, samples held with a vacuum chuck for dry grinding which likely pulls in grinding debris. As such a lack of debris highlights fracture sites on internal ligaments/struts. In Figures 3 and 4 for the cordierite and AT-based materials respectively, microcracks and numerous pores are readily observed. In both the cordierite and AT-based materials, it is well established[5-9] that the microcracking is due to the highly anisotropic thermal expansions coefficients with crystallographic direction within each material. The fracture surfaces of the ligaments are transgranular and likely pre-existing microcracks link up with the primary crack. The RT and 500°C fracture surfaces of double torsion samples were indistinguishable. Microcracks are readily observed in cordierite and AT-based materials but only occasionally observed in SiC-based material. The microcracks in the SiC-based material are thought to originate from the fracture process itself.

Figure 7 shows typical the fracture behavior in the double torsion experiments, and the average fracture toughnesses, K_{IC}, are listed in Table II. The double torsion method was selected to measure apparent fracture toughness as crack length not needed for determination.[10] This is important given the engineered porosity and honeycomb structure as well as microcracks in the DPF materials. Here, the maximum load was used to calculate K_{IC}. The non-zero start-finish of K_I is due to weight of the double torsion jig top load, which pre-loads the sample (and is included in the K_{IC} calculation). The slopes in Figure 7 suggest that the moduli are the same or slightly lower at elevated temperature.

The increase in temperature had a negligible effect on the fracture toughness of cordierite and AT-based materials, but did increase same for SiC-based material. It is speculated that the mechanism for this increase in toughness is due to increased ductility of the free Si nodules. Huang and Zhu[11] also observed slight increase in strength and fracture toughness of RBSC between RT and 800°C. Figure 8 shows the fracture toughness increasing with Young's modulus and decreasing with relative porosity. The trend includes all three DPF materials suggesting the strong influence of porosity on the material behavior. Interestingly, the data from this study fall in as predicted by Ashby[12] (see Figure 9).

Status of FY 2011 Milestones

In the reporting period, the ORNL team continued characterizing new Sic-based DPFs, which is part of the milestone to continue to investigate the interaction and properties of washcoat, soot and substrate on properties of new and field tested DPFs. Later in FY11, we plan to initiate characterization of the dynamic and static fatigue response of SiC DPFs (second milestone).

Travel

ORNL and Cummins personnel traveled to Daytona Beach, FL for a meeting of the ASTM C28.01 Mechanical Properties and Reliability committee on January 23, 2011, which, in part, provides standards for the DPF community. On the same trip, a technical talk was presented by T.R. Watkins at the 35th International Conference on Advanced Ceramics and Composites Meeting, Daytona Beach, FL, January 25, 2011.

Presentation

T. R. Watkins, A. Shyam, R. Stafford, "Elevated Temperature Fracture Toughness Behavior of Porous Ceramic Materials," presented at the 35th International Conference on Advanced Ceramics and Composites Meeting held in Daytona Beach, FL, January 25, 2011.

References

1. Vehicle Technologies Program, Multi-Year Program Plan 2011-2015, Dec 2010, pp. 2.3-4; 2.5-7, 8.
2. A. Shyam, E. Lara-Curzio, T. R. Watkins and R. J. Parten, "Mechanical Characterization of Diesel Particulate Filter Substrates," *J. Am. Ceram. Soc.*, **91** [6] 1995–2001 (2008).
3. J. A. Kuszyk and R. C. Bradt, "Influence of Grain Size on Effects of Thermal Expansion Anisotropy in MgTi2O6," J. Am. Ceram. Soc. 56 [8] 420-3 (1973).
4. J. J. Cleveland and R. C. Bradt, "Grain Size/Microcracking Relations for Pseudobrookite Oxides," J. Am. Ceram. Soc. 61 [11-12] 478-81 (1978).
5. Bush & Hummel, J. Am. Ceram. Soc. 1958, 1959.
6. B. Morosin and R. W. Lynch, " Structural Studies on Al_2TiO_5 at Room Temperature and at 600°C,"Acta Cryst. **28** 1040-6 (1972).
7. M. E. Milberg and H. D. Blair, "Thermal Expansion of Cordierite," J. Am. Ceram. Soc. 60 [7-8] 373-4 (1977).

8. H.A.J. Thomas and R. Stevens, “Aluminum Titanate – A Literature Review,” Br. Ceram. Trans. J. **88** 1989.
9. W. R. Buessem, N. R. Thielke, R. V. Sarakauskas, “Thermal Expansion Hysteresis of Aluminum Titanate,” Ceramic Age **60** [5] 38-40 (1952).
10. A. Shyam and E. Lara-Curzio, “The Double-Torsion Testing Technique for Determination of Fracture Toughness and Slow Crack Growth Behavior of Materials: A Review,” J. Mater. Sci **41** 4093–4104 (2006).
11. Q-W. Huang and L-H. Zhub, "High-temperature strength and toughness behaviors for reaction-bonded SiC ceramics below 1400 °C," Mat. Let. **59** 1732–5 (2005).
12. M.F. Ashby, “Materials Selection in Mechanical Design, 1992.
13. ASTM D3766, Standard Terminology Relating to Catalysts and Catalysis, ASTM International, West Conshohocken, PA 2008.
14. J. H. Wallace and H. R. Wenk, Am. Mineral. **65** 96 (1980).
15. CRC Handbook of Chemistry and Physics, Edited by R. C. Weast, CRC Press, Inc., Boca Raton, FL 33431, p. B-121.
16. S. Aroati, M. Cafri, H. Dilman, M.P. Dariel, N. Frage, “Preparation of reaction bonded silicon carbide (RBSC) using boron carbide as an alternative source of carbon,” J. Euro. Ceram. Soc. 31 841–845 (2011).
17. Q-W Huang and L-H Zhu, “High-temperature strength and toughness behaviors for reaction-bonded SiC ceramics below 1400 °C,” Materials Letters **59** 1732–1735 (2005).
18. C. Bubeck, "Direction Dependent Mechanical Properties of Extruded Cordierite Honeycombs," J. Euro. Ceram. Soc. **29** 3113–9 (2009).
19. S. Bueno, M.G. Hernández, T. Sánchez , J.J. Anaya, C. Baudín, "Non-destructive Characterization of Alumina/Aluminum Titanate Composites Using a Micromechanical Model and Ultrasonic Determinations Part I. Evaluation of the Effective Elastic Constants of Aluminum Titanate," Ceramics International **34** 181–188 (2008).
20. T. R. Watkins, D. J. Green, and E. Ryba, "Determination of Young's Modulus in Chemically-Vapor-Deposited SiC Coatings," *J. Am. Ceram. Soc.*. **76** [8] 1965-68 (1993).
21. P. G. Karandikar, G. Evans, S. Wong S, M. K. Aghajanian, M. Sennett, "A Review of Ceramics for Armor Applications," pp. 163-175 in Advances in Ceramic Armor IV, Ceramic Engineering and Science Proceedings, V. 29 [6]. Edited by L.P. Franks, T. Ohji, A. Wereszczak, Wiley, Hoboken, NJ 2009.
22. C.J. Luis, I. Puertas, G. Villa, "Material Removal Rate and Electrode Wear Study on the EDM of Silicon Carbide," J. Mat. Proc. Tech. **164–165** 889–896 (2005).
23. T. R. Watkins and D. J. Green, "Fracture Behavior of Chemically-Vapor-Deposited SiC-Coated Graphite: I, Experimental Results," *J. Am. Ceram. Soc*. **76** [12] 3066-72 (1993).
24. P. Columbo, V. Sglavo, E. Pippel, J. Woltersdorf, "Joining of Reaction-Bonded Silicon Carbide Using a Preceramic Polymer," J. MAT. SCI. **33** 2405-2412 (1998).

Table I – Various measures of density of the DPF materials studied. Density definitions are given in ASTM D3766.[13]

Measure/Material	Cordierite	Al_2TiO_5	SiC
Literature reference (g/cc)	2.588 [c,14]	3.702 [c,6]	3.217 [§,15], 2.85-3.10 [§§,16], 3.11 [§§§,17], 2.98 [§§§§,17]
Bulk (g/cc)*	1.22	1.65(0.03) **	1.18(0.03)
Skeletal (g/cc)[¥]	2.46	3.43(0.05)	2.83(0.05)
Relative ρ (%)[Ø]	49.6	48.1	41.7
Porosity (%)	50.4	51.9	58.3

* Geometric volume: includes solids plus all open and closed porosity of plate samples, i.e., no channels
** () values = standard deviation
[¥] He pycnometry: volume includes solids plus all closed porosity
[Ø] Relative density (ρ_{bulk}/ ρ_{skel} *100)
[§] 0 v% free Si;[§§] 15-35 v% free Si; [§§§] 12 v% free Si; [§§§§] 26 v% free Si in RBSC
[c] Calculated x-ray density

Table II – Young's modulus, thermal expansion coefficient, room temperature strength and fracture toughness of various DPF materials.

Property/Material	Cordierite	Al_2TiO_5	SiC	
Polycrystalline Young's Modulus for dense material (GPa)		138 [†¬,18]	155 [††,19] 359-407 [21]	420 [∞,20], 320-340 [§,16],
Young's Modulus (GPa)*	16.2(0.2)	6.19(1.17)	20(2.5)	
Polycrystalline CTE for dense material ($x10^{-6}$ 1/°C)	1.14 [22], 0.7 [7]	9.7 [†,8], 1.73 [†,9]	4.85 [∞,23], 4.5 [24], 4.3-4.6 [22]	
CTE parallel[¢] ($x10^{-6}$ 1/°C)	0.48	1.07(0.15)	5.00(0.04)	
CTE perpendicular[¢¢] ($x10^{-6}$ 1/°C)		0.99	2.17(0.15)	5.10(0.08)
Strength (MPa) @ RT[¥]	7.33(0.45)	2.98	19.5(0.63)	
K_{IC} (MPa√m) @ RT	0.31(0.02)	0.13(0.02)	0.42(0.05)	
K_{IC} (MPa√m) @ 500°C	0.25(0.04)	0.16(0.02)	0.55(0.03)	

* Dynamic Mechanical Analysis (DMA); MOI corrected; 2-5 samples, Each remounted >5 X
Linear coefficient of thermal expansion [¢]parallel and [¢¢]perpendicular to the extrusion direction; RT -1000°C
[¥] MOI corrected
[∞,] CVD β-SiC, no free Si, [§] 15-35 v% free Si
[†] based on single crystal data (w/o microcracks)
[††] Indirectly determined, assumed dense.
¬ For hexagonal cordierite: Indialite.

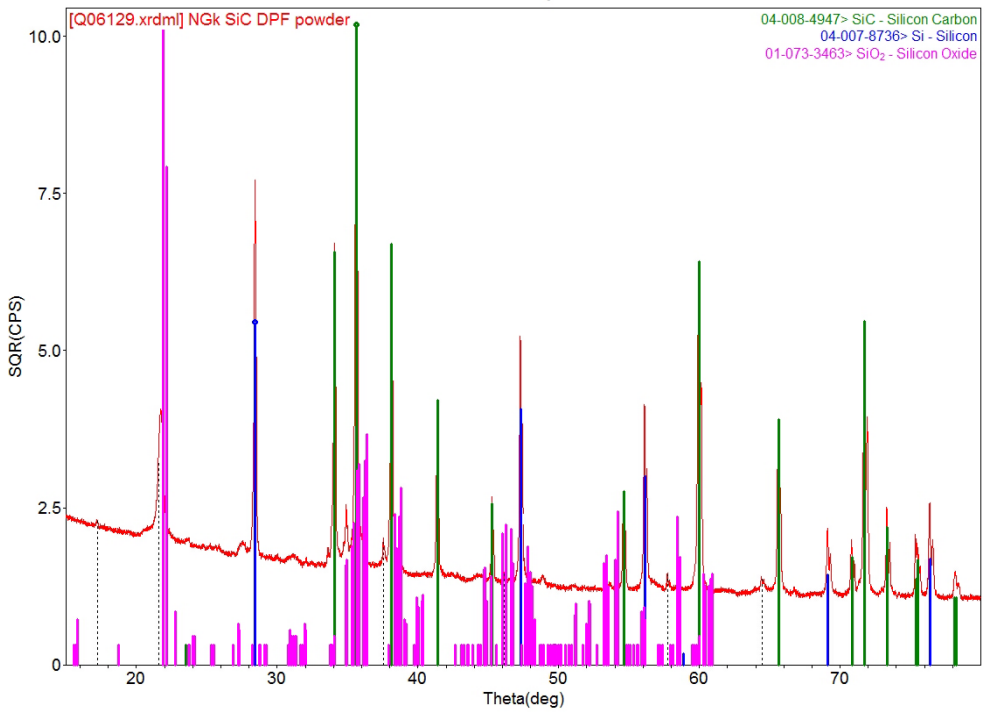

Figure 1 – The x-ray diffraction pattern the SiC-based DPF material.

A. 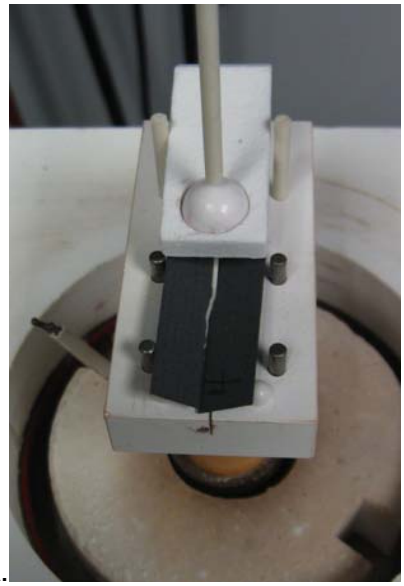 B.

Figure 2 – A. The room temperature double torsion experimental set-up. Note: this is also the interior view of double torsion high temperature experimental set-up. A "successfully" fractured double torsion SiC-based sample is shown. Loading is accomplished through the push-rod shown. A thermocouple is seen to the left. B. The exterior view of the high temperature double torsion experimental set-up.

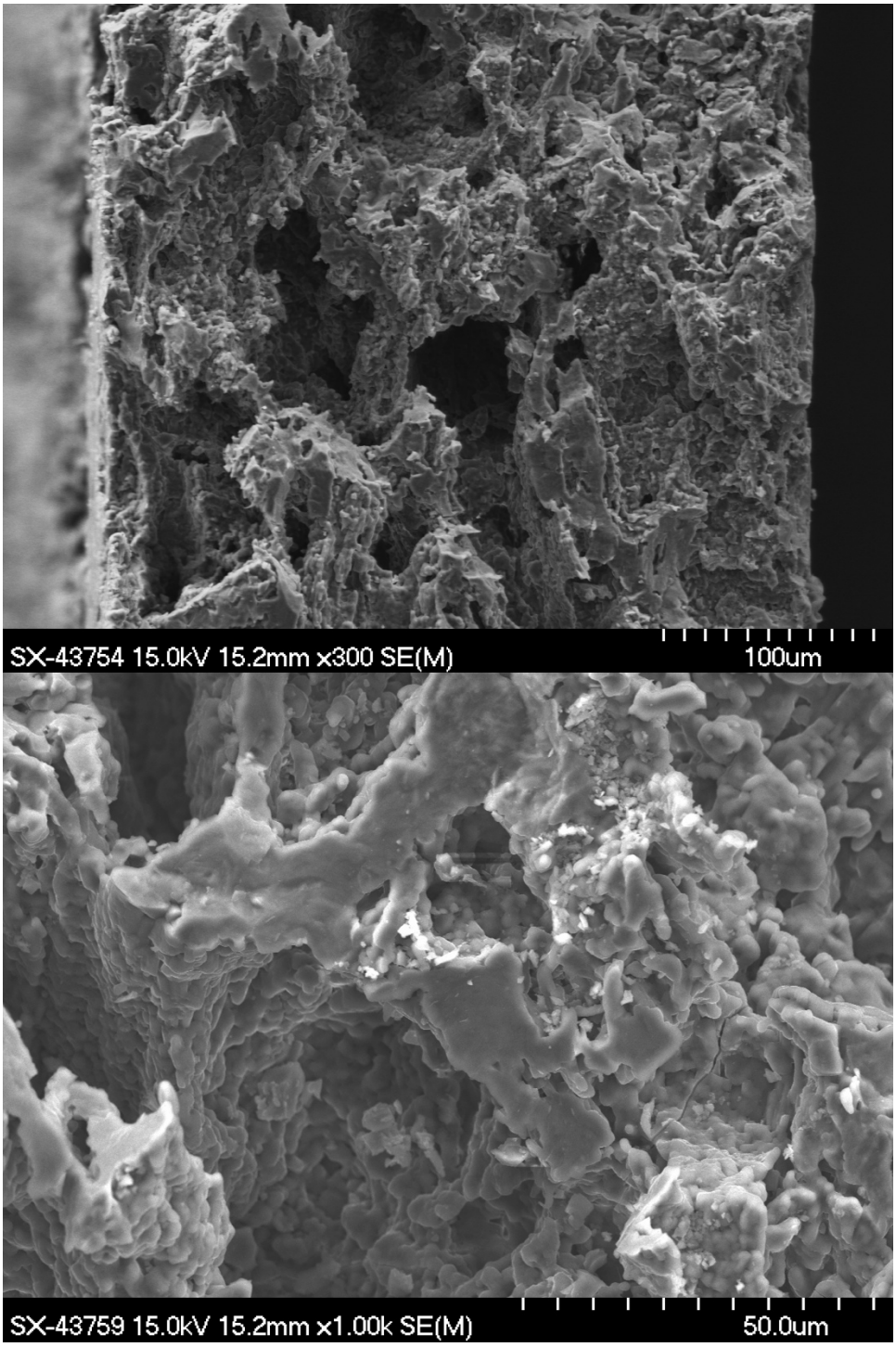

Figure 3 – SEM micrographs of the double torsion fracture surface of a cordierite ($2MgO{\bullet}2Al_2O_3{\bullet}5SiO_2$) DPF material. The upper micrograph covers the entire thickness. Note the numerous microcracks and pores; the grain size ranges from ~2-10+ μm. Some grinding debris (white particles) is shown just off center to the upper right.

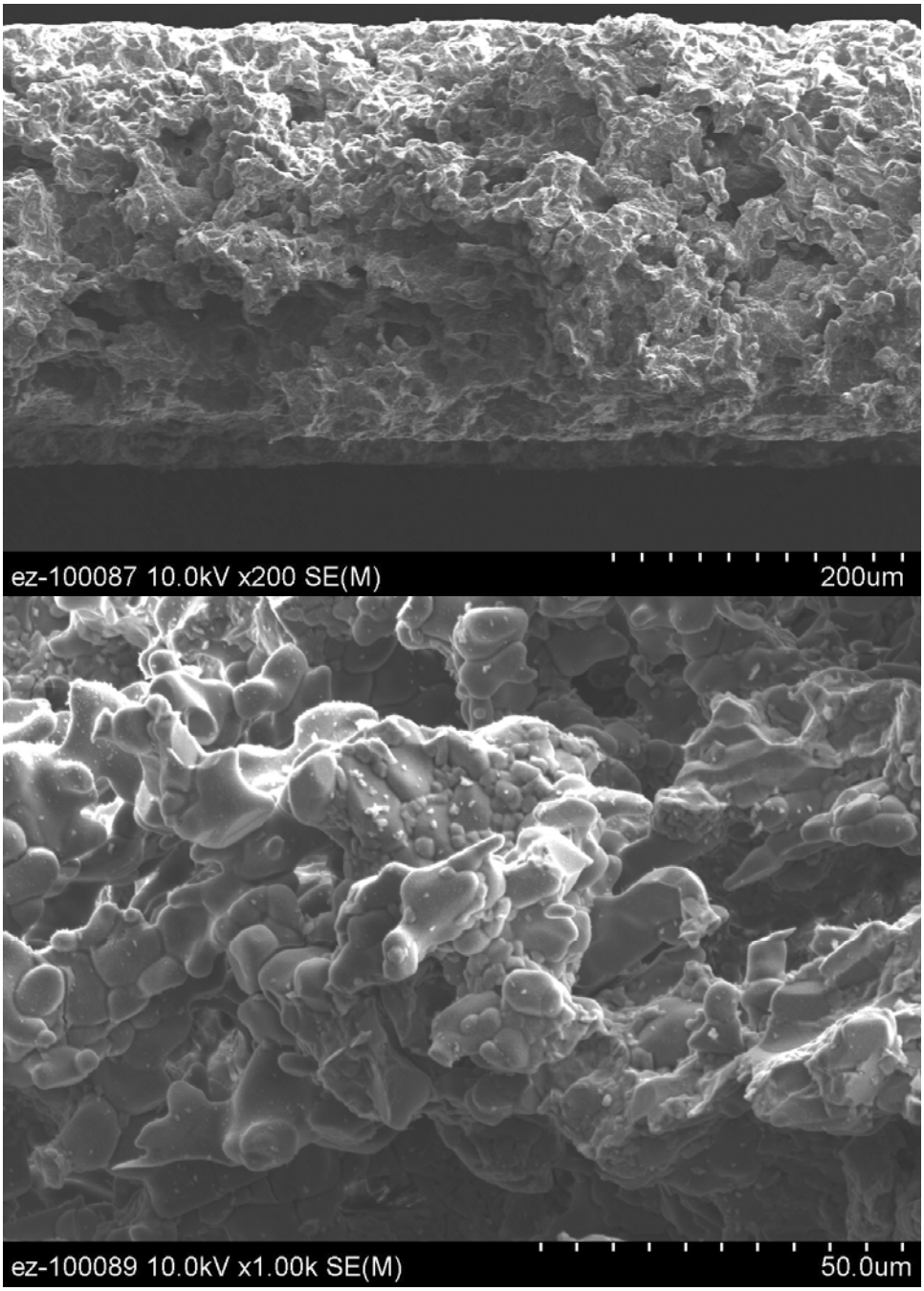

Figure 4 – SEM micrographs of the double torsion fracture surface of an Al_2TiO_5-based DPF material. The upper micrograph covers the entire thickness. Note the numerous microcracks and pores; the grain size ranges from ~5-20 μm. Some grinding debris (white particles) is shown in the center and to the upper left.

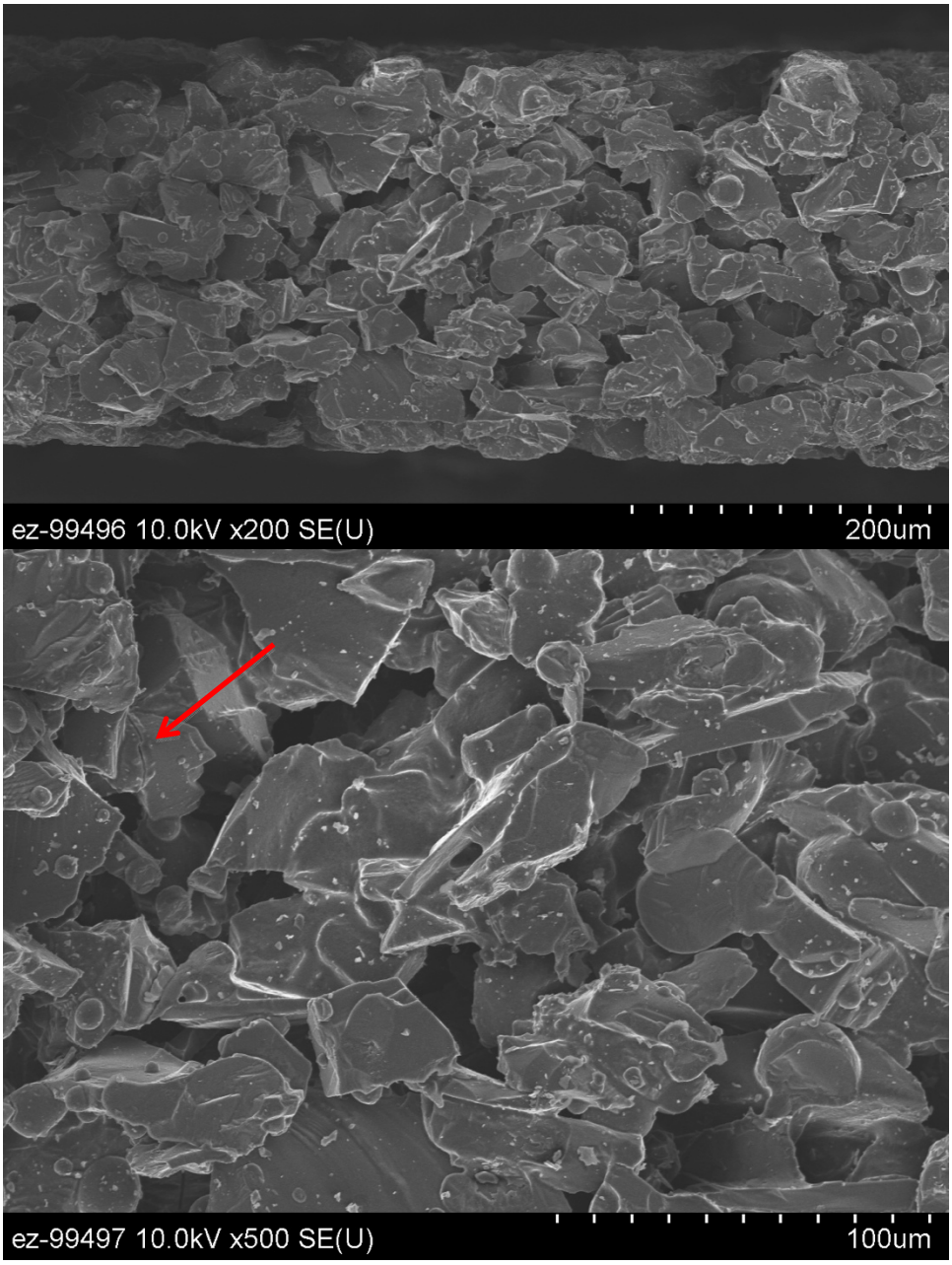

Figure 5 – SEM micrographs of the double torsion fracture surface of a SiC-based DPF material. The upper micrograph covers the entire thickness. Note the numerous pores and abundant grinding debris (white particles); the grain size ranges from 10-50 μm. One microcrack is indicated by the red arrow.

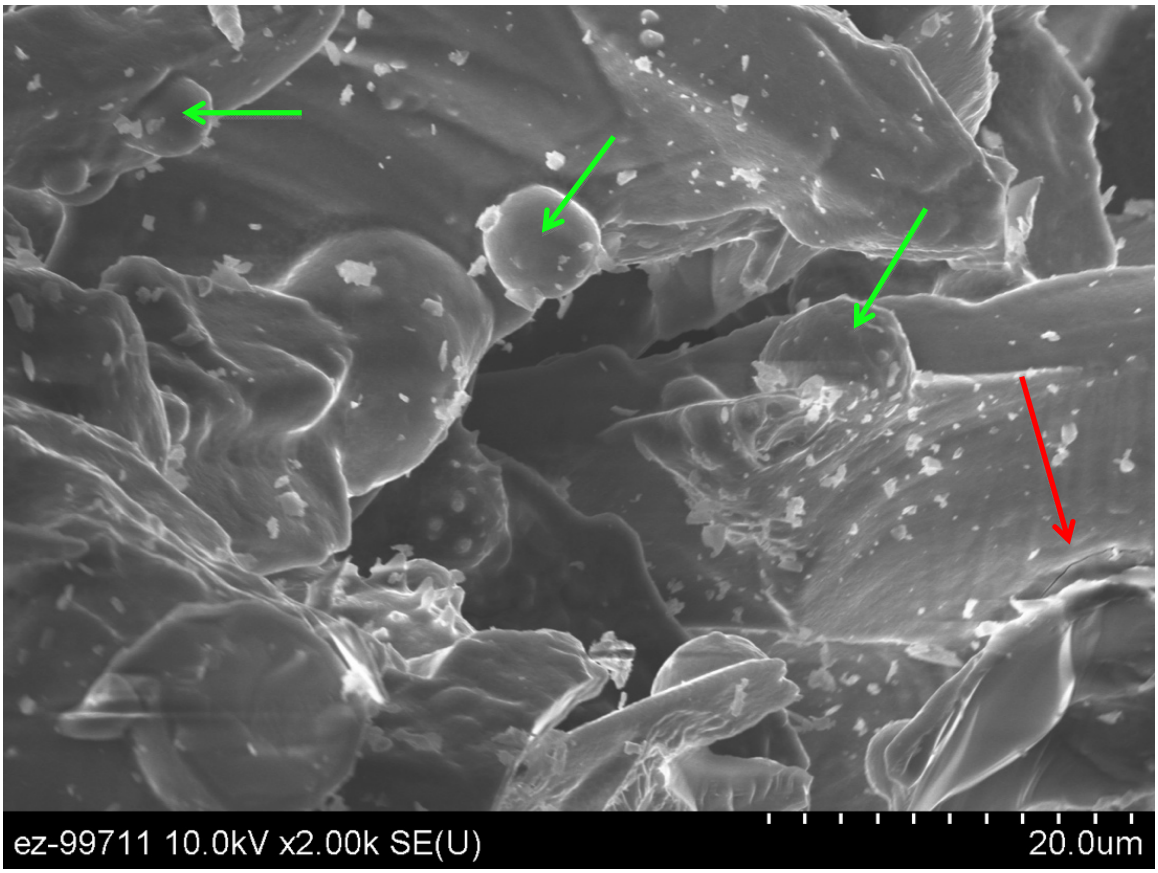

Figure 6 – SEM micrograph of another double torsion fracture surface of a SiC-based DPF material. The green arrows indicate Si-rich nodules (per EDS) when the red arrow indicates a microcrack.

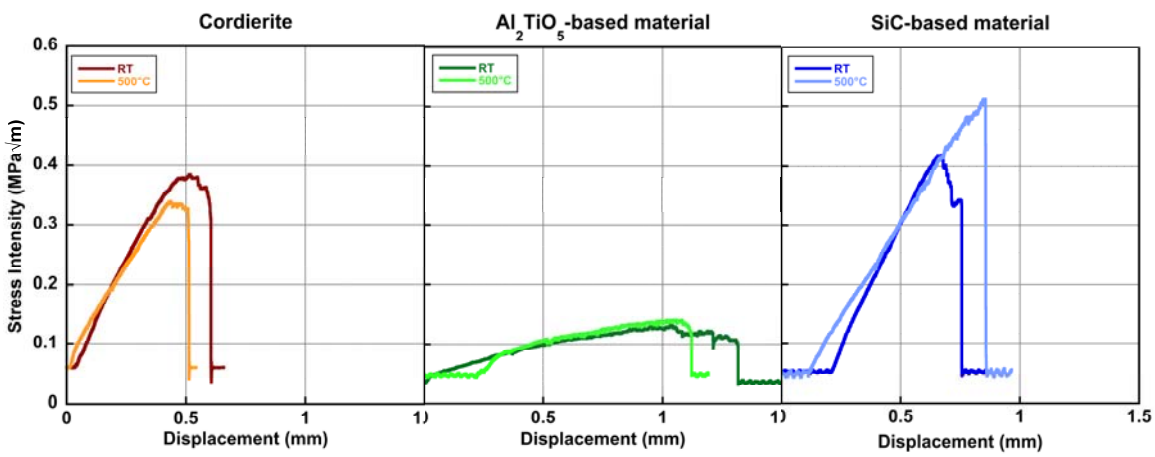

Figure 7 – Stress intensity as a function of displacement for double torsion samples of cordierite, aluminum titanate based and silicon carbide based DPF materials.

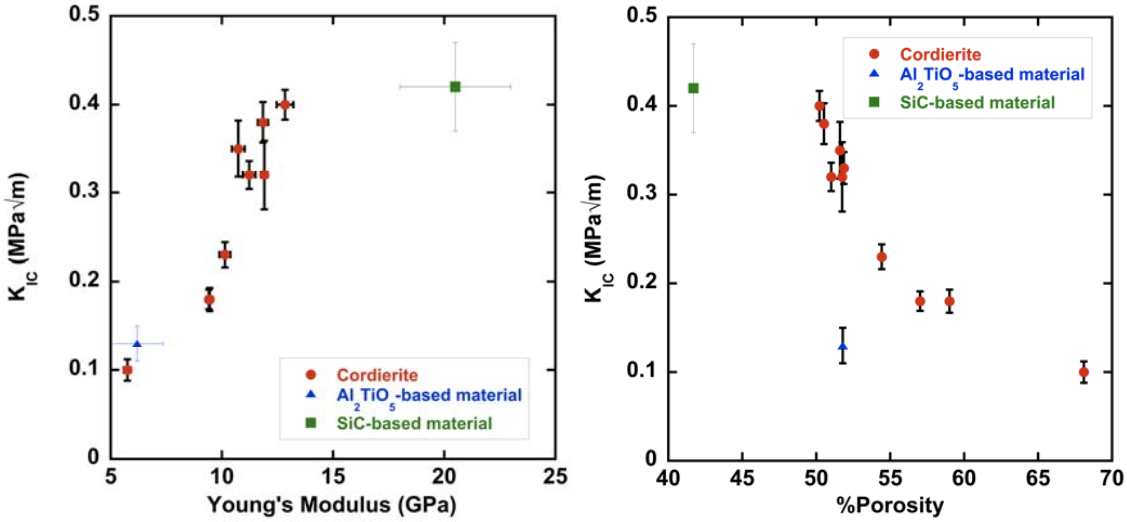

Figure 8 – The fracture toughness as a function of Young's modulus (left) and percent porosity (right) for the SiC-based DPF material.

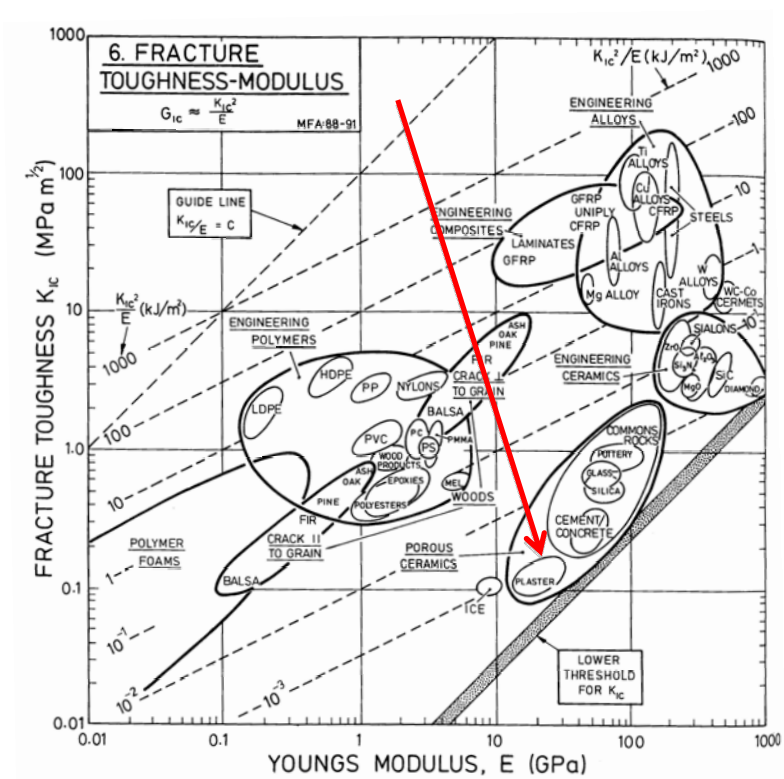

Figure 9 – The fracture toughness as a function of Young's Modulus for various materials. {after M.F. Ashby, "Materials Selection in Mechanical Design, 1992}[12]. The red arrow highlights the region for porous ceramics.

Agreement 10635: Catalysis by First Principles - Can Theoretical Modeling and Experiments Play a Complimentary Role in Catalysis?

C. Narula, M. Moses DeBusk, Xiaofan Yang
Oak Ridge National Laboratory

Objective/Scope

This research focuses on an integrated approach between computational modeling and experimental development, design and testing of new catalyst materials, that we believe will rapidly identify the key physiochemical parameters necessary for improving the catalytic efficiency of these materials. The results will have direct impact on the optimal design, performance, and durability of supported catalysts employed in emission treatment; e.g., lean NO_x catalyst, three-way catalysts, oxidation catalysts, and lean NO_x traps etc.

The typical solid catalyst consists of nano-particles on porous supports. The development of new catalytic materials is still dominated by trial and error methods, even though the experimental and theoretical bases for their characterization have improved dramatically in recent years. Although it has been successful, the empirical development of catalytic materials is time consuming and expensive and brings no guarantees of success. Part of the difficulty is that most catalytic materials are highly non-uniform and complex, and most characterization methods provide only average structural data. Now, with improved capabilities for synthesis of nearly uniform catalysts, which offer the prospects of high selectivity as well as susceptibility to incisive characterization combined with state-of-the science characterization methods, including those that allow imaging of individual catalytic sites, we have compelling opportunity to markedly accelerate the advancement of the science and technology of catalysis.

Computational approaches, on the other hand, have been limited to examining processes and phenomena using models that had been much simplified in comparison to real materials. This limitation was mainly a consequence of limitations in computer hardware and in the development of sophisticated algorithms that are computationally efficient. In particular, experimental catalysis has not benefited from the recent advances in high performance computing that enables more realistic simulations (empirical and first-principles) of large ensemble atoms including the local environment of a catalyst site in heterogeneous catalysis. These types of simulations, when combined with incisive microscopic and spectroscopic characterization of catalysts, can lead to a much deeper understanding of the reaction chemistry that is difficult to decipher from experimental work alone.

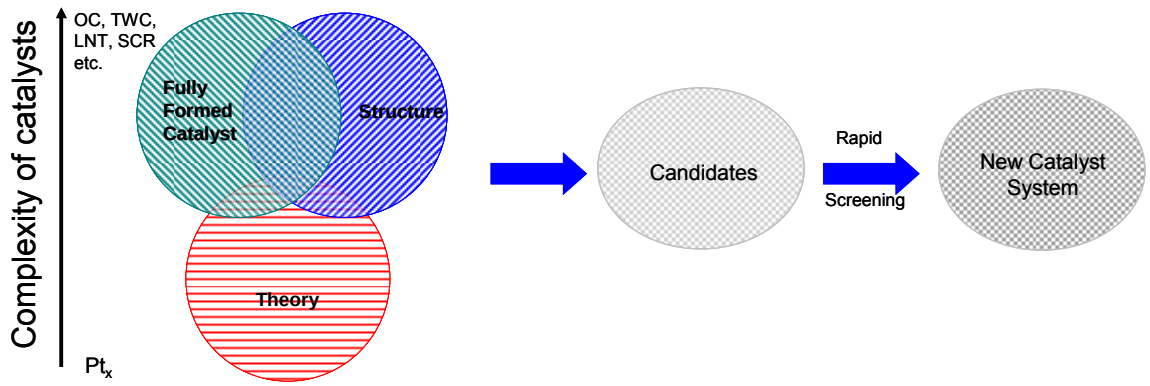

Thus, a protocol to systematically find the optimum catalyst can be developed that combines the power of theory and experiment for atomistic design of catalytically active sites and can translate the fundamental insights gained directly to a complete catalyst system that can be technically deployed.

Although it is beyond doubt computationally challenging, the study of surface, nanometer-sized, metal clusters may be accomplished by merging state-of-the-art, density-functional-based, electronic-structure techniques and molecular-dynamic techniques. These techniques provide accurate energetics, force, and electronic information. Theoretical work must be based on electronic-structure methods, as opposed to more empirical-based techniques, so as to provide realistic energetics and direct electronic information.

A computationally complex system, in principle, will be a model of a simple catalyst that can be synthesized and evaluated in the laboratory. It is important to point out that such a system for experimentalist will be an idealized simple model catalyst system that will probably model a “real-world” catalyst. Thus it is conceivable that “computationally complex but experimentally simple” systems can be examined by both theoretical models and experimental work to forecast improvements in catalyst systems.

We have focused on the oxidation catalyst and SCR catalyst to develop and demonstrate catalyst by design protocol as a prelude to developing catalyst by design protocols for complex emission treatment catalysts; e.g., TWCs, NO_x traps, and HC-SCR catalysts. Our goals are as follows:

- Our theoretical goal is to carry out the calculation and simulation of realistic supported Pt nanoparticle systems (i.e., those equivalent to experiment), in particular by addressing the issues of complex cluster geometries on local bonding effects that determine reactivity. As such, we expect in combination with experiment to identify relevant clusters, and to determine the electronic properties of these clusters. In addition, we plan to study zeolite structures with a view to develop an insight on the mechanistic aspects of catalytic process to enable us to develop better catalysts.
- Our experimental goal is to synthesize metal carbonyl clusters, decarbonylated metal clusters, sub-nanometer metal particles, and metallic particles (~5 nm) on

alumina (commercial high surface area, sol-gel processed, and mesoporous molecular sieve), characterize them employing modern techniques including Aberration Corrected Electron Microscope (ACEM), and evaluate their CO, NO_x, and HC oxidation activity. Furthermore, guided by theoretical studies we plant to synthesize new zeolites and characterize them.

- This approach will allow us to identify the catalyst sites that are responsible for CO, NO_x, and HC abatement. We will then address design of new durable catalysts systems that can withstand the prolonged operations.

Technical Highlights

Until recently, our theoretical studies have focused on supported noble metals. We have shown that single platinum atoms supported on a θ-alumina slab are in the zero oxidation state. This result is very different from that reported in literature on single platinum atoms supported on α-alumina or simplified models of γ-alumina where a platinum atom generally has an unpaired electron. This also means that mechanism of CO, NO_x, or HC oxidation on Pt(0) will be different from that on Pt(I) or Pt(II). We plan to carry out first principle studies of CO oxidation on Pt atoms supported on a θ-alumina slab.

Since our experimental work has already shown that the distribution of platinum on γ-alumina and θ-alumina is almost identical, and the surface properties and CO oxidation of both catalysts are identical, we propose that Pt supported on θ-alumina is a better model for Pt supported on γ-alumina than Pt supported on α-alumina or simplified models of γ-alumina.

We have also shown that incorporation of palladium in platinum particles at sub-nanometer scale is quite ineffective in improving the durability, however, large Pt-Pd nanoparticles tend to be more hydrothermally durable than pure Pt particles. While efforts are in progress to prepare sub-nanometer Pt-Pd particles to validate the results of theoretical studies, we have initiated theoretical studies of SCR-zeolite-catalysts.

In this report, we describe our theoretical studies on single atoms of Ni, Pt, Pd, Cu, Ag, Au employing Gaussian smearing functions with a width of 0.05 eV to states near Fermi level to facilitate convergence and obtain high quality Density of State (DOS) data. The experimental work summarizes our efforts to synthesize a complex containing a Pt-Pd bond which we plan to employ to synthesize sub-nanometer particles of Pt-Pd supported on alumina to validate our theoretical studies.

Theoretical Studies: The ground state of Ni is $3d^9 4s^1$ and excited sates are $3d^{10}$ and $3d^8 4s^2$. The excitation energy of transition from $3d^9 4s^1$ to $3d^{10}$ and $3d^8 4s^2$ are 1.74 and 0.58 eV. [1,2] This makes the interaction of Ni with θ-alumina quite complex. The Nickel atom occupies a position between two surface oxygen atoms and is 0.626Å above the surface. The Ni-O bond distances are 2.022 and 1.977 Å with O-Ni-O angle of 143.61°. There is no magnetic moment associated with Ni atoms allowing us to infer that there are no unpaired electrons on nickel atoms. The DOS analysis [Figure 1] shows that all d orbitals on Ni are filled leading us to suggest a d^{10} configuration.

Furthermore, the Ni s, Ni d and O 2p orbitals are strongly hybridized as a result of mixing of s-d metal hybrids with O2p orbitals. This bonding picture is definitely not a charge transfer from the metal atom to the oxide surface but a covalent bond between Ni and O atoms due to s-d hybridization in Ni with some polar character for Ni. This bonding picture has previously been seen for Ni atoms adsorbed on MgO. [2] In comparison, previous studies of Ni/γ-Al_2O_3 are limited to Nickel clusters in which the Ni-O bond and bond order have been computed to be 2.16 and 0.08, respectively, which decrease to 2.04 and 0.004, respectively, with an increase in Ni cluster size suggesting weak Ni interaction with γ-Al_2O_3. The Ni atom adsorption energy is -18.9 Kcal/mole, which is substantially less than that observed by us for Ni/θ-Al_2O_3.

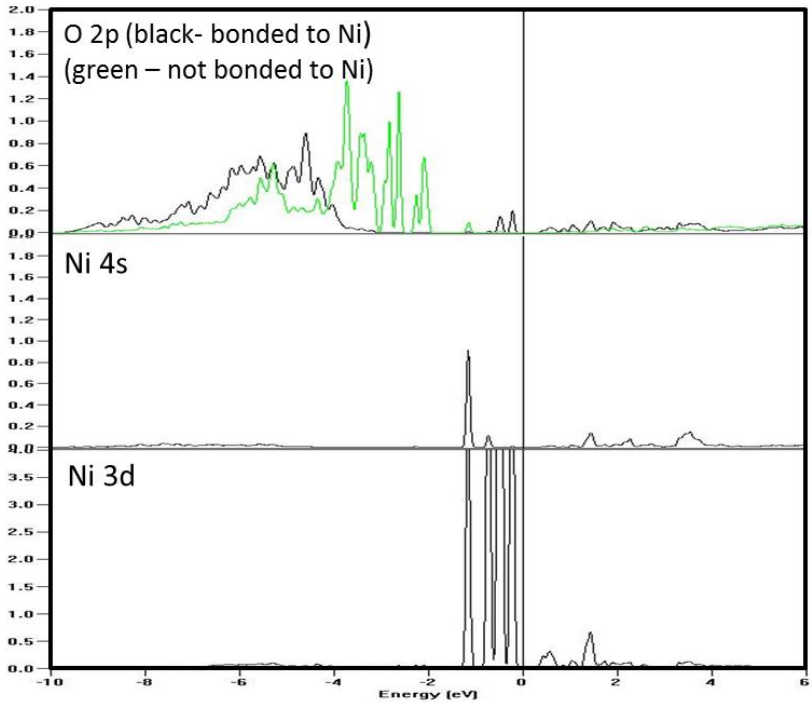

Figure 1: Density of state plots for Ni on (010) θ-alumina surface, surface oxygen (green) and surface oxygen (black) bonded to Ni atom

The lowest energy, equilibrium, adsorption site of platinum on the θ-Al_2O_3 (010) surface is found to be a bridging position between 2 oxygen atoms from adjacent layers and is located above aluminum. The Pt bond distances to the nearest neighbor oxygen sites are 2.18 and 2.13 Å, respectively, with an O_1-Pt-O_2 angle of 140.55º; the platinum atom is located 0.728 Å above the cell surface. These Pt-O distances are larger than Pt-O bond distances calculated for Pt-O clusters in the gas-phase (1.76 Å) and Pt/α-alumina (2.0 Å) but are closer to bulk Pt-O (2.08 Å). We also carried out calculations using a charge-neutral supercell of 420 atoms comprising monoclinic 2 × 3 × 3 unit cells. The platinum atom location and bond distances are essentially identical to those on the 2 × 4 × 2 supercell. We carried out surface mapping of a platinum atom on the alumina surface by moving the platinum atom in *x* and *z* directions in a quadrant of 2.08 × 0.48 Å and allowing the *y*-coordinate to vary, thereby allowing us to ascertain that the optimized position is indeed a minimum.

The lack of a Pt magnetic moment for the Pt/θ-Al_2O_3 system clearly suggests a d^{10} configuration for platinum atoms. This is in contrast with d^9s^1 platinum found for Pt/α-Al_2O_3. Analysis of the local density of state [Figure 2] of Pt/θ-Al_2O_3 leads to a different bonding picture than that reported in literature for α-Al_2O_3 or γ-Al_2O_3. The platinum on α-Al_2O_3 exhibits a $Pt^{\delta+} \leftarrow O^{2-}$ bond. The platinum supported on θ-Al_2O_3 (010), on the other hand, is bonded to two surface oxygen atoms and is essentially d^{10}. The density of states (Figure 2) shows filled Pt d-orbitals hybridized with O 2p orbitals supporting a d^{10} configuration for Pt. Thus, the Pt bond to θ-Al_2O_3 is not simply a charge transfer from the Pt atom to the oxide surface. The strong surface bonding of Pt is not surprising in view of the pronounced tendency of platinum group metals to form s-d hybrids.

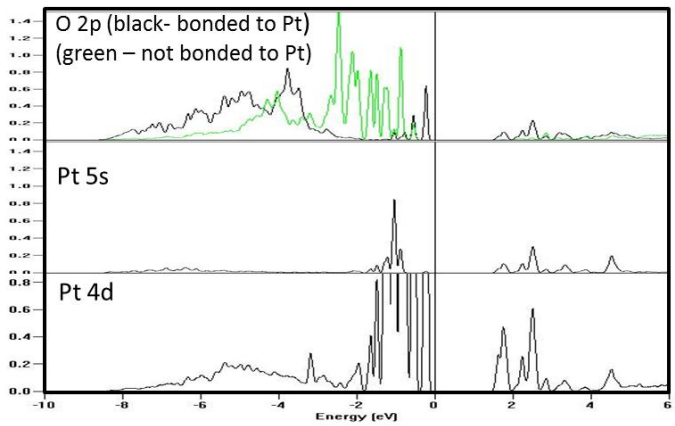

Figure 2: Density of state plots for Pt on (010) θ-alumina surface, surface oxygen (green) and surface oxygen (black) bonded to Pt atom

The hybridization tendency has previously been correlated to s → d transition energy since computed d^9s^1-d^{10} energy separation for Pt is only 0.98 eV.[1,2] Our results are consistent with Pt absorbed on the (001) MgO and (111) ZrO_2 surfaces where it has been shown that Pt changes its configuration from d^9s^1 to d^{10} as it approaches the oxide support.[32-34] The change in configuration is accompanied by quenching of the Pt-atom's magnetic moment. While theoretical modelling studies show that the bonding of Pt with θ-Al_2O_3 results in platinum being in a formally zero oxidation state, experimentally, it is not a stable state for platinum under ambient conditions. The chemistry of platinum zero complexes is quite well developed, and it has been shown that oxygen can bond to platinum zero in η2 mode and form strongly nucleophilic d^8 = Pt(O_2) species. Thus, platinum atoms on θ-Al_2O_3 can be expected to be oxidized species.

The ground state of Pd is $4d^{10}$ and excited state is $4d^95s^1$. The excitation energy of transition from $4d^{10}$ and $4d^95s^1$ is 0.95 eV.[1,2] The bonding behavior of a palladium atom is very similar to that of platinum atom on θ-alumina. The palladium atom occupies a position 0.855 Å above the surface between two surface oxygen atoms. The Pd-O bond distances are 2.22 and 2.20 Å with O-Pd-O angle of 134.55º. There is no magnetic moment associated with palladium also. The DOS analysis shows that all d orbitals on palladium are filled leading us to suggest a d^{10} atom like platinum on θ-alumina 010 surface. This bonding picture is also very similar to the one described for Pd/MgO which has a d^{10} Pd atom with Pd-O bond of 2.28A and a covalent character to the interaction of Pd orbitals with oxygen 2p orbitals. The adsorption energy of a Pd atom on alumina has been reported to be -31.13 Kcal/mole, and its bonding is essentially charge transfer

from Pd to Al^{3+} neighbor with a weak bond to O^{2-} because of a poor match between energy states of the metal atom and oxide.

The ground sate of a Copper atom is $3d^{10}4s^1$ and excited state is $3d^94s^2$ with excitation energy of 1.49 eV.[1,2] As a result, the configuration for a Cu atom does not easily change from $3d^{10}4s^1$ to $3d^94s^2$. The bonding picture is somewhat different from platinum group metals. The copper atom also favors the location between two surface oxygen atoms and is located 1.01 Å above the surface. The Cu-O bond distances are 2.184 and 2.184 Å with O-Cu-O angle of 124.77º. The Cu atom exhibits filled d orbitals and occupied s-orbital with magnetization primarily associated with the 4 s orbital. The DOS shows filled d and s orbitals and supports this bonding picture for a copper atom on a θ-alumina surface. This bonding picture is quite different from that reported for Cu on α-alumina. The adsorption of Cu results in surface displacement, weakening of the attraction of the outermost aluminum atoms by the surface oxide ions suggesting reduction of aluminum atoms by the Cu atoms. The DOS analysis showed the disappearance of Cu 4s band suggesting Cu (I) species.

The ground sate of a Silver atom is $4d^{10}5s^1$ and excited state is $4d^95s^2$ with excitation energy of 3.97 eV. [1,2] The high activation energy prevents a Ag atom from easily changing its configuration from $4d^{10}5s^1$ to $4d^95s^2$ during bond formation. The silver atom favors the location between two surface oxygen atoms and is located 1.46Å above the surface. The Ag-O bond distances are 2.48 and 2.57Å with O-Ag-O angle of 108.5º. The increase in Ag-O bond distance in comparison with Cu-O bond distance is an indication of weaker Ag-O bonds. The high d-s separation results in smaller propensity for s-d hybridization which in turn reduces mixing with 2p orbitals

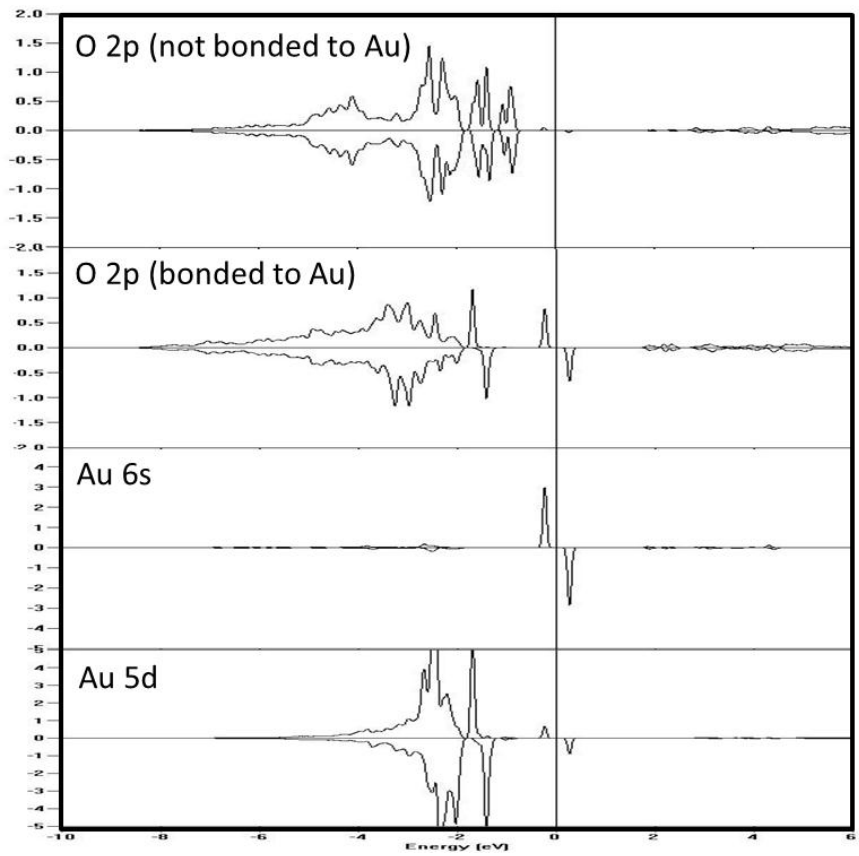

Figure 3: Density of state plots for Au on (010) θ-alumina surface, surface oxygen, and surface oxygen bonded to Au atom

of surface oxygen leading to weaker Ag-O bonds. This bonding picture is somewhat different from that of Ag supported on α-alumina where Ag interacts with α-alumina in primarily ionic fashion.

The ground sate of a Gold atom is $5d^{10}6s^1$ and excited state is $5d^9 6s^2$ with excitation energy of 1.74 eV.[1,2] Like the rest of the atoms, the gold atom also favors the location between two surface oxygen atoms and is located 1.52Å above the surface. The Au-O bond distances are 2.45 and 2.69Å with O-Au-O angle of 107.3º. The Au-O bond distance of the first oxygen (i.e. 2.45 Å) is comparable to the Au-O bond distance observed for Au/α-Al_2O_3 and Au/MgO. However, the second Au-O bond distance of 2.69 Å is almost within nonbonding distance. The DOS of Au [Figure 3] shows filled 5d orbitals and the magnetization centered at the 6s orbital. The partially vacant O 2p orbital of oxygen bonded with Au shows electron transfer from oxygen to Au.

Thus, platinum group metal atoms' interactions with θ-Al_2O_3 010 surfaces follows a simple pattern – all three members (Ni, Pt, Pd) have filled d-orbitals, d-s hybridization, and overlap with surface oxygen 2p orbitals. The interaction of coinage metal (Cu, Ag, Au) atoms with θ-Al_2O_3 010 surface is similar to that of platinum group metals, but Ag and Au interact primarily by charge transfer. The bonding picture of transition metals, especially platinum group metals, with θ-Al_2O_3 010 surfaces differs from that of transition metals on α-Al_2O_3 surfaces. Considering that θ-Al_2O_3 is structurally closer to γ-Al_2O_3, we suggest that a θ-Al_2O_3 surface is a better model for γ-Al_2O_3 than α-Al_2O_3. From an experimental point of view, it should be obvious that platinum group metals in zero oxidation state are not stable under oxidizing condition and can very easily react with atmospheric oxygen to form oxides.

Experimental Studies: The synthesis of *trans*-$[(NH_3)_2Pt(1\text{-methylcytosine})PdCl]NO_3$ is a multistep process and described as follows:

N^4-(N,N-Dimethylaminomethylene)-1-methylcytosine: The literature report [3] on the synthesis of N^4-(N,N-Dimethylaminomethylene)-1-methylcytosine which is the precursor for the synthesis of 1-Me-cytonsine, was found to be irreproducible in our hand. The corrected procedure is as follows:

A mixture of cytosine (4.5 g, 40.5 mmol), N,N-dimethylformamide dimethyl acetal (60 mL) and trifluoroacetic acid (0.3 mL) was heated to a boil under nitrogen for 50 hours. The cloudy solution gradually became red and transparent but contained some insoluble white solid. More white-colored solid separated out upon cooling which was collected by filtration and washed with benzene and was purified by recrystallization from $CHCl_3$/benzene. ^1H NMR was found to be consistent with the literature report.

1-methylcytosine: 6 g of N^4-(N,N-Dimethylaminomethylene)-1-methylcytosine was stirred with 25% ammonium hydroxide solution (600 mL) overnight, and the solution was heated under reflux for 2 hours to eliminate excess NH_3. The powder was collected by filtration.

^{1}H-NMR (400.6 MHz, DMSO-*d_6*): 3.2 (s, 3H), 5.6 (d, 2H), 7.0 (s, br, 1H), 7.6 (d, 1H)
trans-[Pt(NH_3)$_2$(1-methylcytosine)](NO_3)$_2$: This compound was prepared by a reported procedure. [4] *trans*-Pt(NH_3)Cl_2 (0.3799 g, 1.27 mmol) was stirred with $AgNO_3$ (0.4302 g, 2.53 mmol) in 40 mL deionized water under light protection at 40°C for 40 hours, resulting a white slurry. The clear colorless filtrate of the reaction was then introduced to 1-methylcytosine (0.3169 g, 2.53 mmol), and heated under gentle reflux at 80°C for 5 hours. White powder was obtained after drying the water solution, which was further purified by recrystallization from boiling water.

^{1}H-NMR (400.6 MHz, DMSO-*d_6*): 3.4 (s), 6.0 (d), 7.6 (d). The signal at 6.0 ppm also comes with an additional small satellite doublet (~ 1/3 intensity), which may originate from the coupling to the nuclear spin active isotope ^{195}Pt which has a natural abundance of 33%.

trans-[(NH_3)$_2$Pt(1-methylcytosine)PdCl]NO_3: 0.2043 g *trans*-[Pt(NH_3)$_2$(1-methylcytosine)](NO_3)$_2$ was mixed with K_2PdCl_4 in 20 mL deionized water and kept stirring overnight, providing a yellow slurry. Filtrate was green/-yellow, and was dried to yield yellow/brown powder which was identified by NMR as a mixture containing the desired product *trans*-[(NH_3)$_2$Pt(1-methylcytosine)PdCl]NO_3 and unreacted *trans*-[Pt(NH_3)$_2$(1-methylcytosine)](NO_3)$_2$ in an approximate 1:1 ratio.

<u>Status of FY2011 Milestones</u>:

1. We will complete theoretical modeling of large supported Pt clusters and carry out mechanistic studies of CO, NO_x, and HC oxidation.

   Theoretical modeling of large supported Pt clusters is ongoing. We will initiate mechanistic studies after obtaining data for ~10 atom clusters.

2. We will also explore bimetallic subnanomenter supported Pt-Pd clusters to determine lowest energy system, synthesize them, and determine their stability under CO, NOx, and HC oxidation conditions. The results will facilitate the search for optimum catalyst systems for CO, NO, and hydrocarbon oxidation and NO_x reduction.

   We have synthesized subnanometer Pt-Pd supported on γ -alumina and are attempting to characterize them employing ACEM.

<u>Communication/Visits/Travel</u>

We have prepared a manuscript titled “Density Functional Studies of Adsorption of Transition Metal Atoms on θ-Al_2O_3(010) Surface” for Physical Review.

PI is lead organizer of a symposium on emission treatment for energy production and utilization at ACS meeting, Denver, August, 2011. There will be three sessions at the symposium addressing chemistry of emission treatment catalyst.

A joint project on lean NO_x treatment is ongoing with John Deere Co under work for others arrangement.

Problems Encountered

The characterization of Pt-Pd subnanometer catalysts supported on γ–alumina is pending due to ongoing repair of ACEM.

Publications

1. C.K. Narula, M.G. Stocks, "Density Functional Studies of Adsorption of Transition Metal Atoms on θ-Al_2O_3(010) Surface" Physical Review.
2. C.K. Narula, "Catalyst by Design – Bridging the Gap between Theory and Experiments at Nanoscale Level" Encyclopedia of Nanoscience and Nanotechnology, Vol. II, Taylor & Francis, New York, 2008, pp 771-782 (invited).
3. C.K. Narula, L.F. Allard, D.A. Blom, M. Moses-DeBusk, "Bridging the Gap between Theory and Experiments – Nano-structural Changes in Supported Catalysts under Operating Conditions" SAE-2008-01-0416, SAE Int. J. Mater. Manu., 1(2008) 182-188.
4. C.K. Narula, L.F. Allard, D.A. Blom, M.J. Moses, W. Shelton, W. Schneider, Y. Xu, "Catalysis by Design - Theoretical and Experimental Studies of Model Catalysts", SAE-2007-01-1018 (invited).
5. C.K. Narula, M.J. Moses, L.F. Allard, "Analysis of Microstructural Changes in Lean NO_x Trap Material Isolates Parameters Responsible for Activity Deterioration" SAE 2006-01-3420.
6. Y. Xu, W.A. Shelton, and W.F. Schneider, "The thermodynamic equilibrium compositions, structures, and reaction energies of Pt*x*O*y* (*x* = 1-3) clusters predicted from first principles," *Journal of Physical Chemistry B,* 110 (2006) 16591.
7. Y. Xu, W. A. Shelton, and W. F. Schneider, "Effect of particle size on the oxidizability of platinum clusters," *Journal of Physical Chemistry A*, 110 (2006) 5839.
8. C.K. Narula, S. Daw, J. Hoard, T. Hammer, "Materials Issues Related to Catalysts for Treatment of Diesel Exhaust," *Int. J. Amer. Ceram. Tech*., 2 (2005) 452 (invited).

Presentations (last 12 months)

1. Narula, C.K. Stocks, G.M., Density Functional Studies of Adsorption of Transition Metal Atoms on θ-Al_2O_3(010) Surface" American Chemical Society Meeting, Denver, CO, August 28, 2011.
2. Narula, C.K.; Chen, X.; Stocks, G.M., DeBusk, M.M.; Allard, L.F.; "First-Principles and Experimental Studies of the Sub-Nanomenter Platinum Atoms Supported on θ-Alumina" 230th American Chemical Society Meeting, Boston, MA, August 22-26, 2010
3. Narula, C.K.; Chen. X.; Stocks, M.G.; "First-Principles Studies of the Structure and Bonding of Metal Atoms Supported on θ-Alumina," 229th American Chemical Society Meeting, San Francisco, CA, March 21-25, 2010.
4. Moses-DeBusk, M.; Narula, C.K. "Catalyst by design: Combining the power of theory, experiments, and nanostructural characterization for catalyst development," 227th National American Chemical Society Meeting, March 2009 (invited).

References

1. Moore, C.E. *Atomic Energy Levels*: Natl Bur. Stand. U.S. Circ. No. 467; GPO: Washington, DC, 1952.
2. Yudanov, I; Pachhioni, G.; Neyman, K.; Rosch, N.; J. Phys. Chem. B **1997**, *101*. 2786.
3. Hosmane, R.S.; Leonard, N.J.; Synthesis **1981**, 118-119.
4. Lipper, B.; Lock, C.J.L.; Speranzini, R.A.; Inorg. Chem. **1981**, *20*, 808.

Agreement 19214: Effects of Biodiesel Fuel on Diesel Particulate Filter Materials

M. J. Lance, A. A. Wereszczak, E. E. Fox, D. F. Wilson and T. J. Toops
Oak Ridge National Laboratory

Objective/Scope

To characterize changes in the microstructure and material properties of commercial diesel particulate filters (DPFs) in exhaust gas produced by biodiesel blends.

Technical Highlights

Mechanical Properties Measurement as a Tool for Observing DPF Degradation

Mechanical testing of DPF specimens was initiated in Q2 for the estimation of the materials (tensile) failure stress as a function of tensile-stress-direction and location. DPFs do not have an isotropic structure and may not be subjected to symmetric stress fields. Therefore, there is interest in better understanding how a DPF mechanically responds to thermal-induced stress of operation and the direction in which that imposed stress field is applied. Elastic modulus estimation of the DPF materials are also pursued because knowledge of its accurate value is needed for estimating measured tensile failure stresses.

Three considered DPF materials are being examined and are shown in Fig. 1. One is a cordierite and the other two are silicon carbides (SiCs) with different porosity contents. For each material, three specimen geometries are being harvested out of the DPFs for the mechanical evaluations.

- *O-ring specimen*. O-ring specimens, originally developed to measure failure stresses in ceramic tubes [1-2], are cut from DPFs as shown in Fig. 2 and then have an interior hole drilled into each. They are then diametrally compressed to measure failure stress as shown in Fig. 3. Vertically oriented diametral compressive loading of an o-ring specimen will subject the outer diameter to hoop tension at the 3 and 9 o'clock positions and subject the inner diameter to hoop tension at the 6 and 12 o'clock positions. The weakest of those four locations will cause failure and its failure stress will be noted. The measured tensile failure stress represents an allowable hoop tensile stress in the DPF.

- *Biaxial flexure disk*. Biaxial flexure testing of disks will subject the tensile side of the specimen to an equibiaxial radial tensile stress using a ring-on-ring test fixture (i.e., axisymmetric 4-point-bending). Such testing is featured in ASTM C1499 [3]. An illustration of how the harvesting of these disks is conducted is shown in Fig. 4. Disks are machined from the two ends and the interior.

- *Sectored flexure bar*. Four sectored flexure specimens per DPF are harvested at either a 0°- or 45°-orientation as shown in Fig. 5. The specimen, when tested in 4-pt flexure, has its original outer OD subjected to axial tensile stress [4].

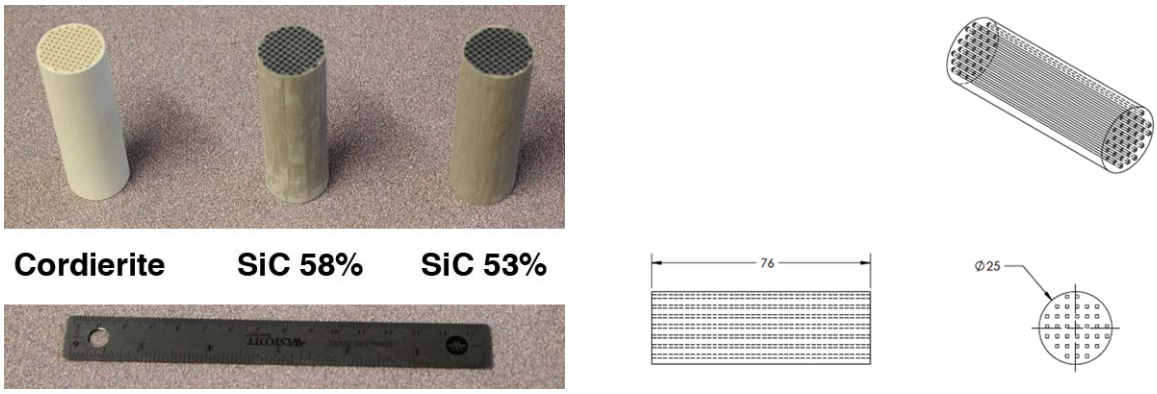

Figure 1. The mechanical properties of three DPF materials (left) are being evaluated. The nominal dimensions (right) of the DPF are 25-mm diameter and 76-mm-length.

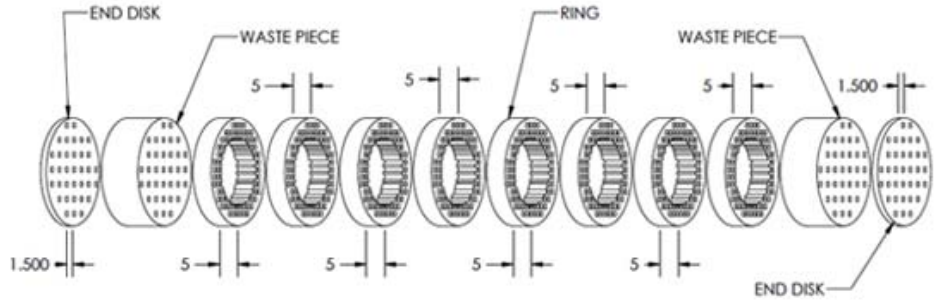

Figure 2. Exploded view showing o-ring specimen geometry harvesting from single DPF. Eight o-ring specimens are yielded per DPF and two end-disks for biaxial flexure testing are also produced.

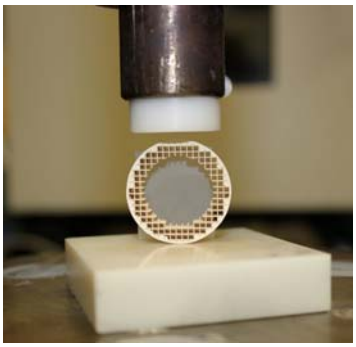

Figure 3. Experimental setup of diametrial compression test of a cordierite o-ring specimen. 0°-orientation shown in this sample (i.e., struts aligned parallel and perpendicular to direction of compressive loading. 45°-orientation is also being tested. Tape (shown behind the specimen) holds the specimen perpendicular until compressive loading and alignment starts. The outer diameter of this specimen is 25 mm.

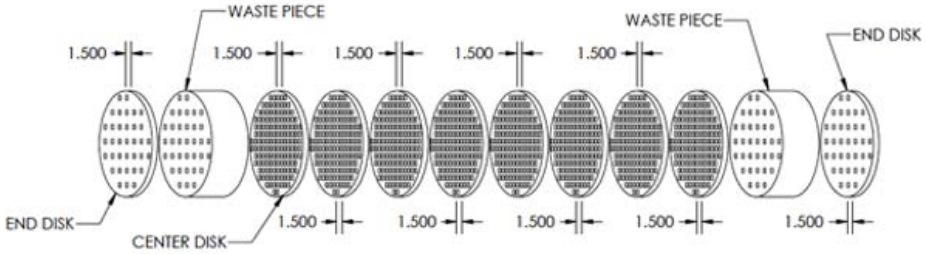

Figure 4. Exploded view showing biaxial disk specimen harvesting from a single DPF. Eight internal biaxial disks are yield per DPF. Two external biaxial disks are yielded for all DPFs.

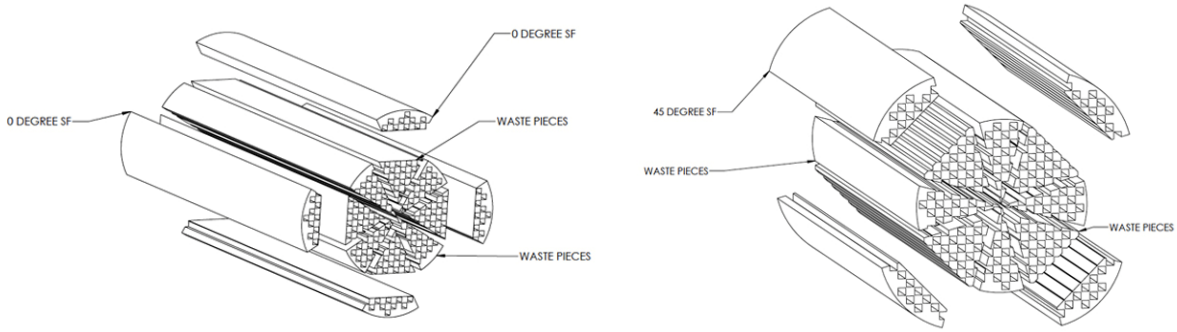

Figure 5. Schematic showing how (left) 0°-oriented and (right) 45°-oriented sectored flexure specimens are harvested out of a single DPF. Yield is 4 sectored flexure specimens per DPF.

Our estimation of specimen failure stress (with all specimens shown in Figs. 2, 4, and 5) occurs via the flowchart shown in Fig. 6. Mechanical testing and finite element analysis (FEA) are combined to achieve this. For example, the diametral compression of the o-ring specimen produces a definitive relationship between compressive force and load-point-displacement. The same loading scenario is then modeled with FEA (enabled thru ORNL's µ-FEA software and the actual capturing of the DPF strut structure) by adjusting the DPF material's elastic modulus until the experimentally measured load-point-displacement jives with the measured maximum compressive force. The arrived-at elastic modulus value is what we report as the material elastic modulus, and is needed for us to estimate failure stress. Strength testings of the o-ring, biaxial disk, and sectored flexure specimens will continue in Q3.

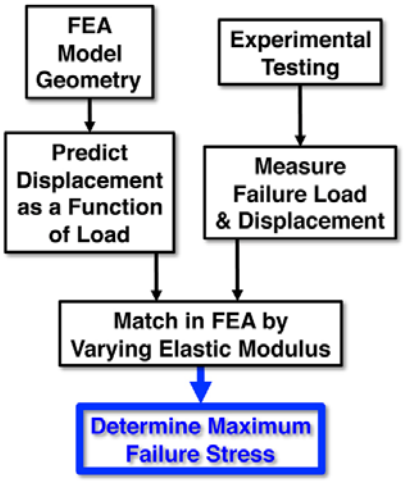

Figure 6. Flowchart (left) describing the modeling and experimentation pathway to determine maximum failure stress.

Ageing of DPF Materials in Condensate Solutions

DPF samples were dip-tested in 1 M solutions of both sulfuric and formic acid and a 50:50 mixture of the two for 2 months followed by 1 month of drying in air. Upon drying, the cordierite formed Al and Mg sulfates as shown in Fig. 7. Figure 8 shows that pure formic acid attack was not observed in either cordierite or SiC DPFs. The skin of the SiC sample contains alumino-silicate fibers that are susceptible to corrosion from sulfuric acid. The most likely mechanism of chemical attack is due to the condensate evaporating slowly, resulting in long exposure to a very concentrated acidic solution. A similar mechanism may have occurred in operation producing the original degradation observed on the as received DPF brick.

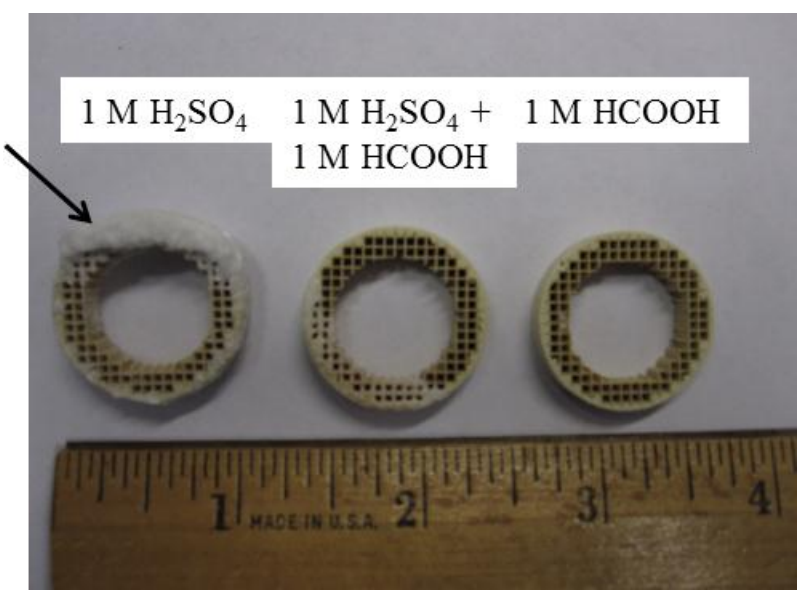

Figure 7. Samples of cordierite following exposure to sulfuric and formic acid solutions. The arrow points to significant corrosion that occurred on the sample exposed to 1 M H_2SO_4.

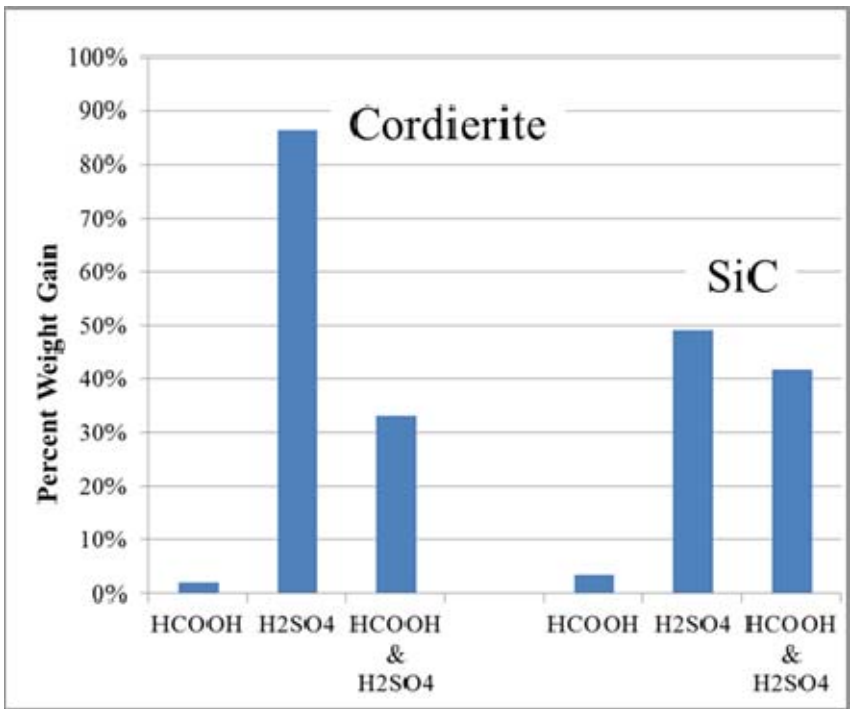

Figure 8. The percentage weight gain following dip-testing in acid for 2 months followed by 1 month of air drying.

Status of FY2011 Milestones

1. Measure the chemical composition and pH of condensate and PM generated by a diesel engine running with ULSD and biofuel blends. (12/10) *On Schedule.*
2. Age filter samples (cordierite, SiC and possibly mullite) in solutions identical to condensate composition. (9/11) *On Schedule.*
3. Monitor microstructural and mechanical property changes in DPF substrates following chemical ageing. (9/11) *On Schedule.*

Communications/Visits/Travel

None.

Problems Encountered

None.

Publications/Presentations/Awards

None.

References

[1] O. M. Jadaan, D. L. Shelleman, J. C. Conway, Jr., J. J. Mecholsky, Jr., and R. E. Tressler, "Prediction of the Strength of Ceramic Tubular Components: Part I - Analysis," *Journal of Testing and Evaluation*, 19:181-191 (1991).

[2] D. L. Shelleman, O. M. Jadaan, J. C. Conway, Jr., and J. J. Mecholsky, Jr., "Prediction of the Strength of Ceramic Tubular Components: Part II - Experimental Verification," *Journal of Testing and Evaluation*, 19:192-200 (1991).

[3] "Standard Test Method for Monotonic Equibiaxial Flexural Strength of Advanced Ceramics at Ambient Temperature," ASTM C1499, Vol. 15.01, ASTM International, West Conshohocken, PA, 2009.
[4] A. A. Wereszczak, S. F. Duffy, E. H. Baker, J. J. Swab, and G. J. Champoux, "Strength of a Ceramic Sectored Flexural Test Specimen," *Journal of Testing and Evaluation*, 36:17-23 (2008).

Agreement 20091: Electrically Assisted DPF Material

M. J. Lance, A. A. Wereszczak, J. E. Parks, W. P. Partridge, and E. E. Fox
Oak Ridge National Laboratory

Objective/Scope

In this CRADA project with General Motors (GM), two research objectives are being pursued:

1. Measure of substrate temperatures during DPF regeneration with optically based techniques that are not susceptible to conductive interferences that are problematic for common thermocouple technologies.
2. Analysis of diesel particulate filter (DPF) substrate materials to understand crack and failure mechanisms and resolve current differences in simulation and experimental results.

Technical Highlights

Engine-based DPF Studies

Development of a fiber optic probe technique for measuring the substrate wall temperature during DPF regeneration continued at ORNL in Q2. Fiber optics were polished to attain angled tips that allowed side viewing of the substrate wall when inserted into the channels of the DPF. Bench rig experiments were conducted to collect blackbody radiation from cordierite monolith samples with a lab furnace. The blackbody radiation curves collected with the fiber optic probe are shown in Fig. 1. Work is continuing and focusing on calibration methods as well as software coding to enable fast data acquisition for the engine-based experiments.

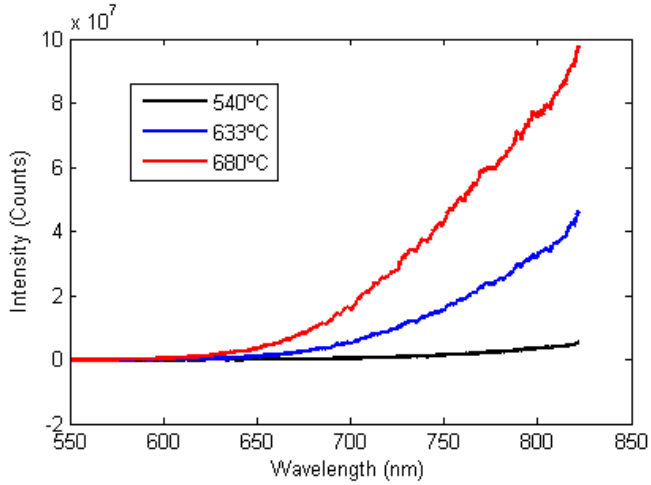

Figure 1. Blackbody radiation spectra obtained with a side viewing fiber optic probe inserted into a cordierite monolith channel.

Engine-based experiments of the electrically-assisted DPF regeneration continued with emphasis on temperature control protocols and measurement. Example temperatures experienced in a DPF regeneration event as a function of location in the exhaust system

are shown in Fig. 2. Results were compared to a 300ºC base engine exhaust temperature. Elevated temperatures downstream of the engine include (in order): exhaust heated by combustion with the Post-80 technique (380ºC), exothermic heating of exhaust by hydrocarbons oxidizing on the DOC (610ºC), and electrical heating of exhaust (910ºC). The resulting DPF temperature was ~750ºC. Work in this area is continuing with the primary focus on repairing thermocouples on the heater that have been found to short at the elevated temperatures experienced during DPF regeneration.

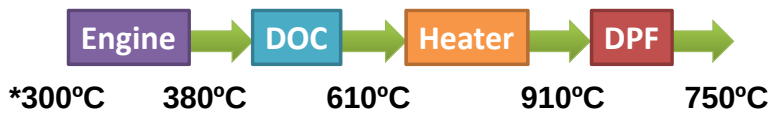

Figure 2. Temperatures achieved in the exhaust system during a DPF regeneration event.

DPF Mechanical Evaluation

The mechanical testing and finite element analysis continued of specimens for the estimation of (tensile) failure stress as a function of tensile-stress-direction and location. Large numbers of tests will occur in Q3 with preliminary tests and their examinations occurring in the present Quarter. Three specimen geometries are being used and are shown in Fig. 3: the o-ring specimen, the sectored flexure specimen, and the biaxial flexure disk specimen. When mechanically loaded as intended, the o-ring specimen enables the examination of DPF response to hoop tension, the sectored flexure specimen enables the study of axial tensile stress on the DPF's outer skin, and the biaxial flexure specimen enables the evaluation of radial tensile stresses on the DPF's inner structure or end-surface (depending where the disk is harvested from).

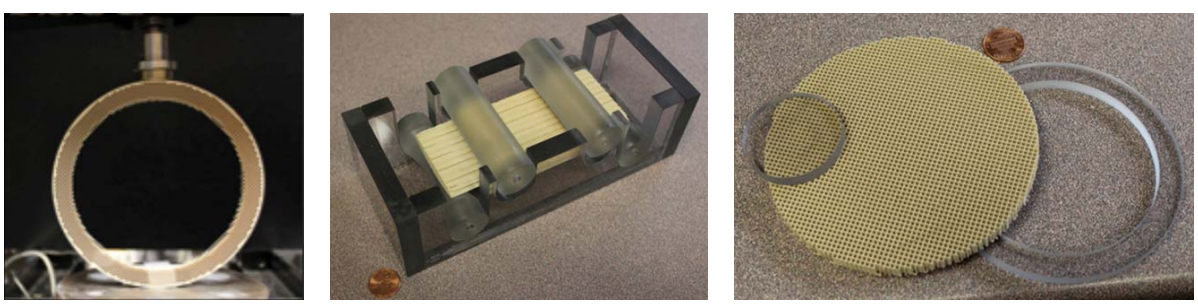

Figure 3. Left to right, examples of the o-ring specimen, sectored flexure specimen, and the biaxial flexure disk specimen.

For all three specimen geometries, mechanical testing and finite element analysis (FEA) are combined to achieve this. For example, the diametral compression of the o-ring specimen produces a definitive relationship between compressive force and load-point-displacement. The same loading scenario is then modeled with FEA (enabled thru

ORNL's μ-FEA software and the actual capturing of the DPF strut structure) by adjusting the cordierite's elastic modulus until the experimentally measured load-point-displacement jives with the measured maximum compressive force. When correlated, an elastic modulus in the range of 1-2 GPa. This is approximately one order of magnitude lower than reported elastic modulus estimated with sonic- or ultrasonically-based, as illustrated in Fig. 4. If this is indeed true, then these lower elastic modulus values will mean that service stresses in DPFs are lower than that previously believed.

Test Method	Elastic Modulus (GPa)*	Source
Resonance Ultrasound Spectroscopy (RUS)	12.3 ± 0.3	Shyam *et al.*, JACS, 2008.
Resonance-Based	4 - 7	SAE 2004-01-0959
Mechanical (O-ring)	1.1 – 2.1	This Project
Mechanical (Biaxial Flexure)	TBD	
Mechanical (Sectored Flexure)	TBD	

** A function of porosity – comparison intended to illustrate coarse comparison.*

Figure 4. Preliminary results suggest elastic modulus of the DPF cordierite is lower than reported sonic-based-measured literature values.

The machine compliance (i.e., machine's "spring-constant) needs to be subtracted out of our experimental measurements. To measure machine compliance, thick steel (i.e., very stiff) test coupons were machined and mechanically loaded in our test frame using the same fixturing and load cell used for our testing of the DPF specimens. From this, we estimated machine compliance as a function of compressive force, and then this component was subtracted from our experimental compressive-load-displacement data measured during our o-ring testing. We determined for the o-ring tests that the machine compliance only constitutes about 1-2% of the entire measured contraction of the o-ring specimen, so this in turn affects our estimation of elastic modulus using our mechanical method of 1-2%. Therefore, our previous estimation of elastic modulus of 1-2 GPa is still 1-2 GPa after machine compliance correction.

Efforts are underway to attempt to estimate elastic modulus of both the (relatively dense) outer DPF skin and the (relatively low dense) inner strut structure using both resonant ultrasound spectroscopy (RUS) and the quasi-static mechanical measuring method advocated in this project (Fig. 5). These measurements are deemed important for two reasons. First, it will help identify and understand any difference in elastic properties of the two different materials in a DPF. Second, it will help us further investigate the apparent disparity between elastic modulus measured with RUS and quasi-static mechanical loading.

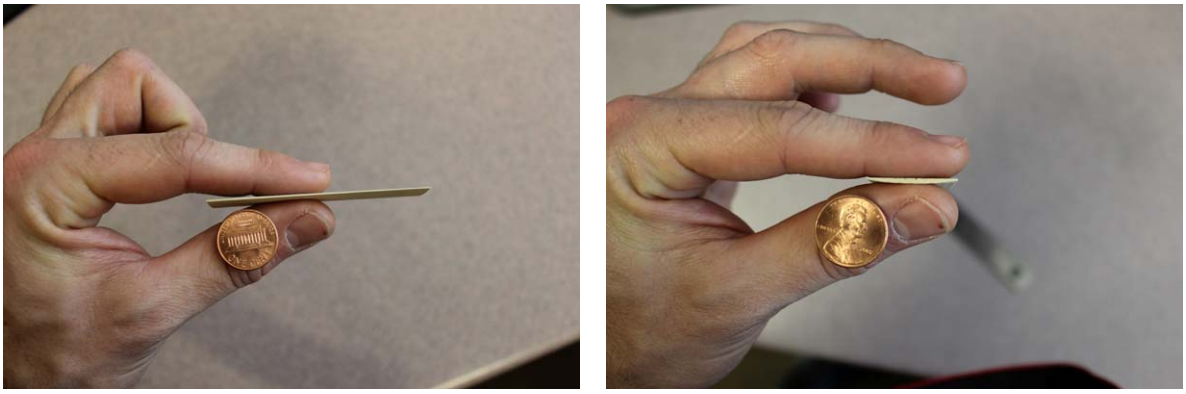

Figure 5. Side view (left) and end view (right) of a "skin specimen" from a 140-mm diameter DPF. Its elastic modulus will be estimated using RUS and quasi-static mechanical loading.

Status of FY 2011 Milestones

1. Measurement of the fuel penalty for both Electrically-Heated DPF and conventional fuel-heated approaches (September 2011). On Schedule
2. Optimization of the fiber-optic temperature measurement technique and a rigged DPF system with fiber-optic and thermocouple probes ready for engine use (September 2011) Delayed- Thermocouple signals are not behaving as expected in the high temperature region. We are in communication with GM to address this problem.
3. Database of strength-size-scaling statistics of ceramic used in EHDPF (September 2011) On Schedule.
4. Rank properties and geometrical parameters that most affect tensile stresses in EHDPFs (September 2011) On Schedule.
5. Rules of design for EHDPF regenerators (September 2011) On Schedule.
6. Recommendations for the best commercial alloy for this application (September 2011) On Schedule.

Communications/Visits/Travel

1. Wereszczak traveled to Daytona Beach, FL in late January to present a talk entitled "Alternative Test Coupons for Failure Stress Evaluation of DPFs" at the 35th International Conference on Advanced Ceramics and Composites.
2. A CRADA review conference call between GM and ORNL occurred on 09Feb2011.
3. A CRADA review conference call between GM and ORNL occurred on 02Mar2011.

Problems Encountered

None.

Publications/Presentations/Awards

A. A. Wereszczak, E. E. Fox, and M. J. Lance, "Alternative Test Coupons for Failure Stress Evaluation of DPFs," presented at the 35th International Conference on Advanced Ceramics and Composites, Daytona Beach, FL, 25 January 2011.

References

None.

Agreement 9105: Characterization of Catalyst Microstructures

L.F. Allard, C.K. Narula, W.C. Bigelow, D.P. Nackashi and J. Damiano
Oak Ridge National Laboratory

Objective/Scope

The objective of the research is to understand fundamental processes in catalytic systems with applications to transportation technologies, such as those used for the treatment of NO_x emissions, and for the production of biomass-derived liquid fuels. The research heavily utilizes new capabilities and techniques for ultra-high resolution transmission electron microscopy with the HTML's aberration-corrected electron microscope (ACEM). The research is ultimately focused on understanding the effects of reaction conditions on the changes in morphology of heavy metal species on "real" catalyst support materials (e.g. oxides and carbon materials), and the understanding of the structures of model mono-, bi- and multi-metallic catalyst systems of known particle composition. A major thrust of these studies has been to develop methods of *in situ* microscopy at elevated temperatures and under controlled gas compositions. This work has expanded with the collaboration with Protochips Inc. (Raleigh, NC), who provide a novel heating technology utilizing MEMS-based heating devices that we have shown to be stable enough to provide sub-Ångström imaging capabilities at high temperature in the ACEM. Model samples of nanoparticulates of controlled composition on carbon or oxide supports are also being studied in collaboration with the catalysis group at the University of Texas-Austin (Prof. P. Ferreira), the University of Texas-San Antonio (Prof. M. Jose-Yacaman), the University of Missouri-St. Louis (Prof. J. Liu), and University of New Mexico (Prof. A. Datye). Studies of the behavior of platinum group metal (PGM) species on oxide substrates are also being conducted with Drs. S. A. Bradley of UOP Co., and C. H. F. Peden of PNNL, and Prof. F. H. Ribiero at Purdue University. NOx trap catalyst materials BaO/Al_2O_3 are being studied with Dr. Peden and Dr. Ja Hun Kwak at PNNL and Pt-Re/C catalysts on model carbon nanotube materials are being studies with Dr. L. Zhang, also of PNNL. We have also initiated a new study of "intelligent catalysts" for automotive emission control applications, based on the self-regenerative phenomenon of heavy metal species such as Pd and Rh in Ca- and La-based perovskite crystal structures. This work is being conducted in collaboration with Prof. Xiaoqing Pan of the University of Michigan, and Ford Research Laboratory colleague Dr. Andrew Drews.

Technical Progress

Further work in collaboration with Protochips Co. has led to the development of the "Gen 3" environmental cell (E-cell), which has several significant advances over the Gen 2 design. The principal change is a complete new design of the gas cell system, which still uses a "two-chip" arrangement similar to the Gen 2 holder, except that the new design does not require the MEMS-based heater chip and the amorphous SiN window to be glued into holder plates that then sealed against O-rings. The separation between the heater plate and the SiN window plate in the Gen 2 designed was controlled by the two Cu-wire electrical leads. The minimum separation therefore was the diameter of the wires, or about 150 m. One problem with this design was that it was

difficult to screw the heater plate down to squeeze against the O-ring for a vacuum seal and to squeeze against the electrical leads to make good contacts, without stressing both the SiN window and the ceramic heater membrane. We also found that, due probably to the epoxy used for sealing the heater chip and window chip into their respective plates, and to the (relatively) large O-rings used to seal the cell, contamination was a significant issue when the catalyst material was imaged under the electron beam.

The Gen 3 E-cell design now uses a new geometry that allows the heater and window chips to seal directly against very small O-rings. The chips are clamped onto the tip of the rod with a clamping plate; Fig. 1 shows the top and bottom views of the holder tip with the plate attached. The clamping plate is precisely positioned by an alignment pin, shown in Fig. 1b. The total thickness of this design is 1.25mm, which allows it to fit comfortably within the narrow 2mm gap of the JEOL 2200FS ACEM pole piece, as shown in the schematic of Fig. 2. The electron beam passes through a hole in the top plate, against which the heater chip seals. Figure 3 shows a schematic of the holder with the clamping plate removed and the SiN window chip in place. Figure 4 is a photo of the tip of the holder also with the clamp removed, showing the two O-rings in place, and dotted lines indicating the positions of the lower window and the heater chip.

The heater chip has two electrode pads microfabricated to be a known thickness, e.g. 5 μm, and the SiN window chip (bottom) also has appropriately designed microfabricated leads on the surface, which contact the Cu-wire electrical leads outside of the O-ring seal surface. The contacts internal to the O-ring that seals the window chip are fabricated to mate against the contacts on the heater chip, allowing the total thickness of the E-cell to be controlled down to a minimum of a mere 5□m. Along with the much thinner cell capability, the new design has the advantage that the clamping forces are uniformly distributed when the screws are tightened, and it is easy to get a good vacuum seal with very little stress on the delicate heater/window ceramics.

Additional improvements with the Gen 3 design include attention to ensuring a clean gas path to the cell, by incorporating very small diameter (100□m ID) stainless steel tubing internal to the rod, which mate with special stainless steel fittings in the rod handle. These fitting, shown in Fig. 5, can connect to 1/16" stainless steel tubing that connects in turn to the gas handling manifold (described in a past quarterly). The handle also incorporates the electrical connector that carries the heating current (Fig. 5a).

We also fabricated a new "clamshell" cover for the specimen goniometer to permit the specimen rod to be sealed from the atmosphere. The clamshell has a removable, replaceable flange on the end that allows electrical and gas feeds into the interior, to connect to the specimen holder as needed. The clamshell provides stability against air pressure changes that can cause specimen drift that affects the highest resolution imaging on the microscope. Figure 6 shows the clamshell in a closed position on the column, with an electrical lead plugged in.

Tests of the Gen 3 E-cell holder showing performance at different atmospheric pressures in the cell, and the ability to do atomic-level imaging will be reported in a later quarterly.

Status of Milestones
On schedule

Communications/Visits/Travel
None this quarter

Publications
None this quarter

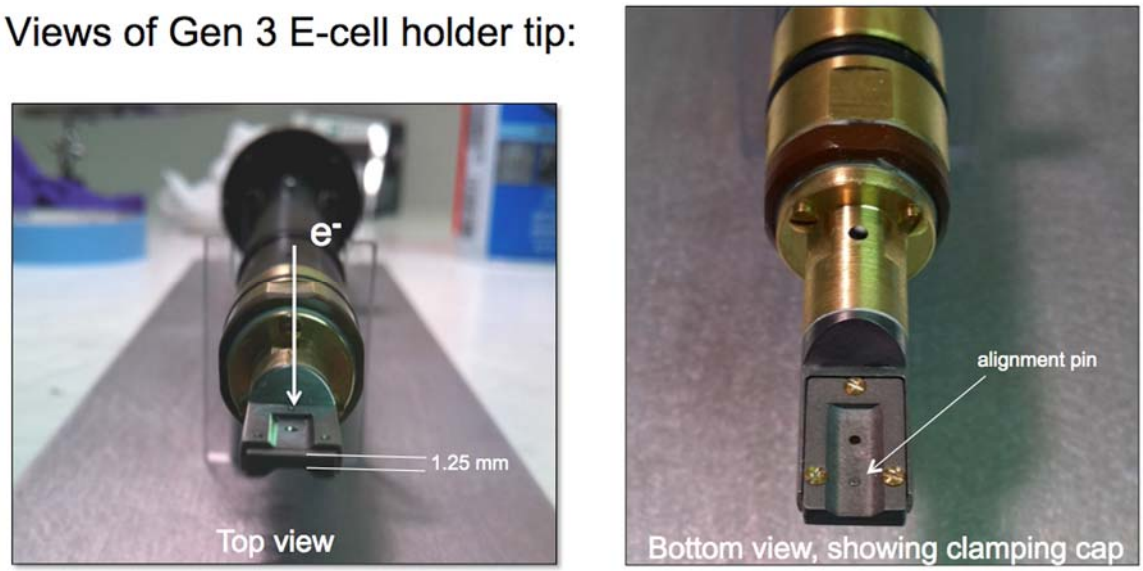

Fig. 1. a) Tip of Gen 3 E-cell holder, showing top surface and 1.25mm thick section that fits into ACEM objective lens pole piece; b) Bottom view, showing clamp and alignment pin to precisely position clamp in tip.

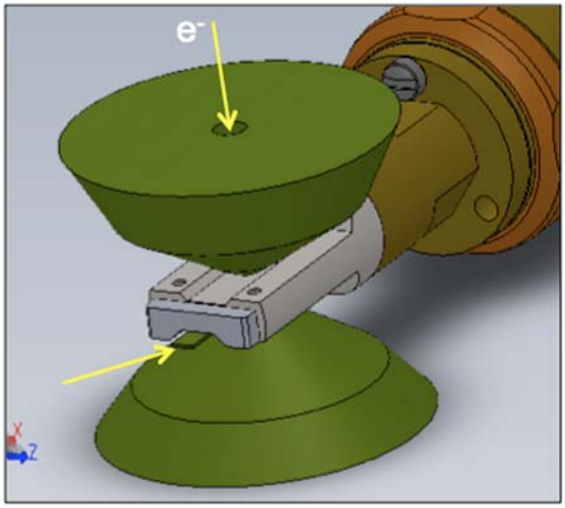

Fig. 2. Schematic showing fit of E-cell holder tip within gap of ACEM pole piece (represented by green sections).

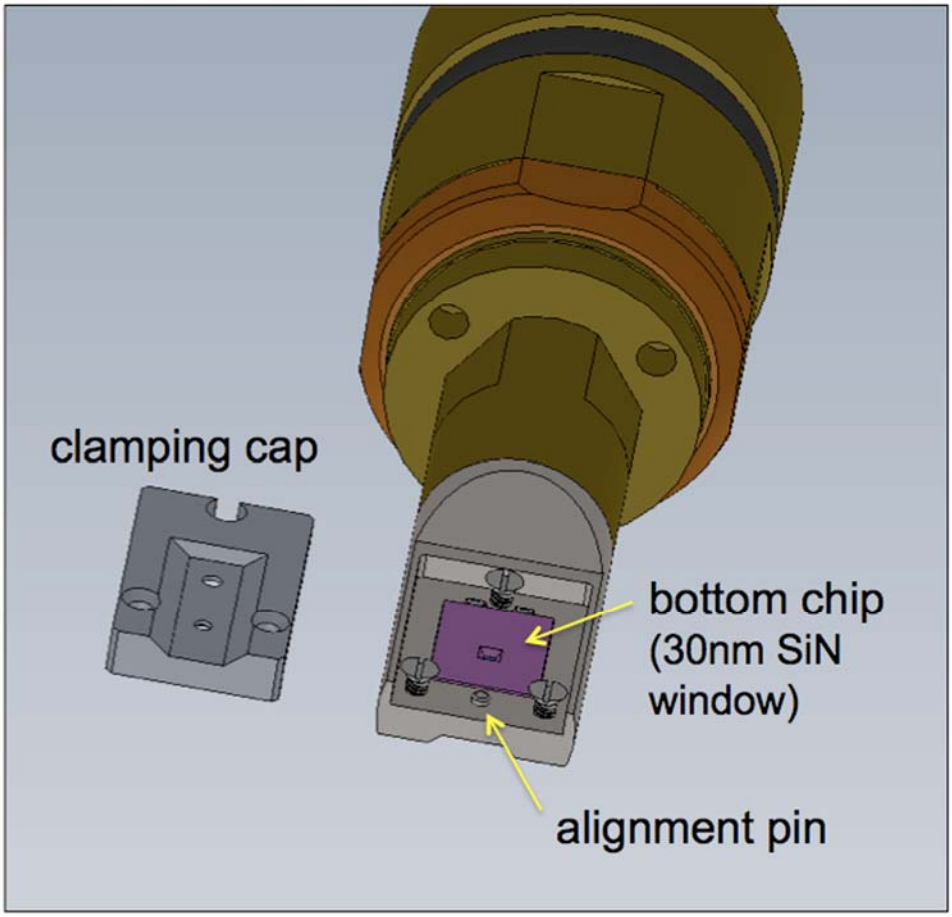

Fig. 3. Schematic of bottom chip section of the holder, with clamping cap removed to show positioning of the 30nm SiN window chip.

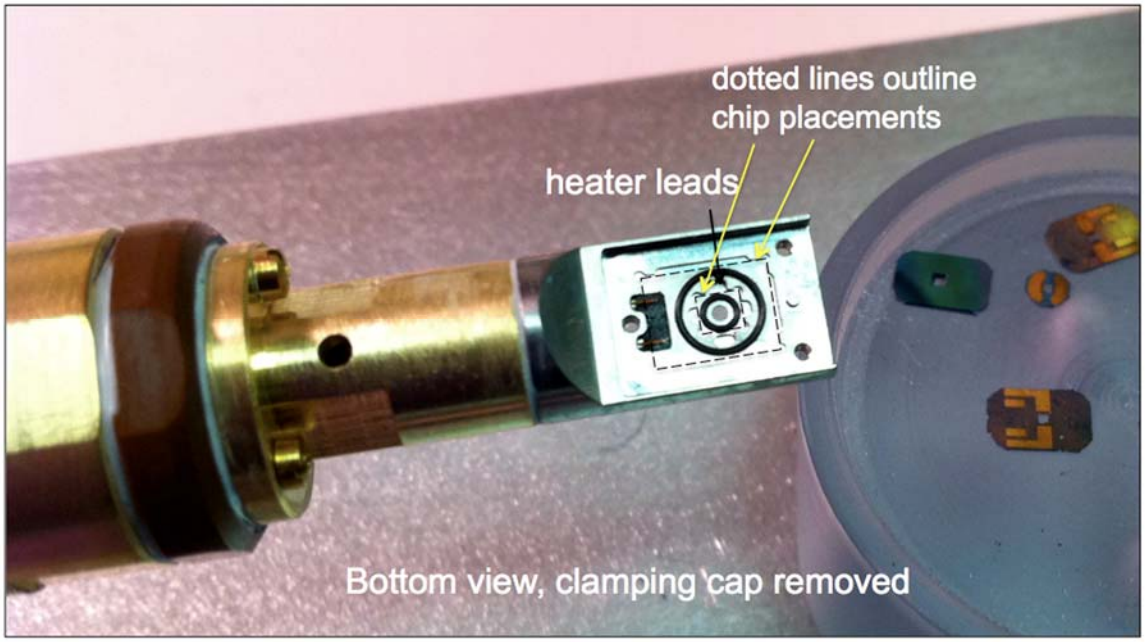

Fig. 4. Holder tip viewed from the bottom with the window chip removed, showing O-rings and positions of both the bottom window chip and top heater chip.

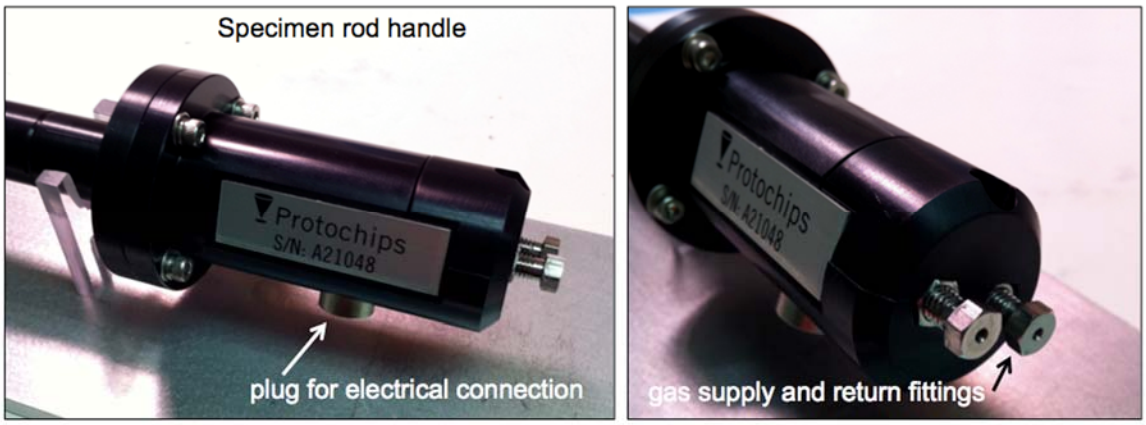

Fig. 5. Handle of E-cell holder, showing electrical connection for heater current (a), and stainless steel fittings for 1/16" gas supply and return lines.

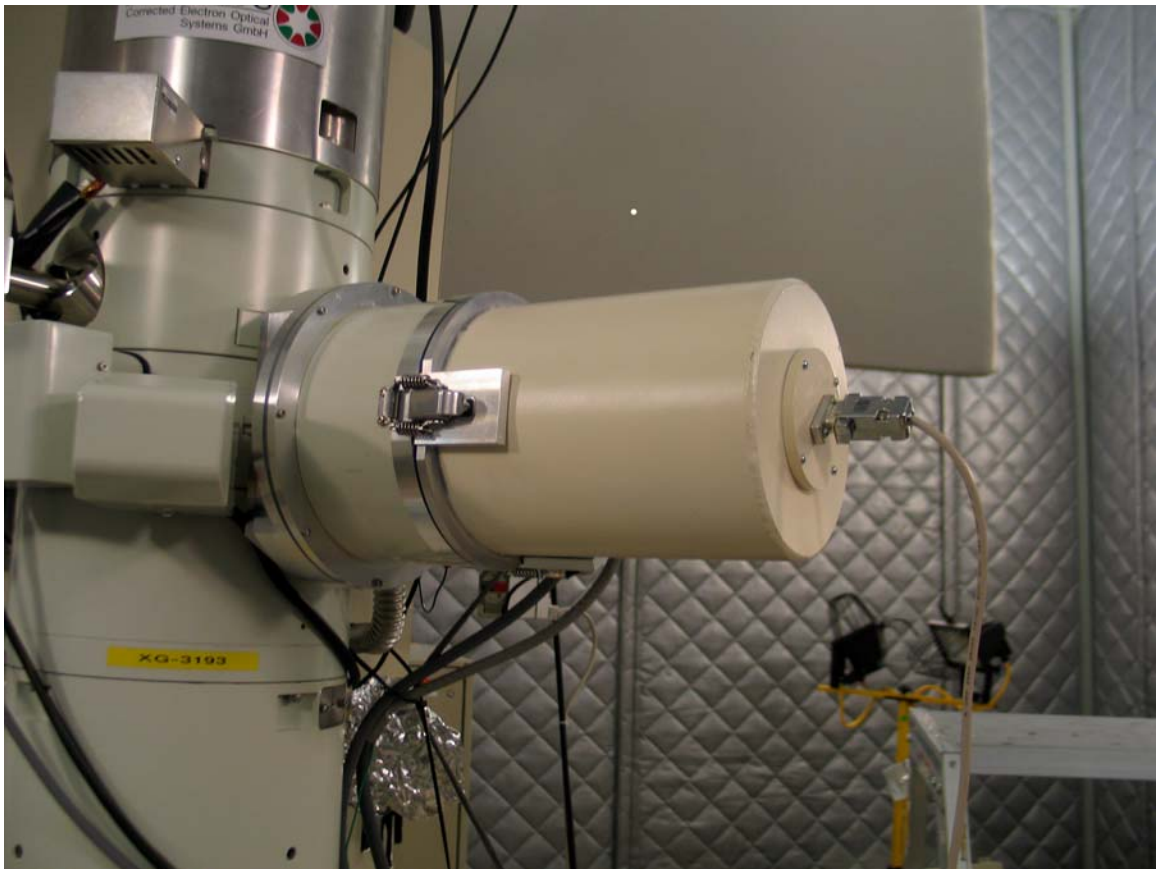

Fig. 6. View of new "clamshell" cover for sealing heater and E-cell holders to minimize effects of pressure changes; plug is connected to a replaceable flange that allows changing accommodate other holder types (e.g. with gas-line fittings).

Agreement 14957: High Temperature Thermoelectrics

A. A. Wereszczak and H. Wang
Oak Ridge National Laboratory

R. McCarty and J. Sharp
Marlow Industries, Inc.

Objective/Scope

Two-thirds of the chemical energy in automotive fuel is rejected to the atmosphere as waste heat. Thermomechanical stresses must be managed and TE material strength must be improved to fully exploit TE devices for waste heat recovery. Toward that, needed thermomechanical and thermophysical properties of candidate thermoelectric (TE) materials are measured in this project and then used with established probabilistic reliability and design models to optimally design automotive and heavy vehicle TE modules. Thermoelectric materials under candidacy for use in TE modules tend to be brittle, weak, and have a high coefficient of thermal expansion (CTE); therefore, they can be quite susceptible to mechanical failure when subjected to operational thermal gradients. A successfully designed TE module will be the result of the combination of temperature-dependent thermoelastic property and strength distribution data and the use of the method of probabilistic design developed for structural ceramics.

Technical Highlights

Thermomechanical and thermophysical testing of Marlow-supplied materials continued during FY11Q2. Hundreds of Bridgeman Bi_2Te_3 specimens were received from Marlow for elastic and mechanical strength testing. Room temperature elastic properties were measured and dilatometry was completed on many dozens of specimens.

High-temperature elastic properties and flexure testing will start and be completed in Q3. An existing oven (capable of heating to 250°C) is being installed in a smaller mechanical test frame. The fabrication of the frame is nearly completed as of this writing and the control and data acquisition software is completed. This system will enable greater throughput of testing.

Room temperature elastic modulus and Poisson's ratio were measured on a wide array of thermoelectric materials. This included new n- and p-type skutterudite specimens supplied by General Motors's J. Salvador.

P-type and n-type skutterudite elements were examined at the High Flux Isotope Reactor (HFIR) for feasibility of neutron strain mapping. Several main diffraction peaks were identified for both compositions on 4x4x5 mm^3 legs. The minimum time to collect neutron diffraction data was estimated. It provided critical information for the follow-on neutron strain mapping of skutterudite modules scheduled for May 2011.

Transport properties on several thermoelectric materials (including bismuth telluride, lead telluride and skutterudite) over the application temperatures were completed

including thermal diffusivity, specific heat, Seebeck coefficient and electrical conductivity. These data are being used in the modeling and product improvement efforts at Marlow.

Residual stresses in the metallization used in Marlow thermoelectric devices is being estimated using a combination of finite element analysis and surface stresses measured using optical fluorescence on alumina substrates.

Status of FY 2011 Milestones

1. Generate thermoelastic and mechanical property database as a function of temperature on candidate p- and n-type TEMats fabricated by Marlow Industries as part of CRADA. [Sep11] *On schedule.*
2. Refine in-situ thermal-gradient-strength test method for TEMats. [Sep11] *On schedule.*
3. Transport properties measurements of selected thermoelectric materials. [Sep11] *On schedule.*

Communications/Visits/Travel

- Conference call was held 31 Jan 2011 between ORNL and Marlow.
- Conference call was held 15 Feb 2011 between ORNL, Marlow, and University of Wisconsin-Platteville's O. Jadaan.
- A presentation describing this project's progress is scheduled for 11 May 2011 at the DOE Merit Review.
- The next semi-annual CRADA review with Marlow is scheduled for 25 May 2011 and will be held at Marlow (Dallas, TX).

Problems Encountered

None.

Publications/Presentations/Awards

None.

References

None.

Agreement 16308: MBD Thermoelectrics Theory and Structure

David J. Singh
Oak Ridge National Laboratory

Objective/Scope

We will use modern science based materials design strategies to find ways to optimize existing thermoelectric materials and to discover new families of high performance thermoelectrics for waste heat recovery applications in vehicles. The emphasis will be on the thermoelectric figure of merit at temperatures relevant to waste heat recovery and on other properties important for applications, especially anisotropy, cost and mechanical properties. The identification of new thermoelectric materials in this project may additionally help with the development of thermoelectric climate control systems for vehicles, which is an important technology in the context of electric and hybrid vehicles.

Technical Highlights

Vehicular applications of thermoelectric materials for waste heat recovery require the identification, development and optimization of high performance thermoelectrics that are applicable to vehicles. A key requirement is related to materials cost. Therefore it is important to identify thermoelectrics that are based on elements that are abundant and low cost. This quarter, we continued our investigation of candidate materials with these characteristics. Specifically we performed a detailed technical analysis combining first principles calculations and Boltzmann transport theory of transition metal doped Mo_3Sb_7. This is a cubic material, which is advantageous from a materials processing point of view.

The compound has a band-gap somewhat above the Fermi level (see Figure 1 below) in the undoped state, but approaches a semiconducting state as electrons are added to the system by doping with commonly available metals such as Iron, Cobalt and Nickel. A ZT of 0.93 at 1050 K (Ref. [2]) has already been attained in this material at a comparatively high carrier concentration of $p = 5 \times 10^{21}/cm^3$, far above the 10^{19}-$10^{20}/cm^3$ range where thermoelectric performance (i.e. ZT) is typically optimized. Thermopowers of approximately 160 μV/K were obtained at this carrier concentration.

The key question for modeling is whether this is the optimum performance of the material, in which case it does not meet the performance requirements for vehicles, or if on the other hand the performance can be significantly increased by control of the carrier concentration or other means. In the latter case, it is important to determine what performance can be achieved and what the required carrier concentration range will be.

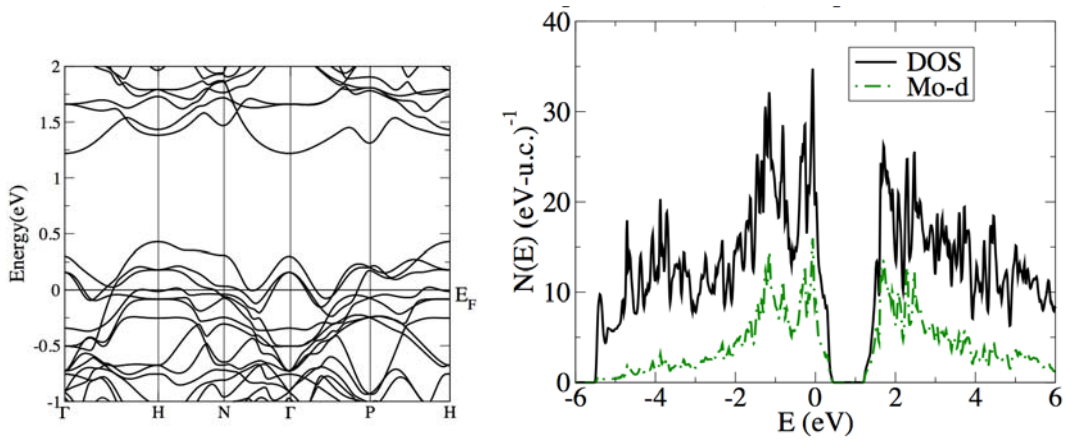

Figure 1: The band structure (left) and density-of-states (right) of undoped Mo_3Sb_7 as obtained in our first principles calculations. Note the band-gap approximately 0.4 eV above E_F (left) and the large density-of-states just below the VBM (right), favorable for large thermopower.

Our analysis (Fig. 2 below) showed that when the material is further doped into a semiconducting state, thermopowers over 300 μV/K – double present values – are likely to be achieved. This is highly favorable for thermoelectric performance. Therefore the present material is not optimized. It is of considerable interest (see Fig. 2) that these thermopowers are attainable in a wide range of temperatures between 500 and 1000 K , as actual performance in an exhaust waste heat recovery application will depend on the average performance across this range of temperatures.

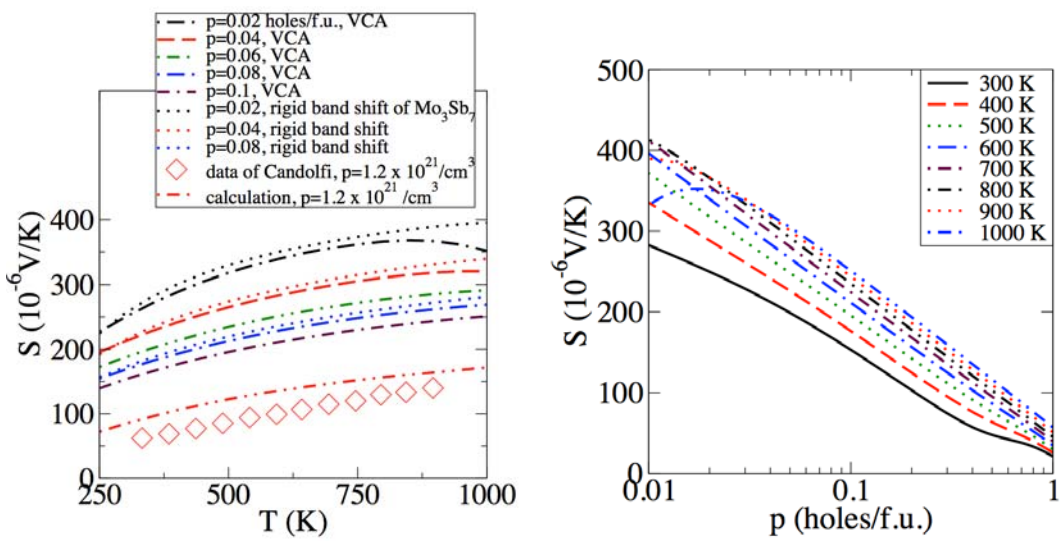

Figure 2: Calculated thermopower (S) at various hole concentrations (left) and temperatures (right) of doped Mo_3Sb_7. Note the very high thermopowers above 500 K (left) and the weak temperature dependence between 500 and 1000 K (right).

The results imply that the optimized power factor $S^2\sigma$ may be as much as twice higher than the currently known highest value, with a concomitant increase in ZT. A remaining

question is how the carrier concentration can be tuned into this high performance region. One possibility that should be investigated is co-doping.

Our Fiscal Year 2010 report presented an analysis of the lead chalcogenide thermoelectric, PbSe, which was not thoroughly studied as a thermoelectric despite a similar chemical structure to the better known high performance material PbTe. Our analysis, which we presented at the 2010 International Conference on Thermoelectrics and published in the form of a technical report [3], showed that if properly doped p-type this material could exhibit high temperature performance surpassing that of PbTe. Recently this prediction has been confirmed. Dr. G.J. Snyder (California Institute of Technology) performed the suggested experiments and found a ZT in excess of 1.2 in partially optimized (Ref. [4]) at temperatures of 850 K (see Figure 3, below). This provides a new high performance Tellurium free material.

Status of FY 2011 Milestones

We are making progress towards our milestone of successfully predicting new thermoelectric compositions. We will continue investigation of the materials mentioned about, and will investigate alternative materials, particularly chalcogenides and Zintl phases.

Problems Encountered

No significant problems encountered this quarter.

Publications/Presentations/Awards

David Singh, “Recent Theoretical Results for Advanced Thermoelectric Materials”, Thermoelectrics Applications Workshop, San Diego, CA, January 5, 2011.

David Parker, M.H. Du and David Singh, “Doping of Thermoelectric Performance in Mo_3Sb_7: First Principles Calculations”, APS March Meeting, Dallas, TX, March 22, 2011.

Award: David J. Singh was appointed Chair of the American Physical Society Publication Oversight Committee, and is serving as a member of the Executive Committee, American Physical Society Division of Computational Physics.

Refereed Papers

None this quarter.

References

1. G.K.H Madsen and D.J. Singh, “BoltzTraP: a code for calculating band-structure dependent quantities”, Computer Physics Commun. **175**, 67 (2006).

2. H. Xu, K.M. Kleinke, T. Holgate, H. Zhang, Z. Su, T.M. Tritt and H. Kleinke, “Thermoelectric performance of $Ni_yMo_3Sb_{7-x}Te_x$ ($y \leq 0.1$, $1.5 \leq x \leq 1.7$)”, Journal of Appl. Physics **105**, 053703 (2009).

3. D. Parker and D. J. Singh, “High-temperature thermoelectric performance of heavily doped PbSe”, Physical Review B **82**, 035204 (2010).

4. Heng Wang, Yanzhong Pei, Aaron D. LaLonde and G. Jeffrey Snyder, “Heavily Doped p-Type PbSe with High Thermoelectric Performance: An Alternative for PbTe”, Advanced Materials **23**, 1366 (2011).